CONTAINS CONFIDENTIAL INFORMATION.
RESPONSIBILITY OF THE RECIPIENT.
WHEN NO LONGER NEEDED, DESTROY
BY BURNING OR SHREDDING

CT-JL-92-06
MARCH, 1990
COPY No. 17

Distribution on last page.

JACKSON LABORATORY
RESEARCH & DEVELOPMENT, TECHNICAL REPORT
CHEMICALS AND PIGMENTS DEPARTMENT
E. I. DU PONT DE NEMOURS & COMPANY

MAXIMUM LOW PVC TIO2 HIDING POWER EFFECT OF PRIMARY PARTICLE SIZE AND AGGREGATION

Work Done By:	D. P. Fields, SVR Mastrangelo
Report Written By:	D. P. Fields D.P. Fields
Approved By:	M. E. Lewis
Previous Related Reports:	CP-JL-90-3, CT-JL-91-16
Project Code:	7053-115129
Type Technical Work:	RE
Period Covered:	January 1984 - December 1988 (Part Time)
Notebook Numbers:	E32956, E39389
Personnel:	R . G. Fernald, Professor John Vander Sande, MIT

Abstract

Commercial TiO2 pigment hiding power potential has been reported to be ~65% of theoretical. Our primary particle size and aggregation experimental programs (low PVC) suggest that our best commercial pigments scatter at about 80% of theoretical. Hiding power losses are ~15% for primary particle size distribution and ~5% for primary particle aggregation.

I. INTRODUCTION

Hiding power is the single most important attribute of TiO2 pigment. If this is true -

A. What is the ultimate hiding power of TiO2? and

B. How do commercial pigments (duPont and competitive) compare with the above?

In order to measure these hiding power losses we need to understand the hiding power theory. The low pigment volume concentration system was selected for study as it represents the simplest system from the standpoint of optical theory and modelling. The major TiO2 hiding power losses in low PVC systems are due to deviation from monosize and monodisperse particles.

II. OBJECTIVES

Optical theory predicts ~15% hiding power improvement for optimum monosize TiO2 compared to commercial pigment particle size distributions. Our program is to show experimentally (for the first time) that the theory is correct and ~15% hiding power potential does exist.

TiO2 aggregates are formed in the oxidation process by collision of primary particles. Hiding power is lost as multiple particle clumps are formed due to inefficient spacing of the TiO2 particles. Past work has suggested that hiding power could be improved ~15% in low PVC systems by decreasing aggregate size from 4 to 1 particles/clump. Our program is to determine the actual aggregation of the TiO2 pigment to accurately assess the potential hiding power improvement.

Optical theory predicts TiO2 scattering values significantly higher than our experimentally measured S values (corrected for width of distribution and aggregation). Investigate the optical theory and suggest reasons for these differences.

III. SUMMARY AND CONCLUSIONS

Primary Particle Size Measurements - Monosize

- o DuPont theoretical scattering calculations predict hiding power can be increased ~15% by narrowing the primary particle size distribution to monosize TiO2.
- o DuPont experimental classification program has demonstrated ~5% increased hiding power by narrowing the primary particle size distribution at constant mean diameter.
- o Extrapolation of experimental program geometric standard deviation data predict monosize TiO2 hiding power can be increased ~15%; thus, the experimental work is in good agreement with the theoretical calculations.
- o Work is currently directed towards narrowing the width of distribution in the oxidation process.

Aggregation Measurements - Monodispersion

- o Apparent aggregation is 2-4 particles/clump (end-use)
- o Actual TiO2 aggregation is ~1.6 particles/clump ~1.6 particles/clump represents ~5% hiding power loss or ~1/3 of calculated theoretical hiding power - the remainder HP (7-10%) is due to TiO2 crowding.
- o Aggregate hiding power variables
  - oo End-use system (random or charge stabilized)
  - oo Pigment volume concentration
  - oo TiO2 pigment (type and grinding energy)

TiO2 Scattering Review

The major difference between TiO2 scattering values by optical theory and corrected experimental measurements may be in our measurement procedures. Data are presented and discussed.

IV. PATENT STATUS

No plans to apply for patent coverage

V. FUTURE PROGRAMS

None by the author - Program suggestions can be found in the discussion

VI. PUBLICATION STATUS

No plans to publish

VII. SPECIAL SAFETY CONSIDERATIONS

No special problems outside of normal laboratory hazards

VIII. ENVIRONMENTAL CONSIDERATIONS

No special problems

IX. ACKNOWLEDGMENTS

This was a part time program conducted over a five year period. Many discussions, suggestions, and constructive criticisms were offered by the R&D community. Hopefully most of these have been incorporated into the report.

TABLE OF CONTENTS

X. Discussion

A. Introduction

The greatest physical attribute of pigmentary titanium dioxide is its ability to scatter light and provide end-use product opacity/hiding power. This TiO2 scattering is dependent upon a number of physical variables including:

- o index of refraction (pigment and vehicle)
- o wavelength of light
- o particle size and distribution
- o particle shape
- o aggregation
- o dispersion
- o impurities (color)
- o end-use formulation - PVC, TiO2 loading, etc.

For most of our studies, the majority of these variables are constant; thus, we can concentrate on the pigment variables - primary particle size, aggregation, etc.

Let's start by defining some terms - you may personally use other definitions but this report is based upon the following definitions.

Primary particle - smallest discrete particle or building block - we will see later that this does include both growth and collision twins

Aggregate - clump of primary particles which is difficult to impossible to break up - once you have formed an aggregate you are stuck with it

Agglomerate - clump of lightly bonded aggregates which is shear sensitive - the grinding operation in the TiO2 process is primarily a deagglomeration process

We do know some of the pigmentary properties are controlled or influenced by particle size. Figure DPF-1 presents a particle size distribution of R-900 08 code (high gloss) product showing general quality parameters as a function of particle size. The distribution is an aggregate distribution for the most part. For comparison let's look at the three most important distributions for oxidation base TiO2 -primary particles, aggregates, and agglomerates (Figure DPF-2). The oxidation base is highly agglomerated as it is produced. High shear wet or dry grinding will produce an aggregate distribution with a median diameter of approximately 0.3-0.4 micrometers. The primary particle size distribution is measured by transmission electron microscopy with a median diameter of about 0.16 to 0.24 micrometers. Oxidation base slurry is really an agglomerate distribution composed of aggregates which in turn are composed of primary particles. The mean size of this agglomeration distribution has varied widely among the oxidation lines. (Ref. 1, 2, 3)

Figure DPF-3 presents some additional particle terminology. Primary particles range is shape as well as size. Some primary particles result from growth or collision twins such as example A. Bonding of primary particles to form aggregates also occurs. Example B shows typical sintered and chemically bonded primary particles. Obviously there is a fair amount of confusion between A and B as the particles overlap. We have used a tilting stage on the electron microscope to make these distinctions. To make life even tougher -most aggregates are composed of more than two primary particles. We try to deal with this by resolving how many scattering centers we have present; that is, how many primary particles are actually in the aggregate.
Table DPF-1 presents common particle size measurement methods for primary particles, aggregates, and agglomerates.

A number of marketing needs originate in the oxidation area and are particle size related. A list of these needs is presented in Table DPF-2. The major needs are higher CBU (smaller size), increased hiding power, and improved gloss. As the individual oxidation lines are slightly different from each other (Table DPF-3), a single solution to these problems in the oxidation area does not exist. A more practical solution is to understand the basic fundamentals of each problem and then work back through the process.

What is the ultimate hiding power of TiO2? Theoretical studies twenty-five years ago suggested that commercial TiO2 pigment has ~30-40% hiding power potential in low pigment

volume concentration systems (enamel, plastics, etc.). (Ref.4) The improved hiding power is split about evenly between:

- o Monodisperse TiO2 (no aggregation) and
- o Monosize TiO2 (all optimum size particles)

We have worked part time over the last few years trying to better understand not only what is theoretically possible but also what is commercially possible; that is, how can we improve our understanding and also demonstrate experimentally improved hiding power in low pigment volume applications.

B. Primary TiO2 Particles

1. Background

Let's first consider the role of primary particles. Table DPF-4 and 5 present some TiO2 primary particle facts and observations.

Figure DPF-4 presents Bill Ross' chart showing relative hiding power as a function of wavelength, and TiO2 primary particle size. An optimum particle size exists for maximum hiding power; that is, all particles produced smaller or larger than this optimum size will decrease the hiding power. Small particles scatter more efficiently in the blue; this is the basis for our CBU test which measures the blue to red ratio and predicts particle size. We are primarily interested in the green curve as the green response more nearly duplicates what the eye sees. Approximately 0.21 micrometers diameter rutile particles are about optimum for maximum HP. A relationship exists between CBU and primary particle size diameter as explained above. The best fit for primary particle size as measured by transmission electron microscopy and CBU for oxidation bases is presented in Figure DPF-5.

Approximately ~15% higher hiding power has been calculated for optimum monosize TiO2 particles (W. D. Ross - Ref. 3). No experimental verification of this higher hiding power for more narrow distributions was ever demonstrated. Figure DPF-6 presents graphically the salient points on Ross' chart Figure DPF-4. What we have is a distribution of primary particles and what we want is for all the particles to be the same size and optimum

diameter. The 15% HP improvement is the theoretical improvement and is not necessarily attainable. Part of our program is to define what is possible and/or reasonable.

The demonstration of significantly higher hiding power by decreasing the primary particle size width of distribution is necessary to justify R&D development efforts in this area but --- production of monosize TiO2 particles is thought to range from difficult to impossible from our current TiO2 agglomeration process. The next two charts (Figures DPF-7 and 8) show the difficulty in the production of monosize TiO2 particles. The first figure on DPF-7 shows that commercial pigment is not monosize and presents distributions for three different mean particle size pigments. Increasing particle diameter increases the width of distribution. This is characteristic of an agglomeration process. The second figure on DPF-7 shows that the width of distribution is commonly expressed as the geometric standard deviation and is calculated by either the ratio of d50/d16 or d84/d50. Figure DPF-8 presents geometric standard deviation as a function of primary particle size for a group of duPont and competitive pigments, both chloride and sulfate processes. Regression analysis shows a linear best fit. Figure DPF-8 also presents an extrapolated version of the same plot. This work predicts a geometric standard deviation of ~1.0 at 0 micrometers. A GSD of 1.0 means monosize particles. This suggests that any finite size particle will exhibit a distribution of particles and the width of distribution will increase as the diameter increases. Significant differences in width of distribution at a given diameter were observed suggesting that some level of hiding power improvement might be attainable.

2. Experimental Program

A laboratory program was undertaken to demonstrate higher hiding power by narrowing the particle size distributions with centrifugal sedimentation techniques. Vinyl film testing was selected for measurement due to its low TiO2 sample end-use requirements. The normal test loading was further reduced by 80%. Table DPF-6 presents early lab tests to show that vinyl TS could be used to measure hiding power. A weight reduction of TiO2 in the formulation showed a comparable loss in vinyl TS. A reduction of TiO2 in the standard formulation yielded

similar relative TS values to the control.

R-101 was selected for study due to its superior performance in vinyl film. Since we were primarily interested in single particle size width of distribution effects, the R-101 was remicronized in the laboratory at 6 S/P to minimize aggregate coarse tail. The vinyl TS increased for 108 to 114. This is our actual starting point from which to measure increased hiding power as a function of decreased width of distribution.

Initial centrifugation efforts produced smaller and possibly more narrow distributions. Highspot hiding power work showed no significant improvement for the fine fractions. We believe we replaced the inefficient oversize particles with inefficient undersize particles. Attempts to remove the inefficient undersize particles (<0.2 micrometers) by sedimentation field flow fractionation were unsuccessful.

Multiple cut centrifugation was conducted to develop hiding power data as a function of particle size and width of distribution. If centrifugation is successful in making primary particle size cuts from a finished R-101 product, then by definition the width of distribution of the fractions would be more narrow than the starting material. Vinyl TS data are presented for the multiple cut centrifugation work as a function of CBU in Figure DPF-9. The optimum CBU appears to be ~16.5 which is in good agreement with past work. Hiding power increased as the TiO2 size increased until a maximum was reached; then hiding power decreased as particle size further increased. This is the familiar HP chart that Bill Ross developed from theoretical Mie scattering (Figure DPF-4) only now developed from experimental data. The maximum HP demonstrated was 119 TS which is 5% higher than our double micronized starting material. While the hiding power improvement is attributed to a more narrow distribution, centrifuge fractions were submitted to MIT for primary particle size distributions (TEM).

Additional centrifuge fractionation work was conducted using a centrifuged fraction as the starting material. No additional hiding power improvement was demonstrated. Evidently the centrifuge classification procedure had reached its limit. Another technique for varying the width of distribution at constant particle size (CBU) is by blending small and large particle size pigments.

In this case the blending of small and large particle size commercial products will have a wider particle size distribution than the commercial TIO2 product with the equivalent mean size. The low PVC hiding power will also be poorer due to the wider width of distribution -see Figure DPF-10.

MIT projected area measurements were converted to diameters and then means, medians, GSD, etc. calculated. A plot of low PVC hiding power vs. geometric standard deviation is presented in Figure DPF-11. All samples plotted have diameters ranging from 0.155 to 0.165 micrometers. To increase the range of GSD's we included a sample (equivalent diameter) that was prepared by blending high and low CBU products (large width of distribution - 1.730. As vinyl TS of the plant R-101 was increased 6% by removal of aggregates/agglomerates (double micronizing), the blended plant product was adjusted accordingly (104 to 110%). Figure DPF-12 presents extrapolation work as well as a summary.

Approximately 5% increased hiding power has been demonstrated at equal median particle size by centrifugation. Centrifuge techniques narrowed the primary particle size distribution. Extrapolation of the linear best fit line predicts that ~15% high hiding power can be attained with a monosize TiO2 pigment (GSD = 1.0). This work is in excellent agreement with Bill Ross' early scattering calculations.

Table DPF-7 presents additional data from the centrifuge series. Noteworthy items include:

- o multiple centrifugation produced samples with CBU's ranging from ~12 to 22 from a feed CBU of 14
- o TEM aggregation measurements show starting material and centrifuge fractions were equal

A summary of this primary particle size work follows:

- o DuPont theoretical scattering calculations predict hiding power can be increased ~15% by narrowing the primary particle size distribution to monosize TiO2.
- o DuPont experimental classification program has

demonstrated ~5% increased hiding power by narrowing the primary particle size distribution at constant mean diameter.

- o Extrapolation of experimental program geometric standard deviation data predict monosize TiO2 hiding power can be increased ~15%; thus, the experimental work is in good agreement with the theoretical calculations.

- o Work is currently directed towards narrowing the width of distribution in the oxidation process.

3. Primary TiO2 Particle Size Measurement

Historic TiO2 measurements yield primary particle size distributions with increasing width as primary particle size increases. These distributions generate excessive specific surface area compared to actual sample measurements; thus, the actual primary particle size must be larger. This decreased surface area and increased particle size can occur via fusion and sintering. Other aggregation mechanisms do occur such as small neck sintering and chemical bonding but these mechanisms would not greatly affect the specific surface area.

Enamel and plastic hiding power (low PVC systems) are controlled by primary particle size, distribution width, and aggregation. We need to develop additional information before we can accurately predict future hiding power improvements and potential. A good first effort would be to measure primary particle size distributions and determine whether the sintering process is constant as a function of CBU and oxidation line. Of equal importance would be to measure the best competitive products for comparison. It is possible that all oxidation products are similar and no short term hiding power improvements are predicted/possible. If this is true we need to know it. It is also possible that we have historically optimized the current chloride process for low PVC hiding power and if we do learn to inhibit fusion/aggregation we will have to produce larger particles for optimum scattering. Experimental evidence for measurement of the sintered particle size distributions does exist (Figure DPF-13). This work by Buchanan, Hench, and Fields shows the classic TEM primary particle size distributions (CRB count) and the sintered

"scattering center" counts by Hench. With the development of smarter image analysis hardware and software, these counting objectives become more realistic.

C. Aggregation

1. Background

TiO2 aggregates are formed in the oxidation process by collision of the primary particles. Bonding is controlled by TiO2 surface chemistry as well as the individual oxidation line conditions. The effect of aggregation on product quality is primarily associated with TiO2 scattering (low PVC hiding power, CBU, etc.) although the coarse tail does effect gloss in both emulsion and solvent systems. Past theoretical and experimental work by WD Ross and RJ Bruehlman (Ref. 5, 6) suggested low PVC hiding power could be improved ~15% by reducing TiO2 aggregate size from ~4 to 1 particles/clump (monodispersion) - see Figure DPF-14. Our program was to determine the actual aggregation of our oxidation bases and products to accurately assess the potential hiding power improvement.

Bill Ross made theoretical calculations on the effect of multiple particle attachment (Ref. 5). He found a hiding power loss for 0.2 micrometer particles of ~4% per particle attachment or ~12% for a 4 particle/clump aggregate -(Table DPF-8). While these calculations were for a linear geometry, Ross stated that they would also be true for other common geometries. This hiding power loss occurs due to particle to particle interference. For maximum scattering we desire particle separations of ~1/4 wavelength or about 1/2 the diameter of the TiO2 particles; thus, we do not want the TiO2 crowded together. Ross' work also showed that aggregation played a minor scattering role as the TiO2 diameter increased. At 0.3 micrometers diameter aggregation had essentially no effect on scattering.

Experimental work by Hennessy and Paulson in 1968 showed a relationship of hiding power with reduction of mean agglomerate size - Figure DPF-15. The size reduction was controlled by grinding. I would interpret this minimum size by grinding to represent sample aggregate size. Extrapolation of aggregate size to mean crystal diameter would represent a reduction in aggregation; thus, the

hiding power improvement is estimated at ~15%. The major problem with this rationale is that most particle size measurement techniques are relative and no two techniques should be used on the same data plot.

A summary chart on aggregation types and measurement techniques is presented on Table DPF-9. A new instrument has been developed for measurement of TiO2 aggregate size - the X-ray scanning disc centrifuge. A comprehensive report on this instrument was issued (Ref. 7) by the author. Our evaluation work suggests that fine particle size measurement (both accuracy and precision) is improved vs. gravitational equipment such as the Sedigraph. A direct comparison of XSDC and Sedigraph particle size distributions for R-900 is shown in Figure DPF-16. The XSDC produces a smaller and more narrow distribution than does the Sedigraph. The number of 0.2 micrometer primary particles possible in the median equivalent spherical diameter of R-900 is 13 particles/clump for the Sedigraph and 4 particles/clump for the XSDC. The equivalent spherical diameter from the XSDC is much more realistic than the Sedigraph when compared to transmission electron microscopy studies and past historical aggregation measurements. Figure DPF-17 shows these relative particle size distributions.

2. Experimental Program

a. DuPont/MIT Program

Much aggregation counting work has been conducted by Professor John Vander Sande, MIT and us through the years. Figure DPF-18 presents a flow chart of how the aggregate measurements were made. Figure DPF-19 and 20 show relationships between researchers and methods. While differences do exist, these techniques must be considered relative rather than absolute. In an effort to document this aggregate counting work, typical oxidation line counts and oxidation line ranking are presented in Figure DPF-21 and Tables DPF-10 and 11. As can be seen, no measurements have been made for the more recent deagglomerated fin flue oxidation line developments.

Aggregation among oxidation lines was originally thought to be constant with aggregate a function of primary size (Sedigraph median size equal to 2.25X primary particle size). While this is still probably true within an

oxidation line, significant aggregation differences do exist at constant CBU among the various lines. The best lines were the high pressure Antioch and JVII lines and the worst line was EMII. EMII appeared not only larger but also much more highly sintered. The addition of co-ox. P205 significantly reduced EMII aggregation.

The examination of both primary particle size and aggregation suggests that CBU is a function of both primary and aggregate size. At constant CBU, the oxidation lines with larger aggregates will have smaller primary particles while the least aggregated lines will have larger primary particles. There is little past evidence to show CBU is a function of primary particle size and aggregate size within a single oxidation line. This may mean that the aggregate bond strength is too great to decrease aggregation by conventional grinding. The one possible exception is Mike Baloga's recent work on the media mill where significant CBU increases have been noted -ostensibly from reduced aggregation.

Table DPF-12 presents typical oxidation line and finished product measurements while Table DPF-13 presents all of our aggregation measurements made during these investigations. A few observations -Table DPF-14 shows that oxidation lines with more sinter bonding have larger aggregates. It should also follow that aggregate reduction should be more difficult due to sinter bonding. Table DPF-15 shows the effect of surface chemistry (co-ox. Al203) on aggregation. Aggregate size is constant even though the bond mechanism changes from chemical to sinter bridges. This suggests that aggregation may occur independent of bond type or in other words mother nature strikes again. Table DPF-16 and Figure DPF-22 show the aggregation changes due to sandmilling and micronizing. Sandmilling reduces aggregate size (as well as micronizing) and when combined with micronizing appears to minimize the oxidation base aggregate differences.

An attempt was made to correlate MIT aggregate counts with Sedigraph clump size data. Table DPF-17 presents aggregate means and medians by both number and weight for a progression of samples through the TiO2 process and typical end-uses. The major observations are:

- o aggregation is a coarse tail problem rather than a primary aggregation distribution problem (low median by number)

- o End-use systems vary in aggregation (same pigment) - possible reasons include system shear, end-use surface compatibility and PVC (TiO_2 crowding)

Seven competitive R-900 products were evaluated vs. DeLisle, Johnsonville, and Antioch R-900 code 08 products. DuPont aggregate counts show the best competitive R-900 products were equal to the best duPont products (Table DPF-18).

A series of variable energy micronizing tests were conducted on JVI R-101DD (Table DPF-19). Aggregate measurements show no significant differences for the micronized products. This suggests grinding harder does not reduce aggregation (TEM). On the other hand vinyl tinting strength does improve as grinding energy increases and has been correlated to the reduction in oversize coarse fraction (%>0.6 micrometers) - Table DPF-20. If agglomerate/aggregate coarse tail is variable and aggregate measurements do not see it, it may be that coarse tail clumps >0.6 micrometers are too large for the TEM mounting process. This would also suggest that the coarse tail is possibly a second distribution (bimodal) as the aggregation data are not at all influenced by the coarse tail.

b. End-Use System Aggregation

If aggregation is a primary player in determining end-use hiding power, then it becomes obvious that we must resolve how may particles/clump our pigments contain in the end-use. Historic counts indicate 4 particles/clump while our work suggests 2-4 particles/clump. Initial end-use evaluations are presented in Table DPF-21. Observations:

- o product quality (gloss) plays a minor role on aggregation unless it is poor
- o significant aggregation differences are observed depending upon pigment volume concentration - aggregation increases as PVC increases

It is logical that as the concentration of TiO_2 increases that the apparent aggregation increases due to TiO_2 crowding. The implications of this work are that TiO_2 aggregate size is smaller than measured in past studies

and may be only 1-2 particles/aggregate. Potential hiding power improvement from a strict aggregate size reduction would appear to be less also. Additional work is required to substantiate this position.

Table DPF-22 presents a graphic summary of our aggregation work thus far. The five oxidation lines investigated are different and range from 3-6 particles/clump. Following wet and dry finishing, the aggregate size decreases about 30% to 2-4 particles/clump. The ranking remains unchanged; that is, the larger aggregate bases exhibit larger aggregate finished products. The main area of concern is not the dry product but the end-use system as it is here where the TiO2 scattering is measured. End-uses studied ranged from about 1.5 to 3 particles/clump (different systems). Limited work suggests that PVC may play a major role in measured aggregation.

c. Variable PVC End-Use Investigation

A computer program was written to produce random particles in two dimensions as a function of time. The pigment volume concentration was calculated from the number of particles, particle diameter, and X-Y area. Computer down loads are presented in Figure DPF-23. Aggregation was measured using similar techniques to those used for TiO2 electron micrographs. The increased particle attachment can be readily observed as PVC increases (TiO2 crowding). We label this aggregation as "perceived" aggregation as all computer simulated particles were single particles (monodisperse). A plot of mean aggregate size vs. PVC is shown on Figure DPF-24. This work suggests that a major part of our end-use aggregation could be "perceived" (TiO2 crowding) and not due to the actual pigment aggregation.

The next step to resolve this issue was to investigate the various end-uses at variable PVC TiO2 additions. Even though a given end-use was designed for a specific PVC, our work would look at a range of PVC's. The vinyl end-use system results are presented in Figure DPF-25. Aggregation increased with concentration. Similar slopes (computer simulation and vinyl system) suggest the vinyl system is randomly aggregated. This is reasonable as the vinyl test is a high shear viscous fast freeze system. The actual aggregate size of the pigment is the aggregation at 0 PVC or approximately 1.6

particles/clump. The hiding power loss for this aggregation would be less than 5%.

Figure DPF-26 presents similar end-use aggregate measurements for an automotive enamel. The actual pigment aggregation is again about 1.6 particles/clump. The higher aggregate sizes measured previously in the standard auto formulation were due to TiO2 crowding. The difference in slope between the computer simulation and the auto enamel suggests that the auto enamel is not randomly aggregated but the system is probably charge stabilized; that is, TiO2 crowding has been minimized.

The third system, emulsion enamel, is presented in Figure DPF-27. This time the TiO2 PVC is significantly higher - around 2.5 particles/clump. We believe that this increase is probably due to poor paint grinding (TiO2 dispersion) as the industry uses a Cowles grinder rather than sandmills. A similar slope to the automotive enamel is observed. This suggests that the emulsion paint is also charge stabilized.

A summary of our low PVC aggregation studies follow:

- o Apparent aggregation is 2-4 particles/clump
- o Actual aggregation is ~1.6 particles/clump - 1.6 particles/clump represents ~5% HP loss or ~1/3 of theoretical hiding power calculated -remainder (7-10%) is due to TiO2 crowding
- o Hiding power variables
  - oo End-use system (random or charge stabilized)
  - oo Pigment volume concentration
  - oo TiO2 pigment (type and grinding energy)

d. Aggregate Reduction by Grinding

We discussed earlier our inability to reduce aggregate size by variable energy micronizing (fluid energy mill). Aggregate grinding might occur if the grind time was increased to some unreasonable level. Ball milling was selected as it is used in the sulfate process to grind TiO2 agglomerates/aggregates. Figures DPF-28 and 29

present ball milling particle size data for both an oxidation base and a finished R-900 product. Significant particle size reduction occurred in 12 weeks and it appeared only a matter of time before the aggregate structure was size reduced to that of single crystals. Aggregate size reduction appeared too uniform and prompted samples for analytical tests. After 16 weeks of ballmilling the oxidation base sample contained 38% SiO_2 and Al_2O_3. The size reduction of the grinding media was the real cause of the observed oxidation base particle size reduction. This would also have to be considered as a potential problem for sand/media milling experiments.

e. Improved Aggregate Size Measurements

Oxidation base agglomerate and aggregate sizes are currently measured in aqueous dispersions on the Sedigraph/XSDC. Agglomerate size is measured on the "as is" (no shear sample), while aggregate size is measured following ultrasonic grinding. "Aggregate" size has been previously defined as a multi-particle structure which is difficult to impossible to break apart. For convenience, this structure has been further defined as the TiO_2 particle clump remaining following rigorous steam micronizing. The oxidation base mean aggregate size (ultrasonic grinding) is always larger than the post micronizer aggregate size due to lower grinding energy. This difference is due to the presence of hard agglomerates that are not broken down in ultrasonic grinding, but are reduced by micronizing. The aggregate differences are oxidation line dependent; that is, the more agglomerated oxidation lines exhibit the largest aggregate size (constant CBU) following ultrasonic grinding.

The measurement of oxidation base "true aggregate" size requires development of a high energy laboratory mill that simulates micronizer grind conditions. In addition to mean aggregate size, this mill would also be useful for measurement of the oxidation base coarse tail that controls both alkyd and emulsion gloss.

A vibrating mill employing small glass spheres has been investigated (dry impact). This mill was originally developed by Tioxide for the preparation of TiO_2 samples for electron microscopy. EMII, JVI, and JVII oxidation bases were milled using a 20 second grind time. These data are shown in Figures DPF-30, 31 and 32. vs.

Sedigraph distributions for both oxidation base and finished R-900 products at three micronizer grind intensities (S/P = 2, 4, and 6). In each case, the vibrating mill overground the oxidation base samples. This is the first time we have observed a grind technique superior to fluid energy milling.

Grind time was investigated from 10 to 80 seconds. These data (JVI R-101 base) are shown in Figure DPF-33. It would appear that a grind time could be selected to match a given coarse tail or mean aggregate size. Whether this will be constant for all the oxidation bases is not known. A 10-second mill time was selected for evaluation of EMII, DEL, and JVII bases. The oxidation base coarse tails are plotted vs. their respective coarse tails for laboratory R-900 (S/P = 6) products (Figure DPF-34). A 10-second grind time appears to be getting close to matching the R-900 micronized product coarse tails. The aggregate mean sizes for the vibrating mill samples (oxidation bases) were identical to the lab R-900 (S/P = 6) product samples. We appear to have a laboratory grind technique capable of measuring both the finished product aggregate mean size and coarse tail starting with oxidation base samples.

D. Agglomeration

TiO2 agglomeration has been extensively addressed in our past oxidation base studies but a few words are in order. TiO2 agglomeration forms in the oxidation base and continues through wet and dry finishing. TiO2 agglomeration in oxidation is currently not totally inhibitable but is certainly reducible by grinding in finishing. It is true that flocculation, a form of agglomeration, can be a severe end-use problem. Flocculation is formed from particles already size reduced thus flocculation is concerned with TiO2 stabilization rather than size reduction. Our goal is to size reduce or remove all agglomerates as the agglomerates are equally as bad as aggregates in the end-use. Figure DPF-35 presents the effect of finished product coarse tail (agglomerates) on film properties (gloss). Figure DPF-36 overlays the oxidation base agglomerate distribution onto the finished product aggregate distribution. The difference in these distributions (marked) represents the agglomerate fraction in the oxidation base that must be inhibited, removed, or size reduced. We have shown in our previous oxidation base studies that agglomeration is reduced by increasing CBU and decreasing oxidation base turbulence. See Figures DPF-37 and 38.

Sandmilling is also a viable candidate for oxidation base deagglomeration (Ref. 8). Representative data is presented in Table DPF-23.

To produce high quality finished products for today's markets, we must reduce our oxidation base agglomeration. Recent studies suggest that our current oxidation base target is:

25% >0.6 micrometer coarse tail maximum at
12.5 CBU and 20+ tons/hour

A TiO2 agglomeration summary follows:

- o Finished product coarse tail controls end-use performance [film properties (gloss) and HP (vinyl TS)]
- o Finished product coarse tail is a function of oxidation base coarse tail
- o The origin of the coarse tail is unknown - it may be the coarse tail of the growth distribution or a separate distribution such as wall scale
- o Oxidation base/finished product coarse tail is reduced by:
  - oo increased CBU
  - oo decreased agglomeration (turbulence, etc.)
  - oo surface chemistry (coox. P or Si)

E. TiO2 Scattering Review

The greatest physical attribute of pigmentary titanium dioxide is its ability to scatter light and provide end-use product opacity and hiding power. This TiO2 scattering is dependent upon a number of variables including:

- o Index of refractions
- o Wavelength of illumination
- o TiO2 particle size

While we cannot do much to alter the first two variables, we need to understand their basic relationships. Lets's start with the index of refraction.

TiO2 hiding power is proportional to M^2 where (Ref. 9)

M = ([Np/Nv]^2 - 1)/([Np/Nv]^2 + 2) Lorentz-Lorenz Expression

and Np = pigment refractive index
Nv = vehicle refractive index

An approximation for TiO2 hiding power is proportional to

0.16(Np-Nv)]^2

This approximation formula is limited to Nv = ~1.5 and Np = 1.5 to 2.75 (low PVC applications)

Optimum TiO2 particle size can be estimated from the above relationships.

d(optimum) = wavelength/([2]^(1/2)*Nv*HP*Pi

The above refractive index relationships were programed in Quick-Basic. The program INDXREF1.BAS and sample output are appended (ATT - 1, 2, & 3). Hiding power (arbitrary scale) for both Anatase and Rutile TiO2 as a function of vehicle refractive index is presented in Figure DPF-39. TiO2 scattering (hiding power) increases as the vehicle refractive index decreases. Rutile has approximately 25% more hiding power than Anatase at 1.5 vehicle refractive index. Figures DPF-40 and 41 present plots of Rutile and Anatase hiding power (both calculated and approximated from above equations) at variable vehicle refractive index. While not identical, both relationships would appear to be fine for calculating relative scattering differences.

A plot of optimum diameter for Rutile TiO2 at variable vehicle refractive index is presented in Figure DPF-42. Optimum diameters for Rutile TiO2 at 1.5 vehicle refractive index are ~0.16, 0.18, and 0.20 for blue, green, and red wavelengths. Figure DPF-43 compares Rutile and Anatase (green wavelength). Ross Mie scattering calculations do not seem to be in agreement (Figure DPF-44); in fact, Ross's work does not show a diameter dependence on vehicle refractive index.

We have very little input into these hiding power variables as end-use system design determines the vehicle refractive index and we do not know how to significantly increase the refractive index of TiO2 above that of Rutile. The refractive index is also dependent upon the wavelength of illumination and on crystal axis orientation for anisotropic pigments. The use of average

refractive index vs. ordinary and extra-ordinary refractive indices for Rutile is acceptable for scattering calculations. Refractive index is higher for the short wavelengths (blue) than for the longer wavelengths (red).

WD Ross calculated Mie scattering relationships as a function of TiO2 particle size and wavelength (blue, green, and red) (Ref-10). This work was programed for convenience in WDR1SCAT.BAS and PRTSCAT1.BAS. Sample output from these two programs is appended. A plot of these relationships is presented in Figure DPF-45. This is the familiar Ross chart presented earlier as Figure DPF-4.

The undertone (B/R) can be calculated from Ross' work. Figures DPF-46 and 47 present undertone as a function of TiO2 particle size diameter. This relationship is pretty much linear over the pigmentary size range (0.16 to 0.24 micrometers). This undertone relationship is for monosize TiO2 particles at low pigment volume concentration. Let's compare this response with actual experimental reflectance measurements. Figure DPF-48 presents the primary particle size-CBU relationship for oxidation bases (TEM counting -mean data). This relationship is for commercial TiO2 not monosize TiO2. We next determined the relationship between the undertone (B/R) and CBU for the TiO2 CBU test in silicone oil (Figure DPF-49). Figure DPF-50 uses these above relationships and presents a plot of undertone vs. particle diameter for the experimental data. This plot looks identical (similar slope) to the original plot (DPF-47) from Ross' Mie calculations. The difference in absolute undertone might be explained by the addition of carbon black in the experimental CBU test or due to the aggregation in the commercial pigments. The above is reasonable evidence that the CBU test is measuring primary particle size differences in oxidation bases.

We are next interested in determining the Ross Mie scattering for Rutile TiO2 as a function of vehicle refractive index and primary particle size distribution. This work was reported by Ross in CP-JL-87-08. Figure DPF-51 presents monosize TiO2 scattering as a function of diameter for a single vehicle refractive index. Figure DPF-52 presents similar data for different widths of distribution. The absolute decrease in TiO2 scattering is readily observed as the width of the primary particle size distribution increases (monosize to commercial distributions). At optimum particle size this difference has been calculated to be ~15% hiding power using actual TEM particle size data.

Monosize Rutile TiO2 scattering is presented in Figure DPF-53 as a function of particle diameter for a number of vehicle refractive indices (Ross -CP-JL-87-08). Figure DPF-54 presents TiO2

scattering as a function of vehicle refractive index. These data were obtained from Figure DPF-53. Additional Ross data were found in WP-ESI-75-2 report (Figure DPF-55) and converted to Figure DPF-56. Scattering data from Figures DPF-54 and 56 were combined and are presented in Figure DPF-57. Why spend so much time determining the theoretical TiO2 S values as a function of vehicle refractive index? WD Ross proposed that the observed scattering loss at high pigment volume concentration (TiO2 crowding) might simply be due to the change in the paint film refractive index. This reasoning also would explain the increase in scattering observed above the critical PVC (decreased paint film refractive index due to entraped air). The paint film refractive index is a function of both the vehicle refractive and the pigment refractive index thus increases at high TiO2 loadings. Again these S value calculations are for monosize TiO2. The calculated loss in relative hiding power is about 15% comparing monosize particles with actual commercial pigment particle size data (TEM data).

Ross and others measured paint film refractive index for Rutile TiO2 as a function of pigment volume concentration (Figure DPF-58) (Ref. 10). The Ross/Armstrong and Kawabata data appear reasonably uniform. My estimate of the line of best fit is noted on Figure DPF-58 and replotted in Figure DPF-59. We can now convert pigment volume concentration to medium refractive index and use the medium refractive index in the Mie scattering equations to predict TiO2 scattering at higher PVC's. Figure DPF-60 presents calculated TiO2 scattering as a function of PVC for monosize Rutile TiO2 particles as a function of particle diameter. This curve looks similar to the experimental TiO2 S curve determined in coatings. Figure DPF-61 presents Figure DPF-60 data at 0.2 micrometers particle diameter in addition to experimental data developed by Ross and Bruehlman. The slopes appear to be right in line but the absolute S values do not; the measured S values are significantly lower than calculated.

Can we explain these differences? Monosize TiO2 scatters ~15% greater than a commercial TiO2 product. The observed scattering difference is significantly larger than 15%. The next biggest influence on scattering is probably TiO2 aggregation. Figure DPF-62 presents Figure DPF-61 with the addition of aggregated commercial TiO2 pigments at 2, 3, and 4 particles/clump. Scattering was reduced 4% for each additional particle/clump in keeping with Bill Ross' aggregate calculations. The theoretical scattering is still too high even when aggregated to 4 particles/clump. This means that the experimental scattering measurements are not as high as they should be (or the Mie scattering calculations are too high). A number of reasons suggest that the experimental data are probably too low. Our day

to day hiding power measurements are low because we measure specular green reflectance instead of diffuse reflectance and make no corrections for sub-surface reflection. The Ross data set did measure diffuse reflectance and transmittance but neglected sub-surface reflection.

Our dilemma is summarized on Table DPF-24. Ross and Bruehlman measured commercial TiO2 pigments at 0.52 M^2/GM with a vehicle refractive index of 1.514 (low pigment volume concentration). The calculated Mie scattering S value for monosize TiO2 is 0.785 M^2/GM. The calculated loss in S value for the commercial pigment is 0.265 which suggests that scattering can be increased ~ 51% ([0.265/0.52]*100) above current levels or ~ 34% ([0.265/0.785]*100 of theoretical. We feel confident that the loss in hiding power for commercial products is ~15% for width of primary particle size distribution and ~5% loss for aggregation - thus we have an impasse. This coupled with the observation that we have not significantly increased low PVC hiding power in coatings in the last 25 years suggests that a problem exists in our measurement techniques.

Sophisticated TiO2 S value determinations were made by Cairns and Spooner in the 1960's at Chestnut Run (Ref. 11). This work was part of their color matching program. Their work showed a significantly higher experimental S value than those derived today. The work utilized mylar drawdowns for diffuse reflectance and transmittance measurements as well as corrections for sub-surface reflection. This work is presented on Table DPF-25. Cairns and Spooner measured the TiO2 S value at 0.70 for a 1.48 vehicle refractive index (low pigment volume concentration). The calculated Mie scattering S value was 0.885. The difference in S values is ~21% (loss from theoretical) and compares favorably with our estimated S value losses for width of distribution and aggregation (~20%). If these data are correct then the obvious conclusion is that there is no significant HP loss in today's commercial pigments that has not been accounted for in low PVC systems.

Where do we go from here? Current TiO2 products should be measured at low PVC by the methods of Cairns and Spooner and then compared to Mie scattering S value calculations. If we can duplicate Cairns and Spooner's original work, we can feel confident that we understand TiO2 scattering at low pigment volume concentration. If this work is successful then TiO2 scattering work at higher PVC's can be followed-up using Ross' proposal for utilization of paint film refractive index. TiO2 crowding (particle separation as a function of surface treatment and geometry) will also have to be addressed.

XI. REFERENCES:

1. DP Fields, CS Daw, TiO2 Oxidation Base Characterization/ Optimization, CDP-EM-79-5

2. DP. Fields, TiO2 Oxidation Base Optimization, CP-EM-81-8

3. DP Fields, Reactor Discharge Slurry Products, CP-EM-84-11

4. WD Ross, Theoretical Computation of Light Scattering Power, Journal of Paint Technology, Vol. 43, No. 563, Dec. 1971

5. WD Ross - Unpublished Calculations

6. RJ Bruehlman, Effect of Aggregation on the Hiding Power of Rutile Pigments, WP-ESI-65-13

7. DP Fields, TiO2 Particle Size Measurement, CT-JL-91-16

8. DP Fields, Emulsion Gloss - Particle Size Studies and Laboratory Sandmilling Studies, CP-JL-90-3

9. PB Mitton, Chap.III-D-c, Pigment Handbook, Wiley and Sons,1973

10. WD Ross, Light Scattering by Titanium Dioxide Pigment, CP-JL-87-08

11. DL Spooner, Determination of Absorption and Scattering Coefficients for 5 White Pigments using an Improved Method, WG-66-74

FIGURE DPF-1

TIO2 AGGREGATE PARTICLE SIZE DISTRIBUTION

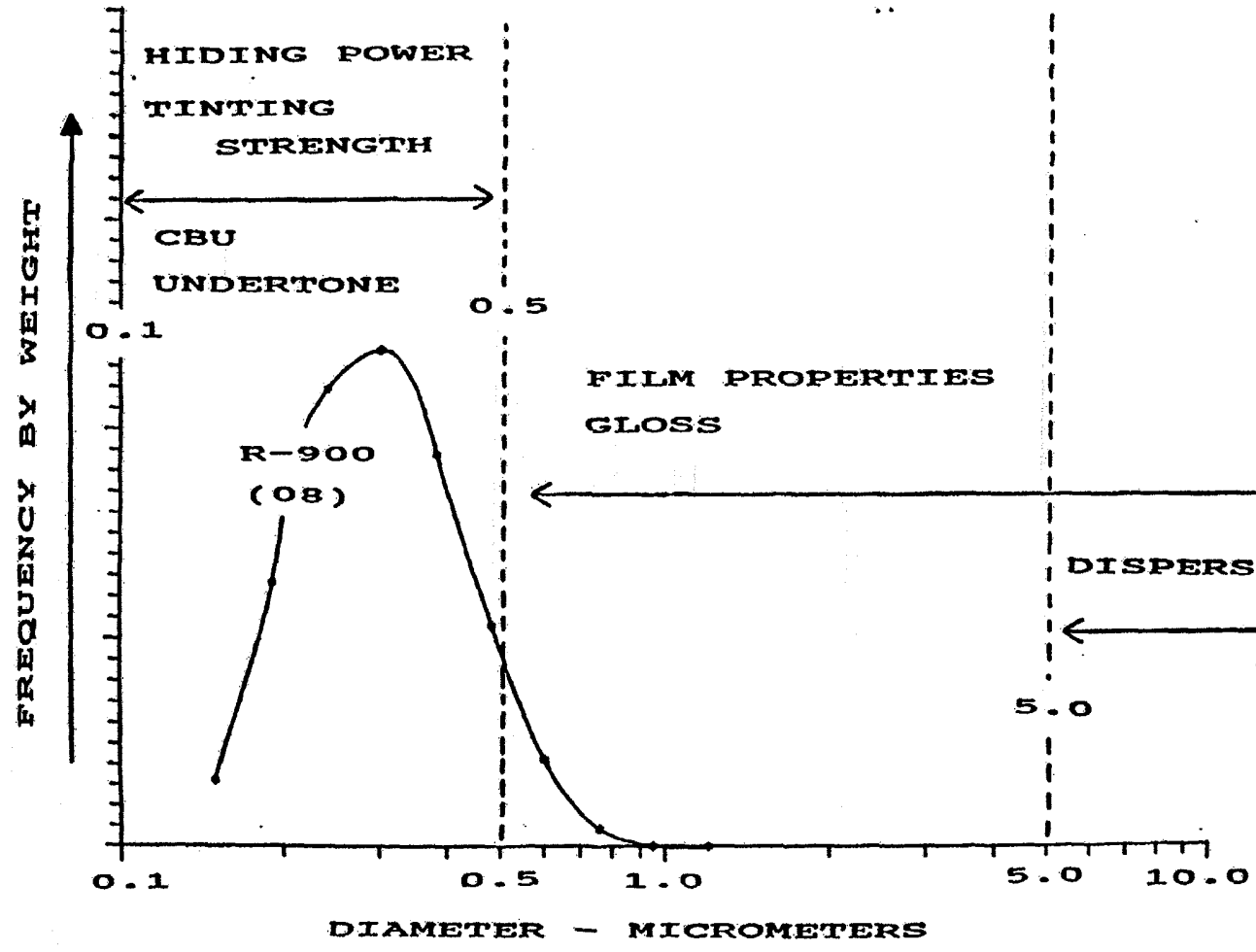

FIGURE DPF-2

TIO2 PARTICLE SIZE DISTRIBUTIONS
RAW TIO2

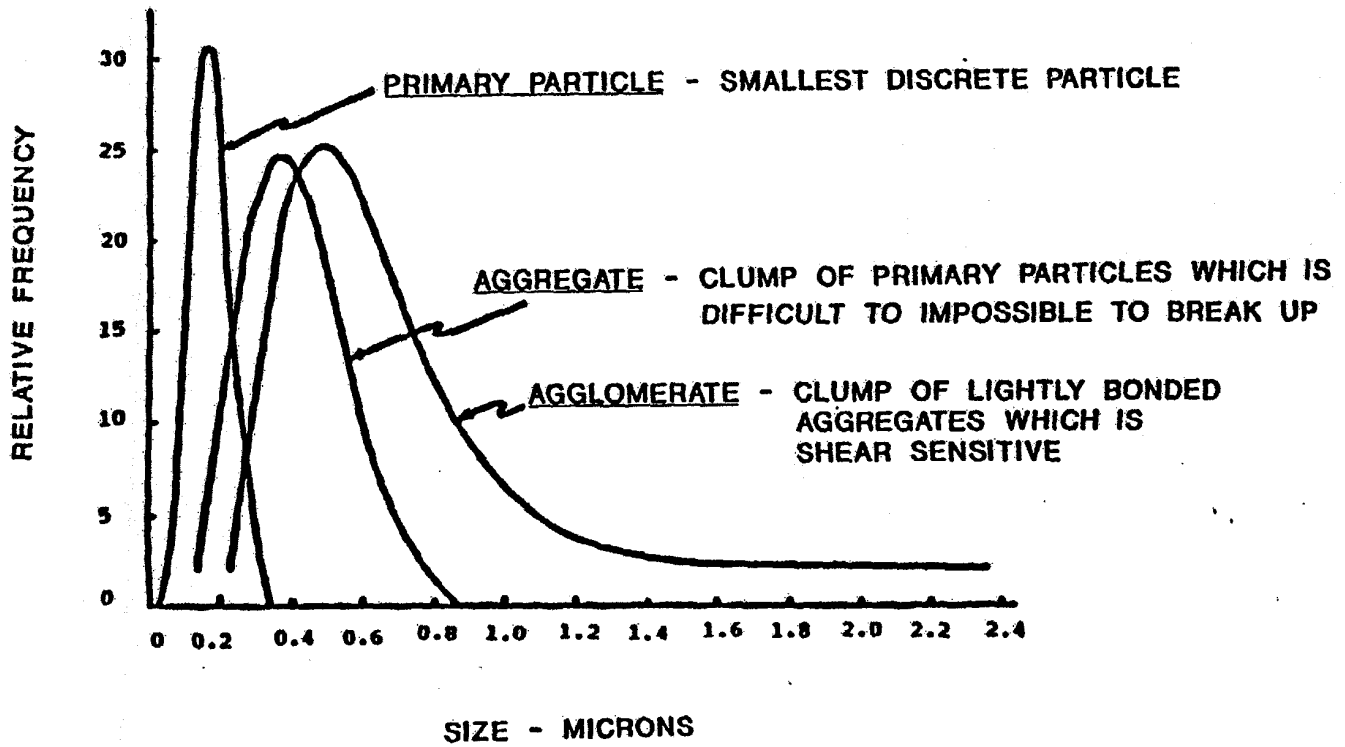

FIGURE DPF-3

PRIMARY PARTICLE BONDING

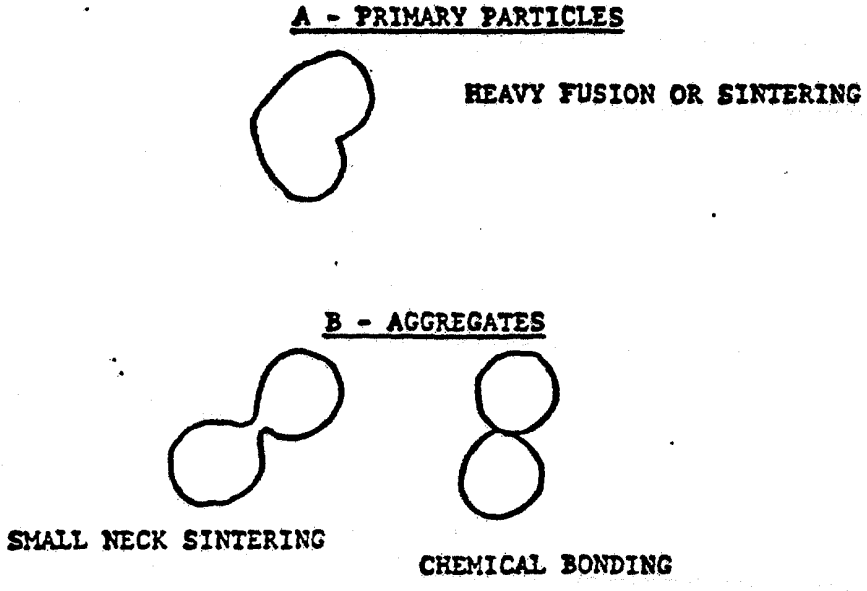

AGGREGATE FORMATION - SCHEMATIC

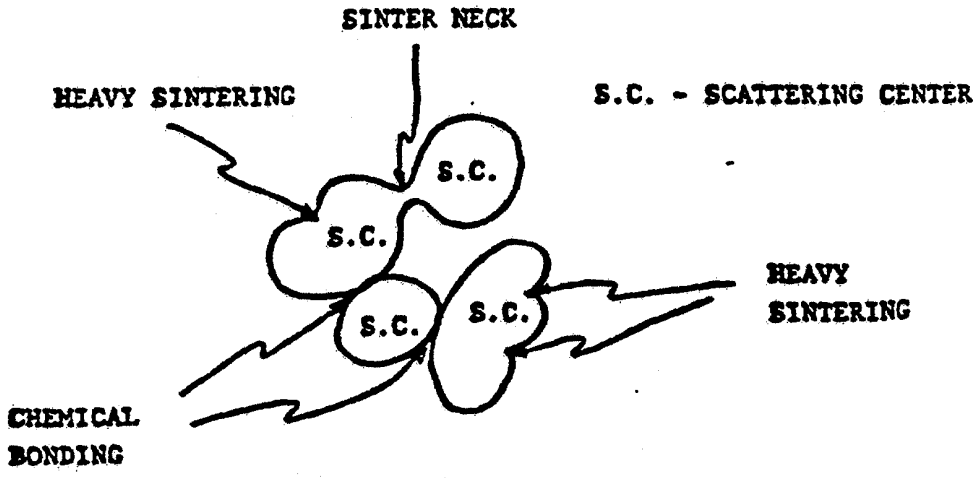

TABLE DPF-1

TIO2 PARTICLE SIZE DETERMINATIONS

PRIMARY PARTICLE SIZE	
DISTRIBUTIONS	-TEM -SEM
MEAN SIZE	-CARBON BLACK UNDERTONE (CBU) -SURFACE AREA -SEDIMENTATION (SONICATED) FINES SEDIGRAPH, XSDC, SFFF
AGGREGATE SIZE	
DISTRIBUTION	-TEM -SEM -SEDIMENTATION (SONICATED) SEDIGRAPH, XSDC, SFFF
AGGLOMERATION	
DISTRIBUTION	-OPTICAL MICROSCOPE -SEDIMENTATION (AS IS) SEDIGRAPH
MEAN SIZE	-BULK DENSITY -OIL ABSORPTION -HG POROSITY

TABLE DPF-2

TIO2 OXIDATION

MARKETING NEED	BACKGROUND	TECHNICAL CHALLENGE
HIGHER CBU/UNDERTONE	CBU IS F(1/PARTICLE SIZE) PRIMARY OPERATING VARIABLES o PRESSURE (CONCENTRATION) o COOLING RATE (QUENCH) o CHEMICAL ADDITIVES	PRODUCE HIGH CBU AT HIGH PRODUCTION RATE
INCREASED ULTIMATE HIDING POWER	HIDING POWER IS DEPENDENT UPON PARTICLE SIZE DISTRIBUTION (OPTIMUM SIZE) AND AGGREGATION (DISPERSION)	DEMONSTRATE SIGNIFICANT HP IMPROVEMENT FOR NARROW PARTICLE SIZE DISTRIBUTION (LAB)
IMPROVED GLOSS	GLOSS IS CONTROLLED BY PARTICLE SIZE (COARSE TAIL)	DECREASE OXID BASE AGGLOMERATION AND COARSE TAIL AT HIGH PRODUCTION RATE

TABLE DPF-3

OXIDATION FACTS

- OXIDATION LINES ARE NOT EQUIVALENT
- OXIDATION BASE QUALITY VARIES WITHIN A LINE
- MAJOR OXIDATION LINE OPERATING DESIGN VARIABLES
  - PRESSURE
  - TURBULENCE
  - COOLING RATE
- MAJOR OXIDATION BASE QUALITY PARAMETERS
  - PARTICLE SIZE (CBU)
  - CLUMPING / AGGREGATION, AGGLOMERATION \ COARSE TAIL
  - SURFACE CHEMISTRY

TABLE DPF-4

PRIMARY PARTICLES

ULTIMATE BUILDING BLOCKS - SCATTER LIGHT TO PROVIDE MAXIMUM END-USE HIDING POWER

OPTIMUM MEAN SIZE

- o UNDERTONE
- o HIDING POWER, TINTING STRENGTH
  - oo REFRACTIVE INDEX
  - oo WAVELENGTH OF LIGHT
  - oo PARTICLE SIZE
  - oo PIGMENT VOLUME CONCENTRATION

WIDTH OF DISTRIBUTION

AS ABOVE

TABLE DPF-5

PRIMARY TIO2 PARTICLES - OXIDATION BASE STUDIES

- MEASUREMENT - UNDERTONE (CBU), TEM, SURFACE AREA
- MANY CRYSTALLOGRAPHIC TWINS
- LARGE NUMBER OF HIGHLY SINTERED MULTIPLE PARTICLES
- RUTILE WITH SOME ANATASE AND POSSIBLY BROOKITE
- VARIABLE SHAPE - SMOOTH TO ANGULAR
- WIDTH OF DISTRIBUTION (GSD) INCREASES WITH INCREASING MEAN SIZE
- ALL OXIDATION LINE HAVE SIMILAR MEAN SIZE AND WIDTH OF DISTRIBUTION FOR A GIVEN CBU (ASSUMPTION)
- 1% CO-OXIDIZED AL2O3
  - APPROX. 50% OF AL2O3 IS ON PARTICLE SURFACE
  - NON-UNIFORM SURFACE (AL2O3 THICKNESS)
- VARIABLE SURFACE SIO2 (UP TO 15% OF TOTAL SURFACE)

FIGURE DPF-4

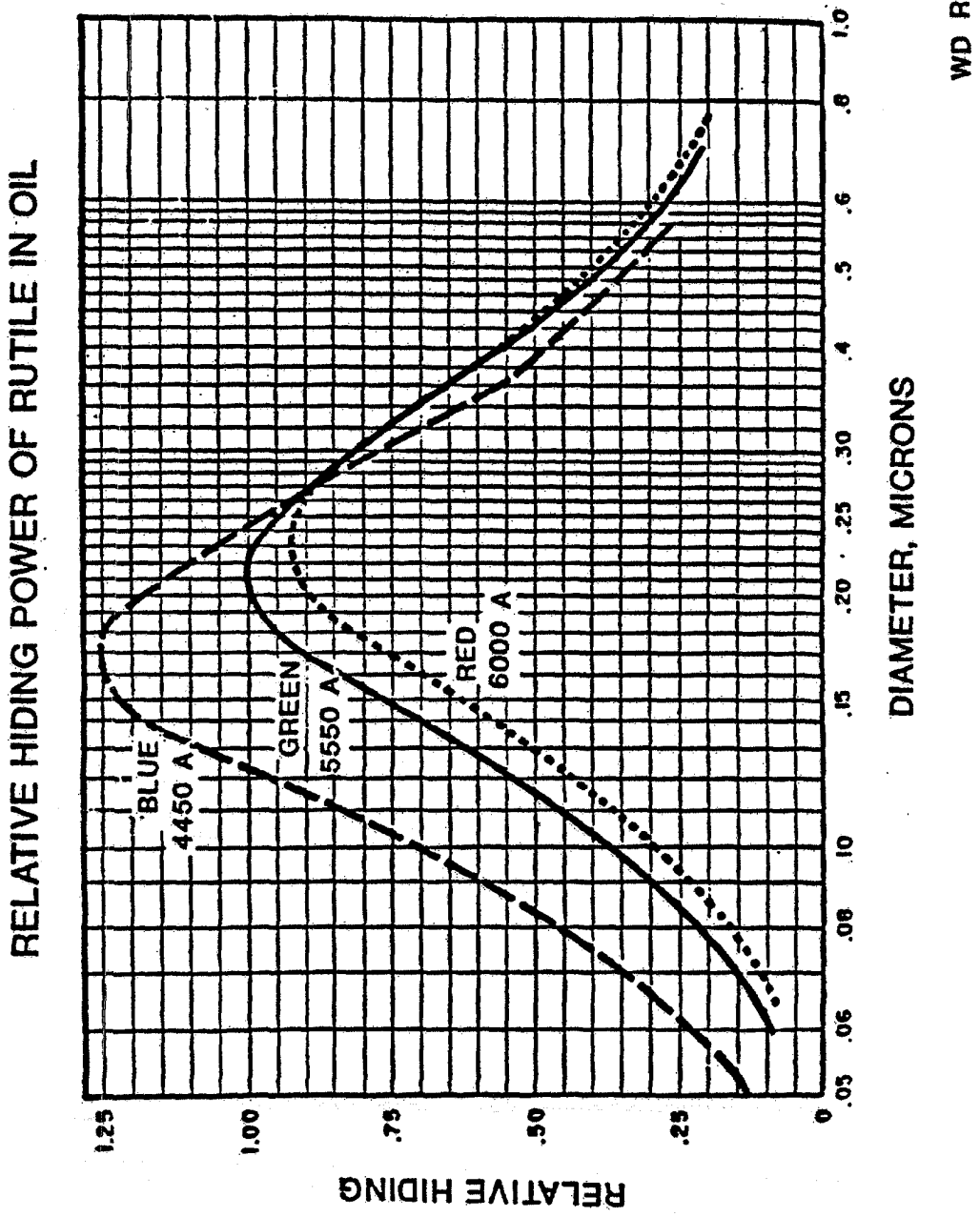

FIGURE DPF-5

TEM PRIMARY PARTICLE SIZE VS. CBU
OXIDATION BASES, FINISHED PRODUCTS

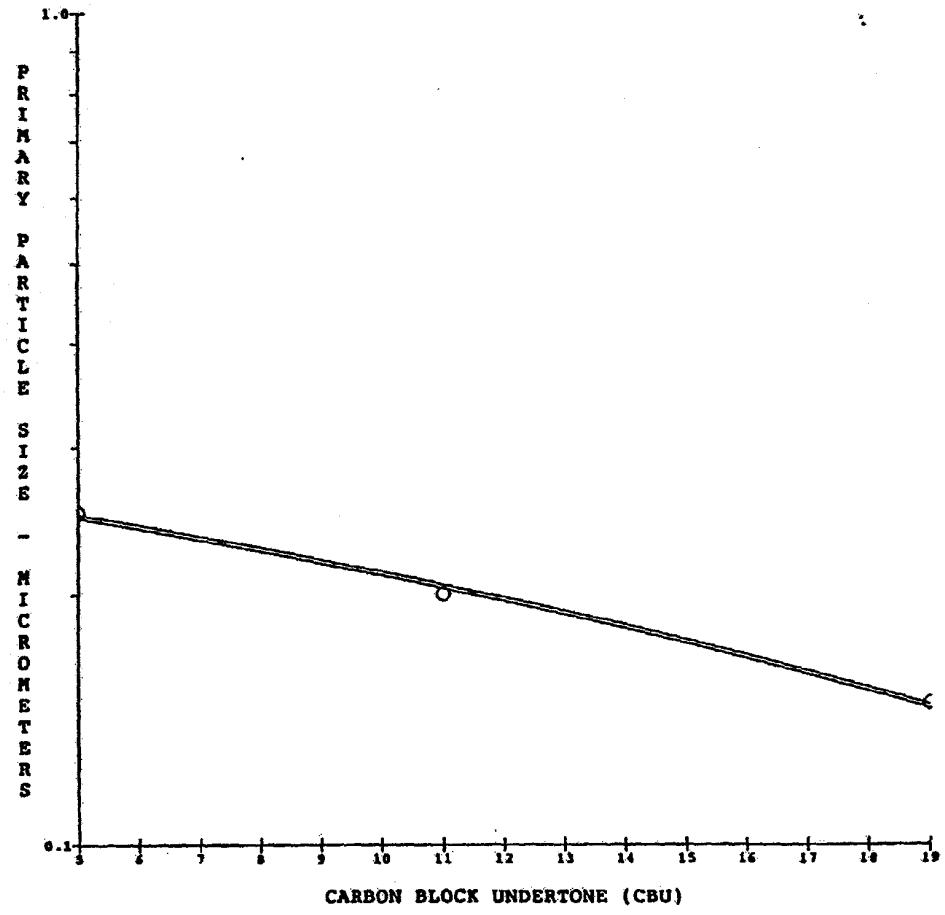

FIGURE DPF-6

HIDING POWER IMPROVEMENT (LOW PVC SYSTEMS)

OPTIMUM PARTICLE SIZE EXISTS FOR GIVEN WAVELENGTH OF LIGHT. FOR MAXIMUM HIDING POWER WE DESIRE OPTIMUM MONOSIZE TIO2 PARTICLES.

OPTIMUM MONOSIZE PARTICLES

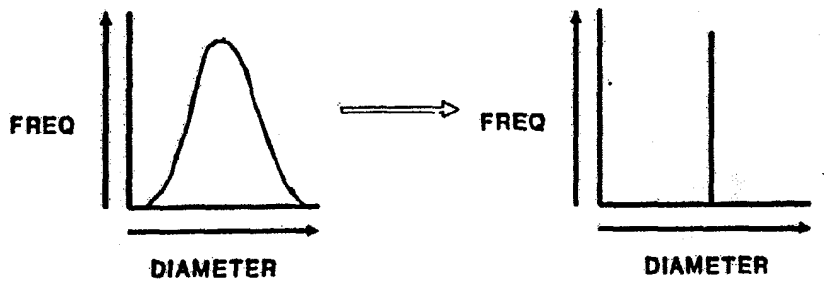

PREDICTED HIDING POWER IMPROVEMENT - 15%

FIGURE DPF-7

PRIMARY PARTICLE SIZE DISTRIBUTIONS

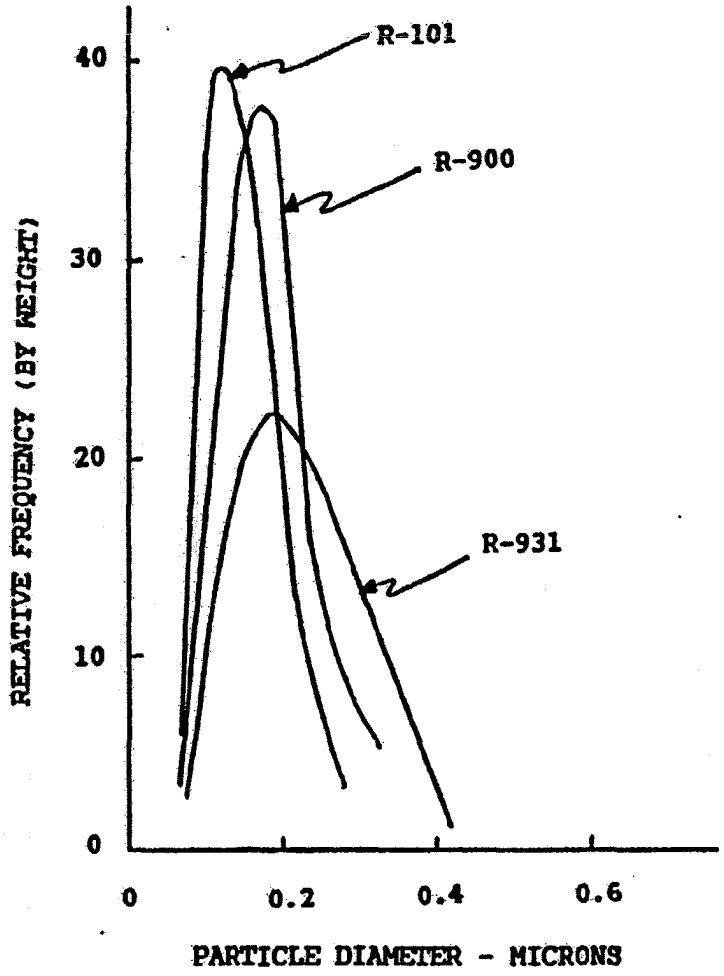

WIDTH OF DISTRIBUTIO

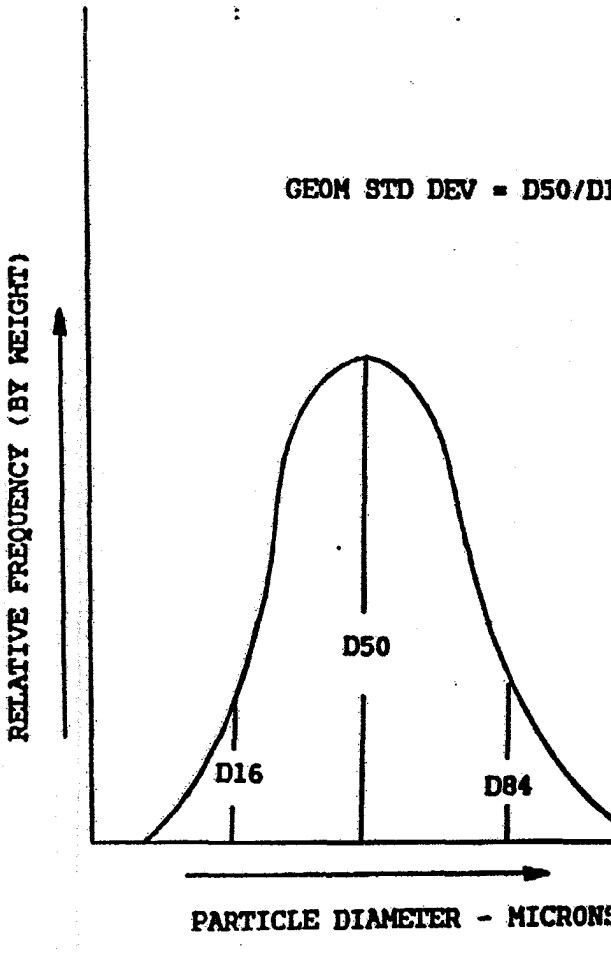

FIGURE DPF-8

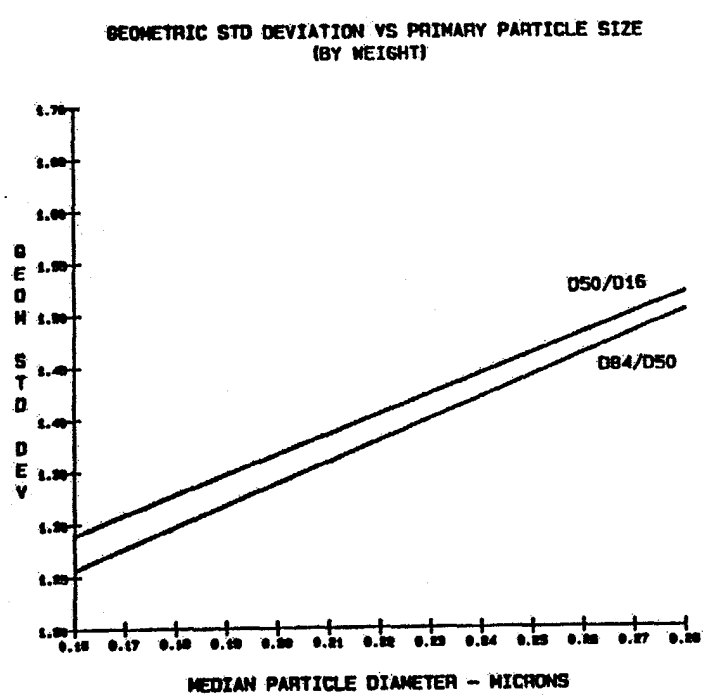

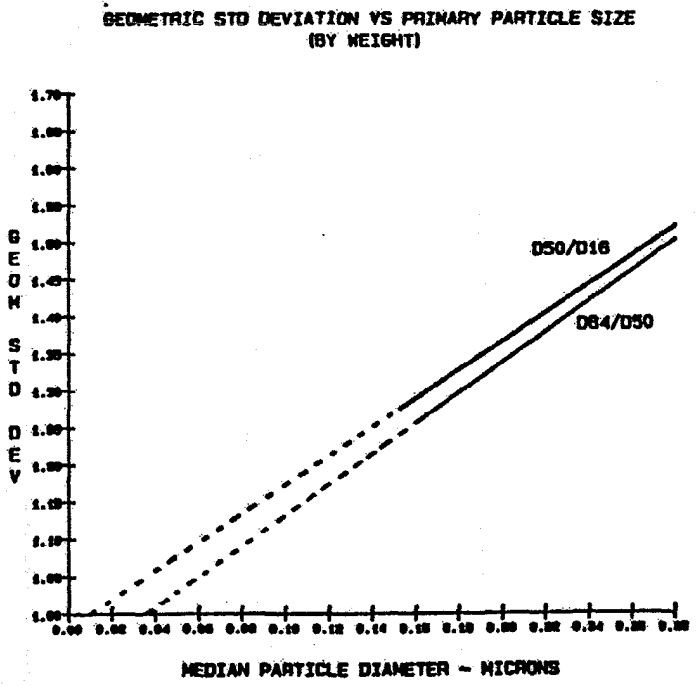

TABLE DPF-6

MAXIMUM LOW PVC HIDING POWER

VINYL FILM EVALUATION - VARIABLE TIO2 LOADING

HP (TS) AS f(LOADING)

% TIO2 LOADING	REL. VINYL TS
100 (STD)	100
90	89
95	94
99	98
101	100
105	104
110	109

REDUCED TIO2 LOADING

	VINYL LOADING (GMS)	REL. VINYL TS
PRODUCT A	5	109
	2	107
	1	106
PRODUCT B	5	113
	2	112
	1	113

FIGURE DPF-9

MAXIMUM LOW PVC HIDING POWER

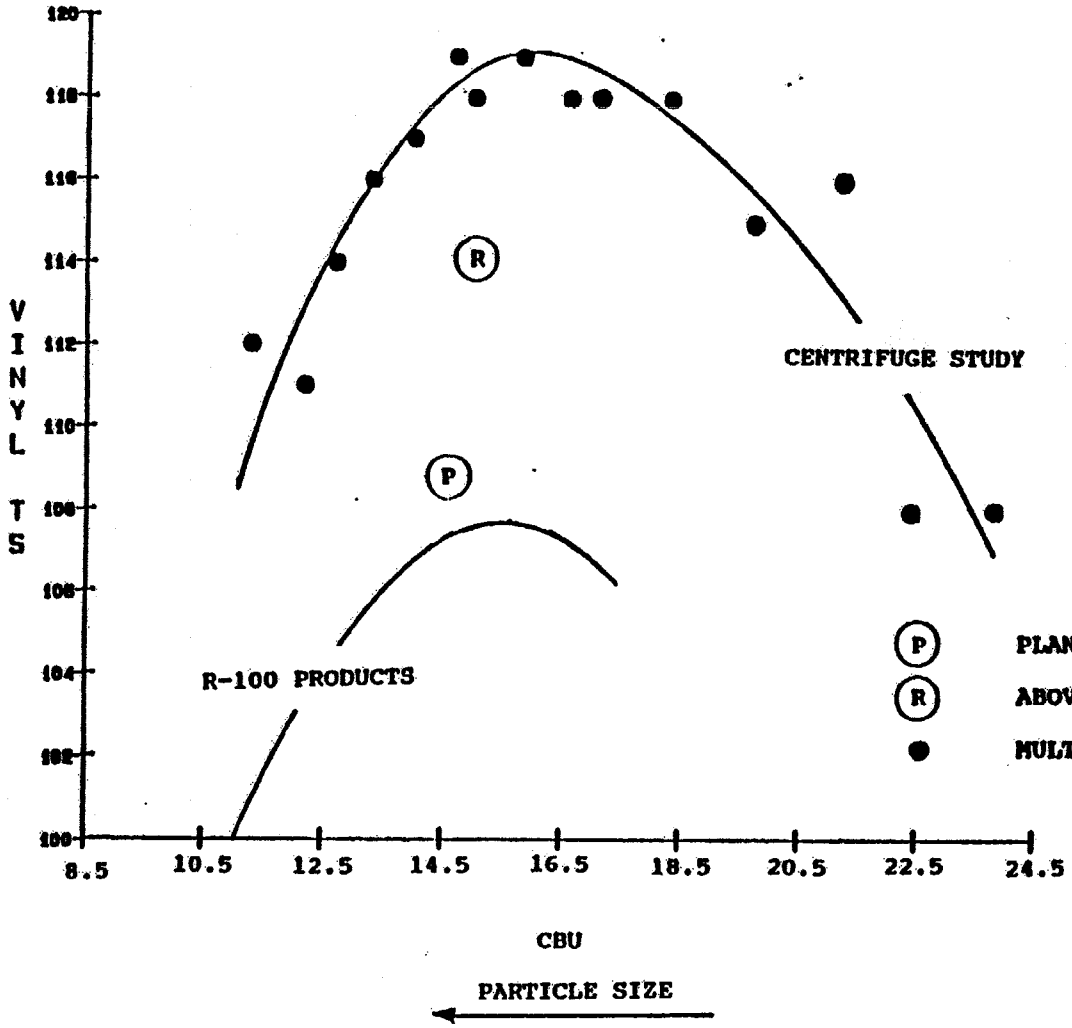

FIGURE DPF-10

PIGMENT BLENDS
VARIABLE WIDTH OF DISTRIBUTION

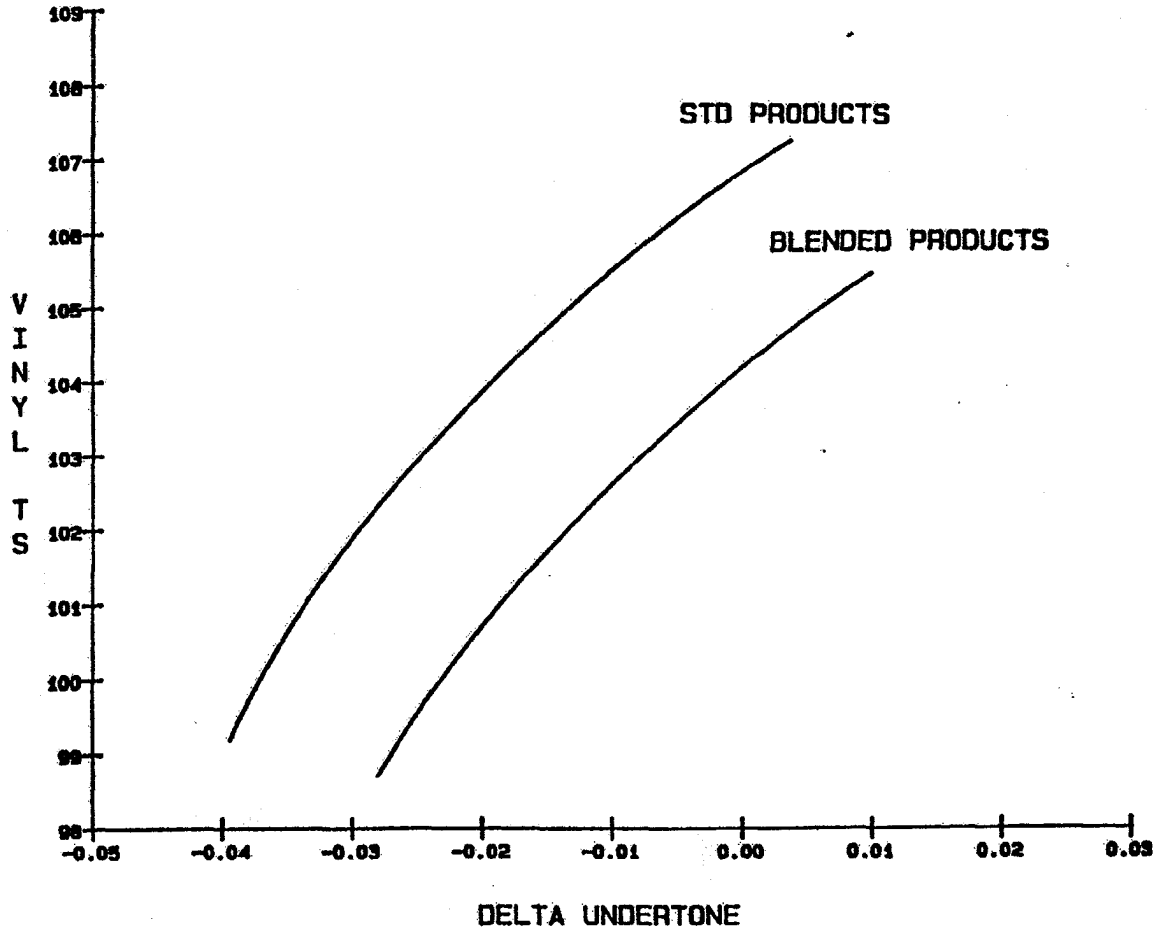

FIGURE DPF-11

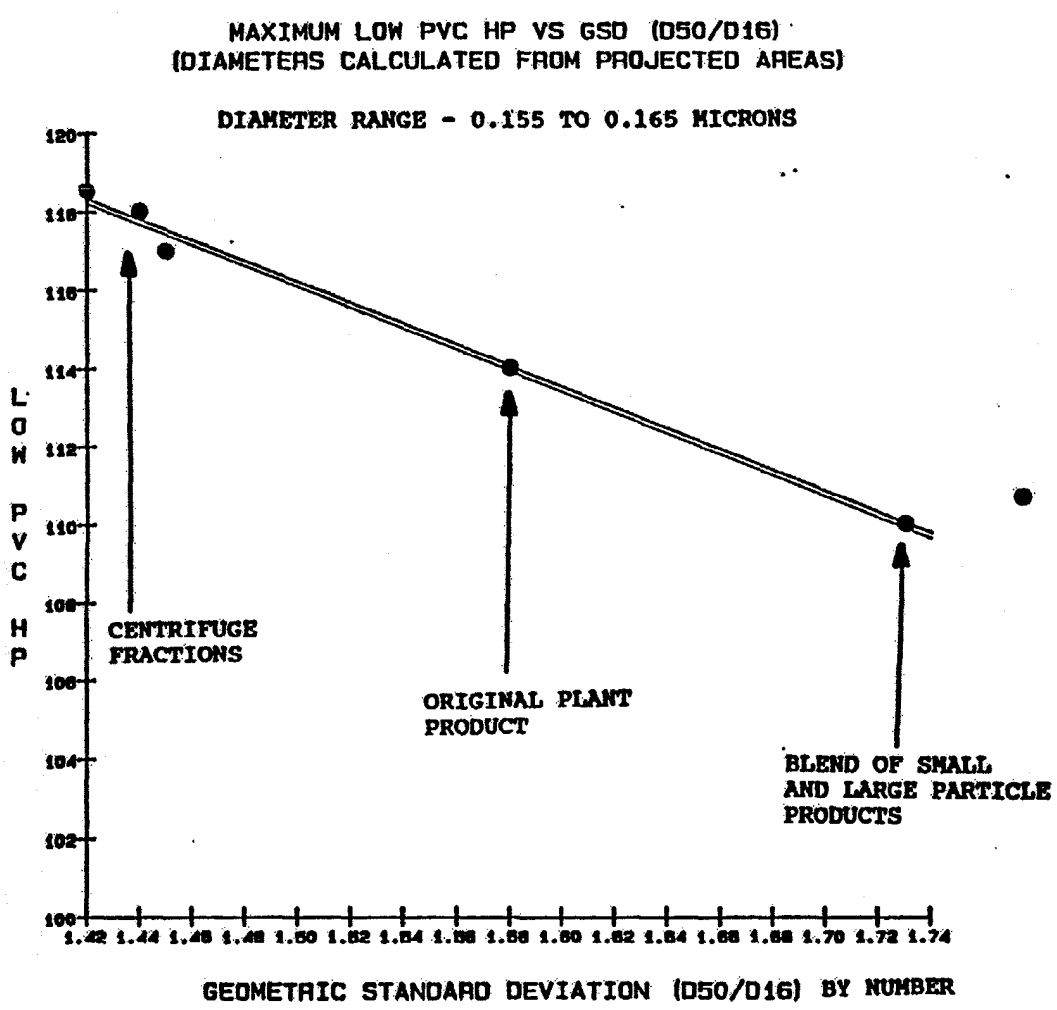

FIGURE DPF-12

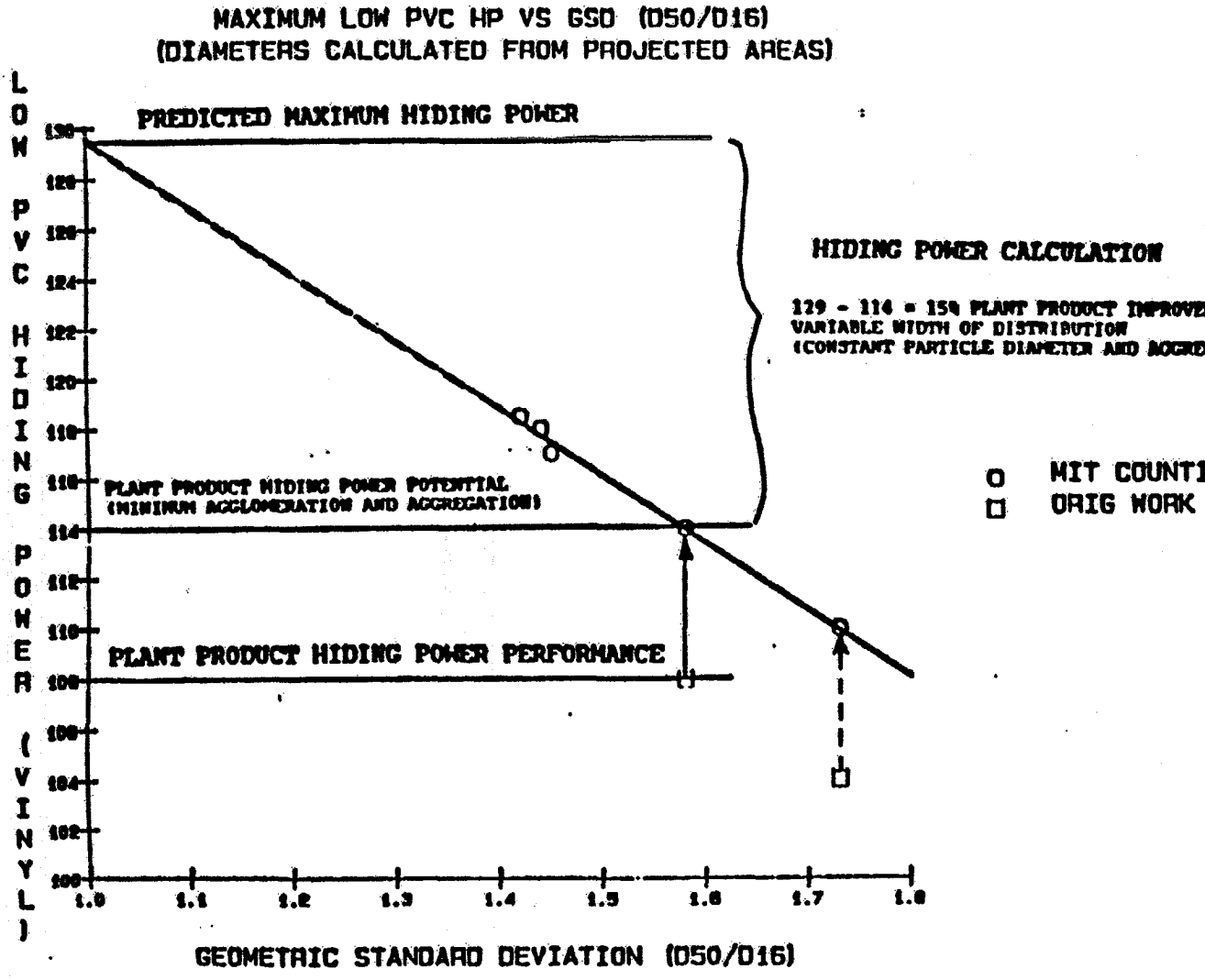

TABLE DPF-7

CENTRIFUGATION WORK

DESCRIPTION	VINYL TS	CBU (VINYL UT)	CBU (TESTED)	AGGREGATION PART/CLUMP	MEAN LENGTH	STD DEV
FEED	114	14.5		3.5	.180	.087
FRACTION 1 (COARSE)	112	10.8	11.3	3.5	.224	.074
FRACTION 3	114	12.2		3.6	.220	.085
FRACTION 5	117	13.5		3.2	.209	.073
FRACTION 7	118	14.5		3.2	.196	.048
FRACTION 9	118	16.1		3.1	.192	.058
FRACTION 11 (FINE)	108	23.3	21.8	2.2	.150	.066

FIGURE DPF-13

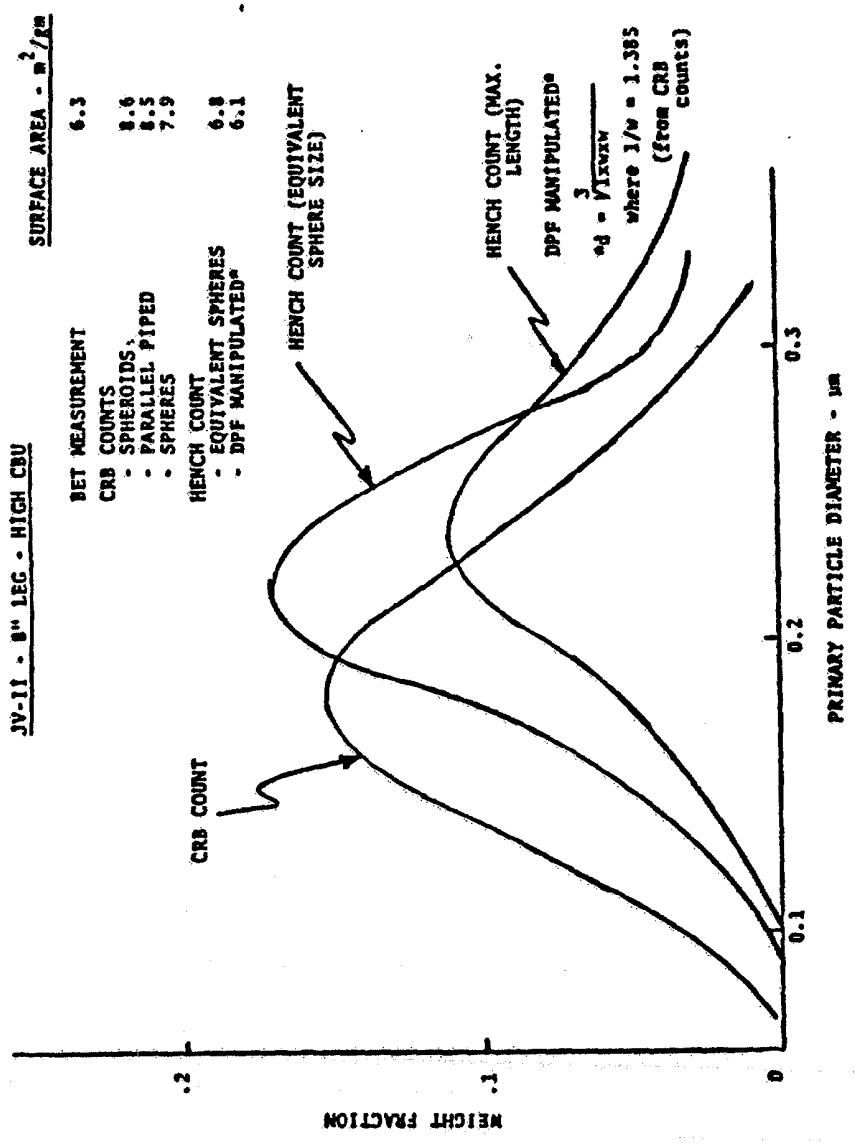

FIGURE DPF-14

HIDING POWER IMPROVEMENT (LOW PVC SYSTEMS)

MONODISPERSED TIO2 PARTICLES (NO AGGREGATION)

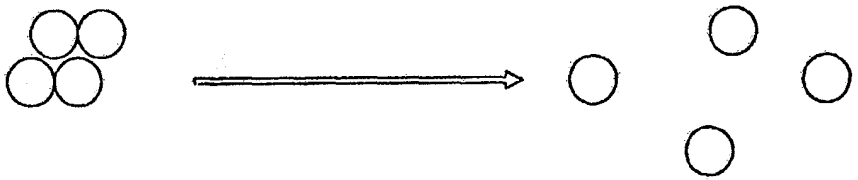

PREDICTED HIDING POWER IMPROVEMENT - ~15%

TABLE DPF-8

RELATIVE HIDING POWER CALCULATIONS
VARIABLE TIO2 AGGREGATION

	RELATIVE HP @ 0.20 MICRONS DIAMETER
ONE PARTICLE	100
TWO PARTICLES	96
THREE PARTICLES	92
FOUR PARTICLES	88

WD ROSS

FIGURE DPF-15

ENAMEL HIDING POWER VS. MEAN PARTICLE SIZE
(HENNESSY AND PAULSON - 1968)

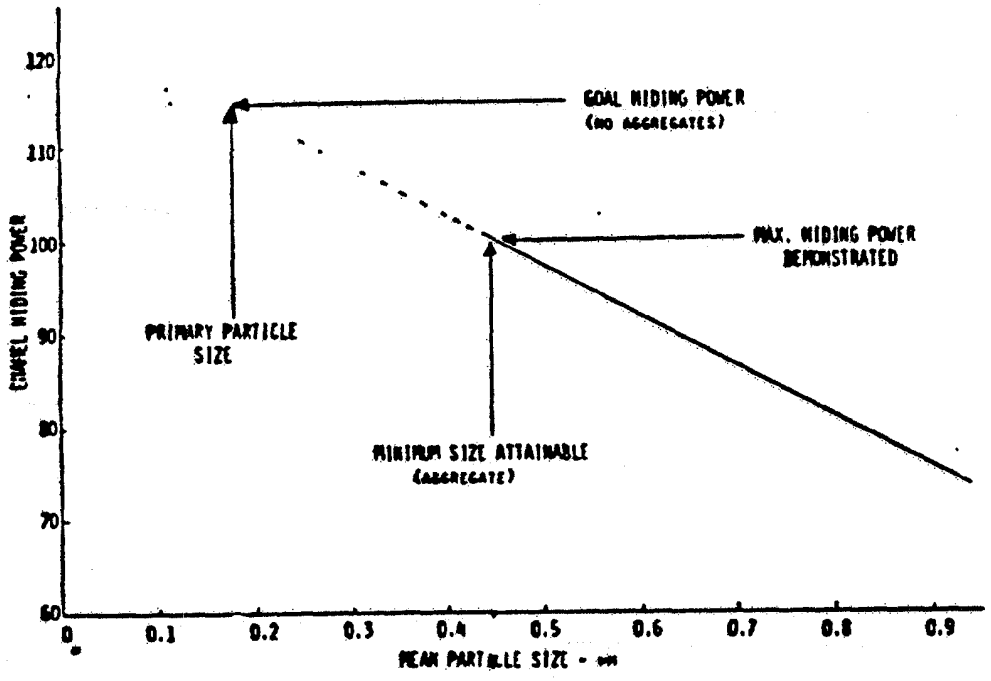

TABLE DPF-9

AGGREGATION

AGGREGATES - STRONGLY BONDED PARTICLES (RESISTANT TO SHEAR)

TWO TYPES

- o SINTER BONDS
- o CHEMICAL BRIDGES

AGGREGATE MEASUREMENT

TEM - PARTICLES/CLUMP FOLLOWING HIGH SHEAR GRIND

STOKES LAW (SEDIGRAPH) - EQUIVALENT SPHERICAL DIAMETER FOLLOWING HIGH SHEAR GRIND

ABOVE TECHNIQUES DO NOT AGREE - SEDIGRAPH » TEM

NEW INSTRUMENT

STOKES LAW (X-RAY SCANNING DISK CENTRIFUGE)
BETTER AGREEMENT WITH TEM

FIGURE DPF-16

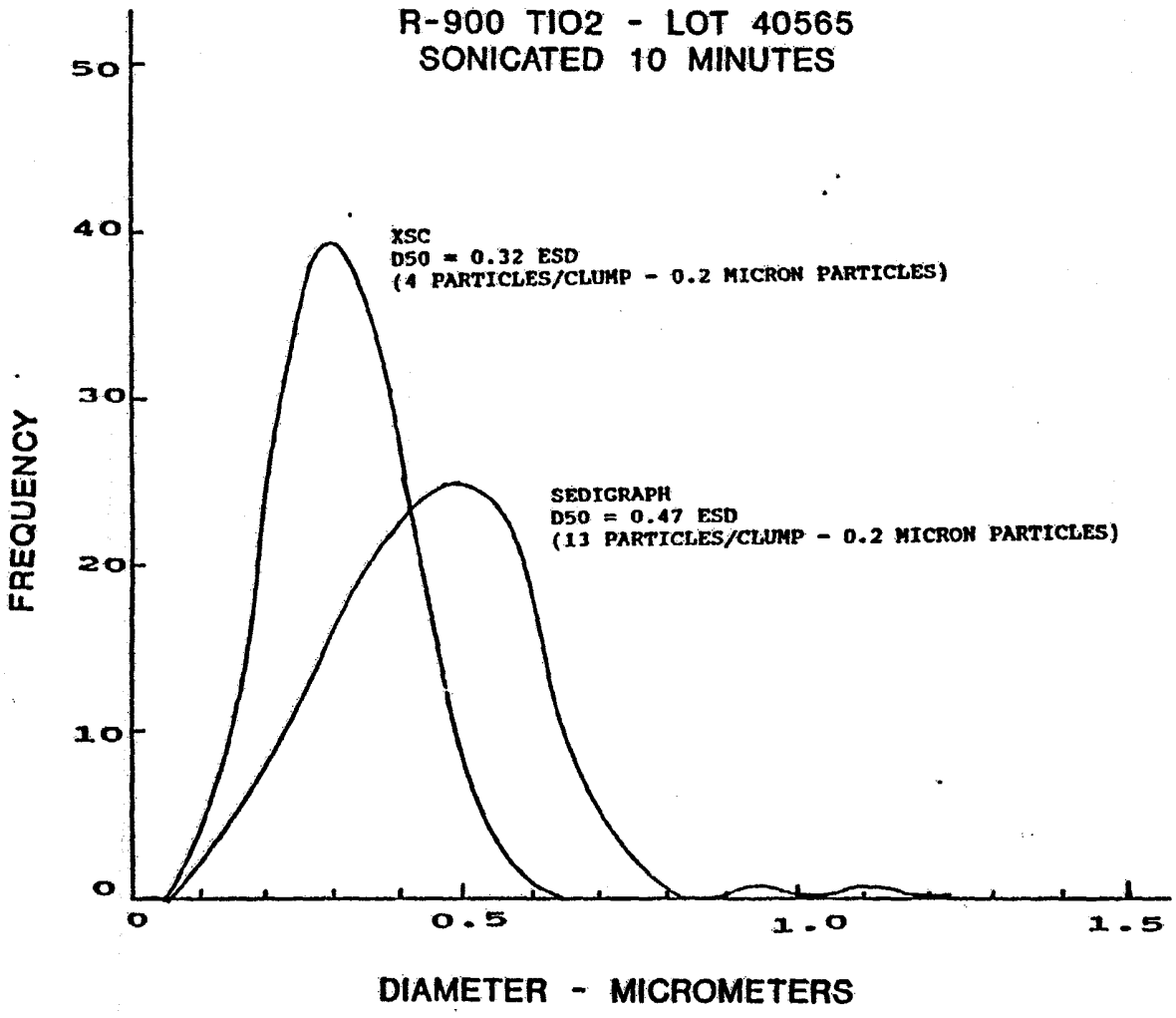

FIGURE DPF-17

R-900 TiO2 PARTICLE SIZE DISTRIBUTIONS (SEDIGRAPH, X-RAY CENTRIFUGE, TRANS. ELECT. MICROSCOPY)

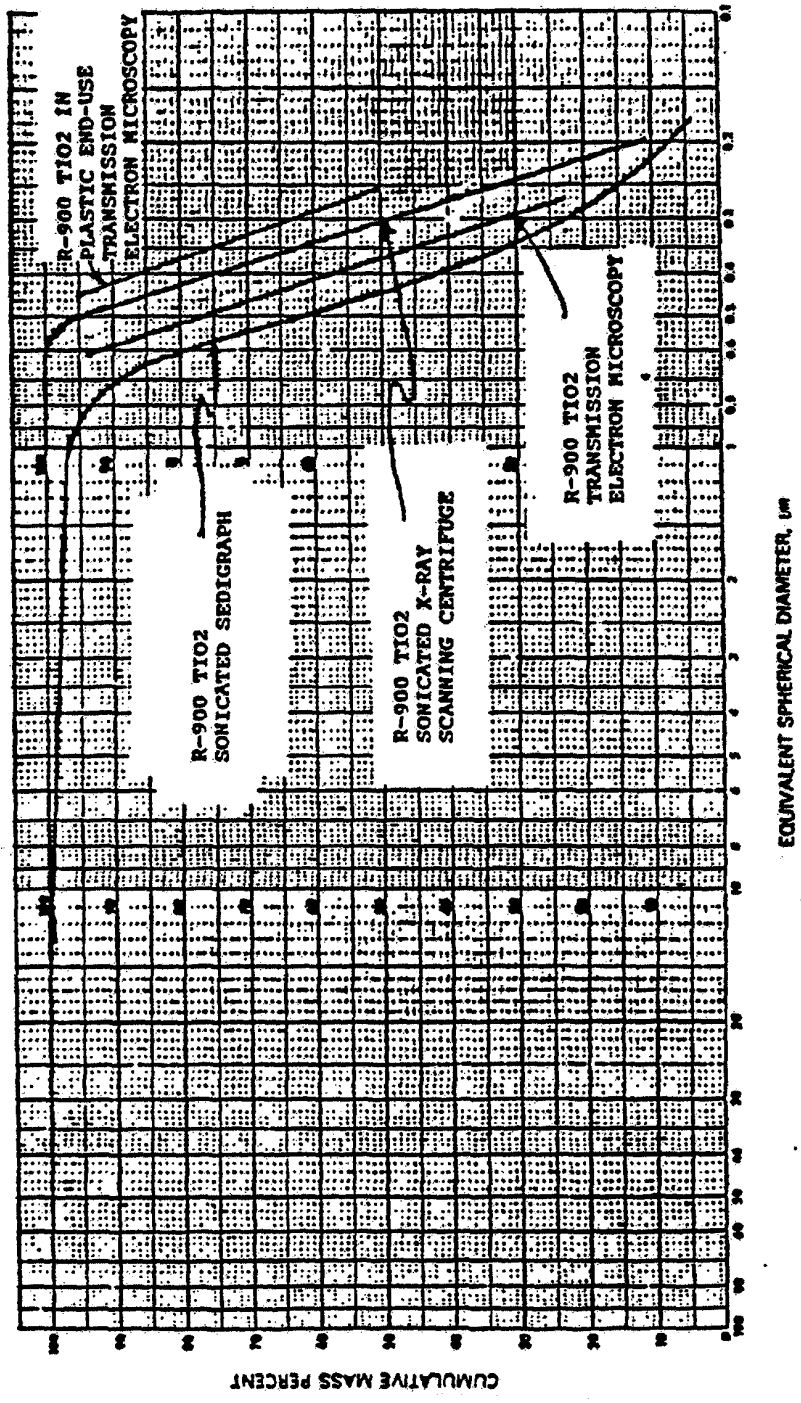

FIGURE DPF-18

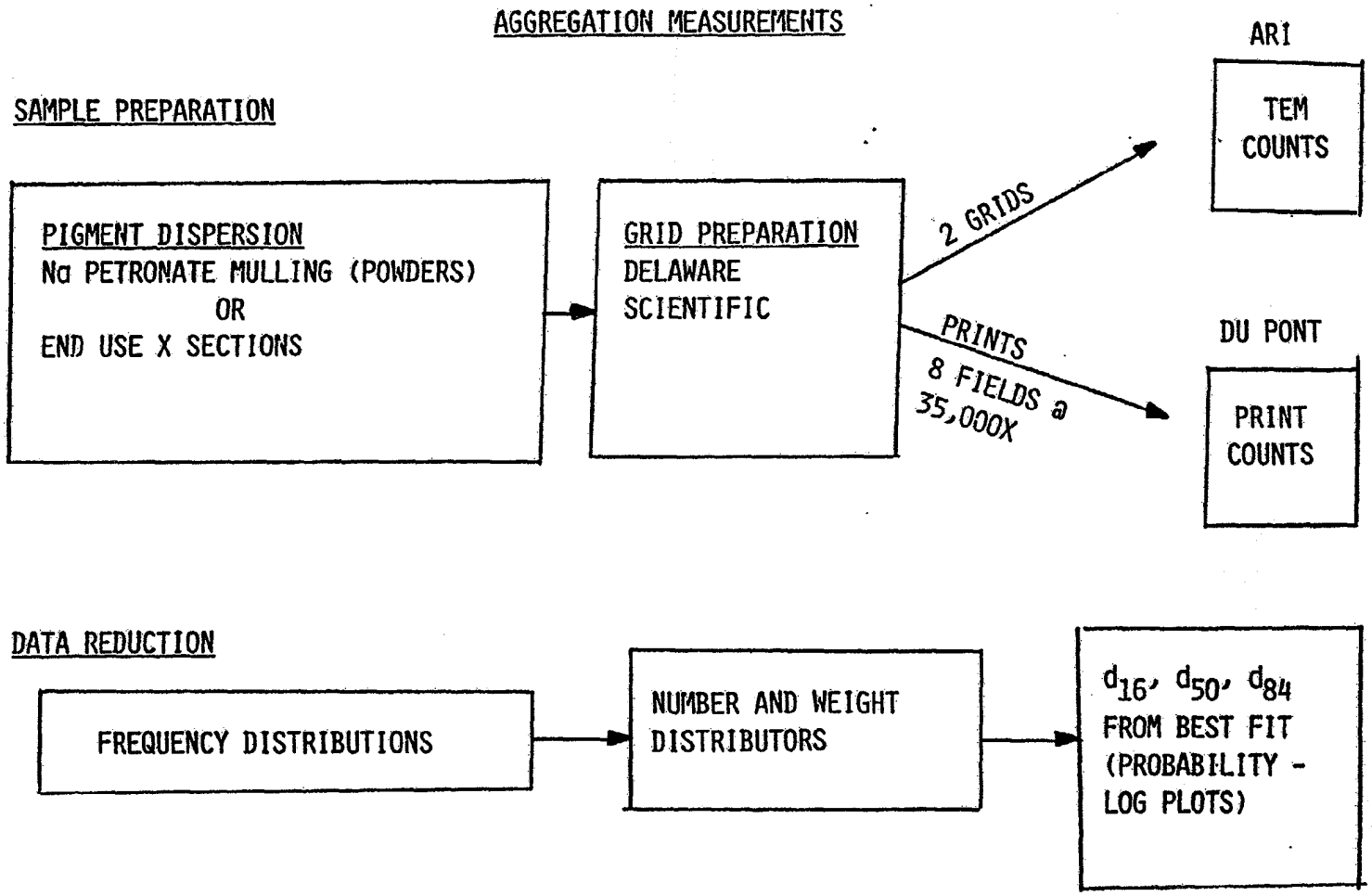

FIGURE DPF-19

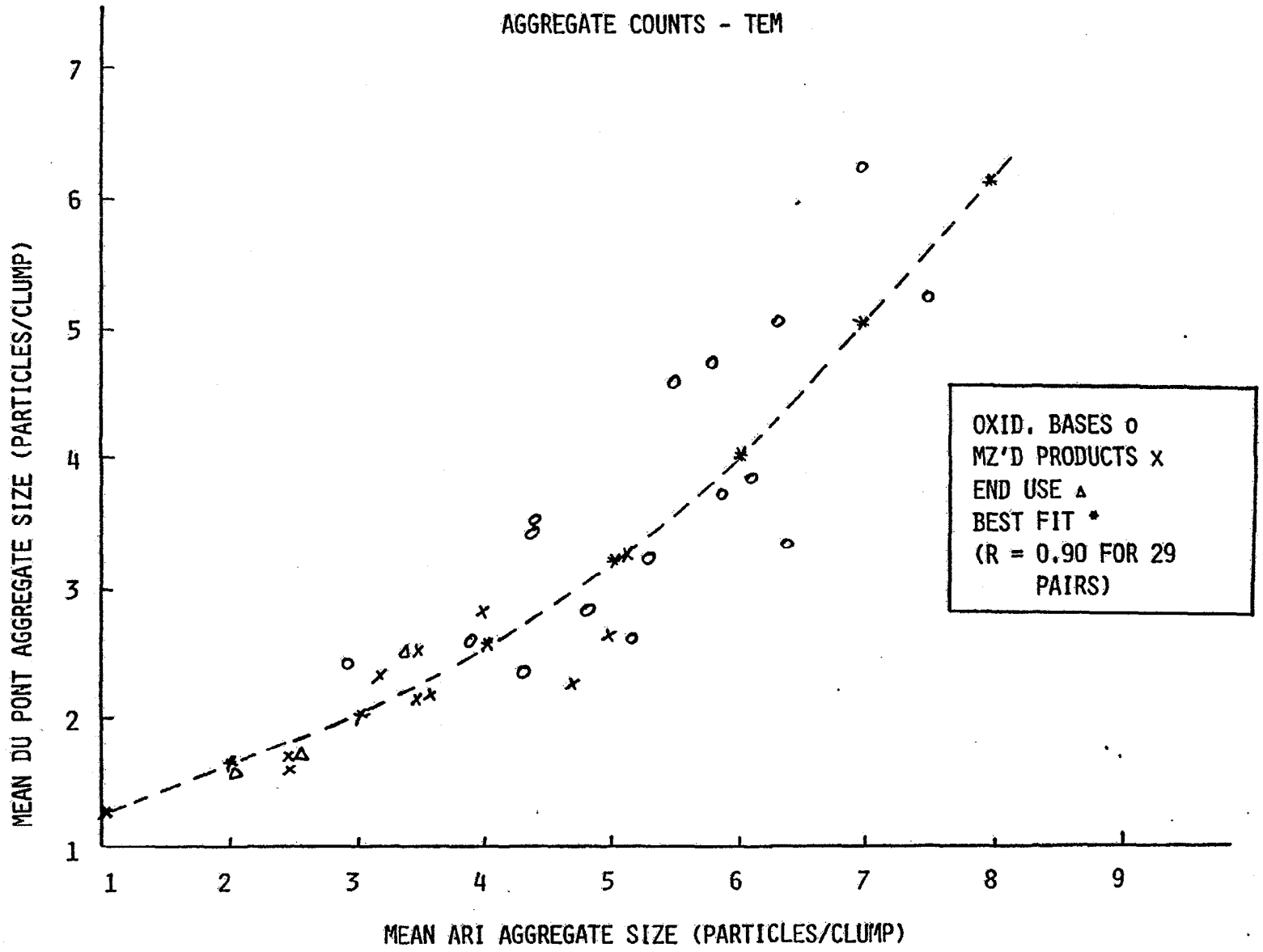

FIGURE DPF-20

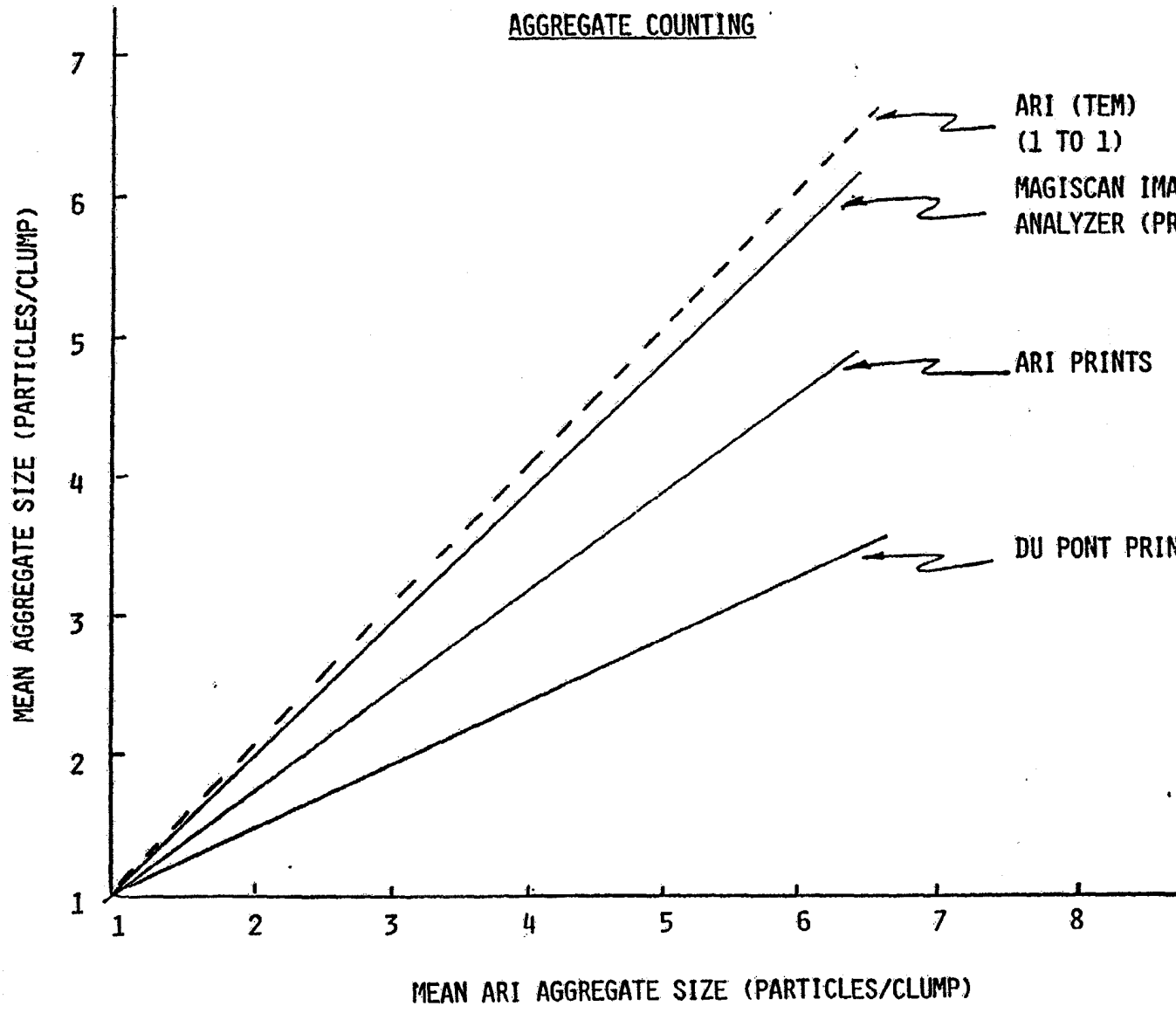

FIGURE DPF-21

AGGREGATION MEASUREMENTS

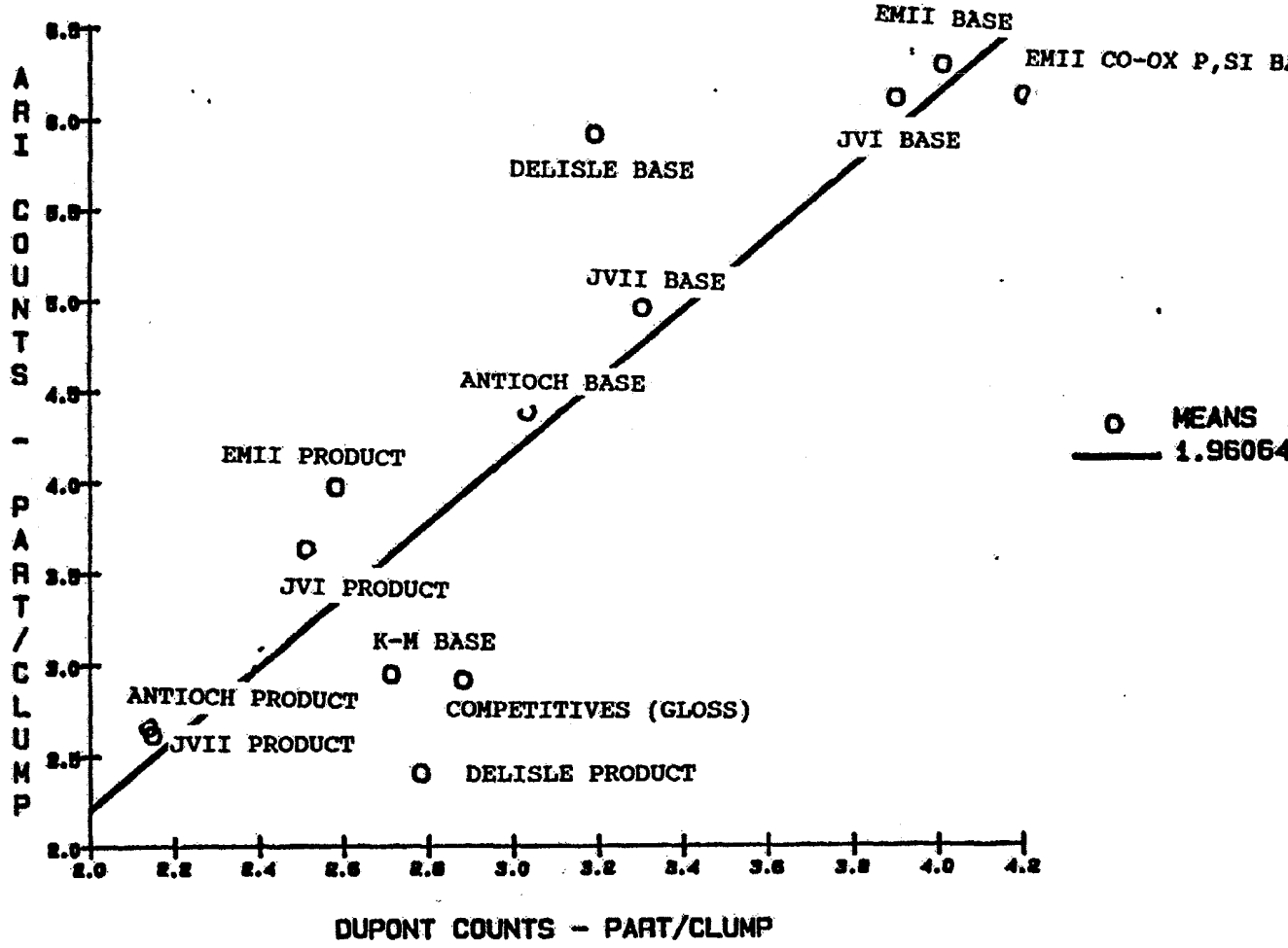

TABLE DPF-10

AGGREGATION

OXIDATION LINE RANKING

SAMPLE	DUPONT MEASUREMENTS	ARI MEASUREMENTS
KERR-MCGEE	2.71 +/- 0.41	2.94
ANTIOCH	3.03 +/- 0.64	4.38 +/- 0.38
DELISLE	3.19 +/- 0.51	5.91
JVII	3.30 +/- 0.64	4.95 +/- 0.22
JVII W/CO-OX P	3.60 +/- 0.48	
EMI	3.76 +/- 0.12	
JVI W/CO-OX P	3.87 +/- 0.55	
JVI	3.90 +/- 0.84	6.10 +/- 0.49
EMII	4.01 +/- 1.23	6.28 +/- 1.08
EMII S/CO-OX P,SI	4.20 +/- 1.22	6.11 +/- 1.13

FINISHED PRODUCTS

ANTIOCH	2.14 +/- 0.18	2.66 +/- 0.13
JVII	2.15 +/- 0.55	2.62 +/- 0.24
JVI	2.51 +/- 0.38	3.63
EMII	2.58 +/- 0.36	3.97 +/- 0.73
DELISLE	2.78	2.40
COMPETITIVES	2.88 +/- 0.46	2.91 +/- 0.60

TABLE DPF-11

AGGREGATION COUNTS

0 SAMPLES	1 DUPONT # TESTS	2 DUPONT MIN	3 DUPONT MAX	4 DUPONT MEAN	5 DUPONT STD DEV	6 ARI # TESTS	7 ARI MIN	8 ARI MAX	9 ARI MEAN	10 ARI STD DEV
1 OXIDATION BASES										
2 ANTIOCH	14	2.08	4.60	3.03	0.64	4	3.92	4.85	4.38	0.38
3 DELISLE	3	2.73	3.74	3.19	0.61	1			5.91	
4 EM I	3	3.62	3.85	3.76	0.12					
5 EM II	6	3.05	6.23	4.01	1.23	2	5.51	7.04	6.28	1.08
6 EM II W/COOX P,SI	23	2.84	7.83	4.20	1.22	5	4.36	7.52	6.11	1.13
7 JV I	9	3.13	5.17	3.90	0.84	2	5.75	6.44	6.10	0.49
8 JV I W/COOX P	3	3.28	4.36	3.87	0.55					
9 JV II	18	2.31	4.64	3.30	0.64	3	4.79	5.20	4.95	0.22
10 JV II W/COOX P	6	3.16	4.25	3.60	0.48					
11 KERR-MCGEE	2	2.42	3.00	2.71	0.41	1			2.94	
12 GEMMELL LAB BASE	1			4.03						
13 FINISHED PRODUCTS										
14 ANTIOCH	2	2.01	2.26	2.14	0.18	2	2.57	2.76	2.66	0.13
15 DELISLE	1			2.78		1			2.40	
16 EM I										
17 EM II	7	2.22	3.07	2.68	0.36	6	3.15	5.00	3.97	0.73
18 JV I	2	2.24	2.78	2.51	0.38	1			3.63	
19 JV II	4	1.63	2.73	2.15	0.55	3	2.47	2.89	2.62	0.24
20 COMPETITIVE (GLOSS)	7	2.36	3.76	2.88	0.46	7	2.41	4.20	2.91	0.60

TABLE DPF-12

AGGREGATE COUNTS

0 SAMPLE TYPE	1 CODE	2 DESCRIPTION	3 MEAN AGG SIZE DUPONT	4 MEAN AGG SIZE ARI
1 ANTIOCH BASES				
2	4369-87		3.54	4.40
3	E21826-130-A	0% COOX AL203 NO Q	2.28	4.34
4	E21826-130-B	0% COOX AL203 W/Q	2.56	3.92
5	4383-159-1	HIGH CBU	3.10	4.85
6	E32949-16	HIGH CBU	3.13	
7	E32949-109-E		4.60	
8	E32949-109-F	W/ LOW COOX P	3.50	
9	ANTIOCH #48	HIGH Q	2.08	
10	ANTIOCH #50	LOW Q	2.51	
11	E32949-67-A	300 PPH CL2	3.01	
12	E32949-67-B	600 PPH CL2	3.30	
13	E32949-67-C	900 PPH CL2	3.09	
14	E32949-67-D	1200 PPH CL2	2.48	
15	E32949-67-E	300 PPH CL2	3.20	
16 ANTIOCH PRODUCTS				
17	4369-86-F	LAB R-900 (4369-87)	2.01	2.57
18	R-900 1868	PLANT R-900	2.26	2.75
19 DELISLE BASES				
20	E18746-27		3.74	5.91
21	E27076-16		3.11	
22	E32949-99		2.73	
23 DELISLE PRODUCTS				
24	R-900 10510	PLANT R-900	2.78	2.40
25 EDGE MOOR I BASES				
26	4369-81-A	0.6% COOX AL203	3.81	
27	4369-81-B	1.12% COOX AL203	3.85	
28	4369-81-E	2.43% COOX AL203	3.62	
29 EDGE MOOR II BASES				
30	E13730-1-4		3.70	
31	E13728-7-10	HIGH Q	3.05	
32	E13728-10-4	LOW Q	3.12	
33	4369-146		6.23	7.04
34	E13730-18-A		4.62	5.51
35	130-Z	DFR REACTOR	3.33	
36	E13730-18-B	.18%COOX SIO2 (SLOT)	5.23	7.52

TABLE DPF-12 CONT'D

AGGREGATE COUNTS

0 SAMPLE TYPE	1 CODE	2 DESCRIPTION	3 MEAN ACC SIZE DUPONT	4 MEAN ACC SIZE ARI
37	E13730-18-C	.18% COOX SIO2 (RECYCLE	5.00	6.29
38	127-4	CONTAM W/COOX SIO2	3.82	6.06
39	127-2	W/COOX SIO2	3.43	4.36
40	E21826-97-B	COOX P RPS	3.01	
41	ABOVE	CROSS CHECK	3.10	
42	108-3	COOX P (HIGH P205)	3.16	5.32
43	E27076-116-A	COOX P RPS	4.68	
44	E27076-116-B	"	7.83	
45	E27076-116-C	"	4.05	
46	E27076-116-D	"	6.42	
47	E27076-116-E	"	4.88	
48	E27076-116-F	"	5.39	
49	E32949-90-A	"	3.28	
50	E32949-90-B	"	4.11	
51	E32949-90-C	"	3.02	
52	E32949-90-D	"	2.84	
53	E27076-147-A	"	4.09	
54	E27076-147-B	"	3.92	
55	E27076-147-C	"	3.31	
56	E27076-147-D	"	4.19	
57	E27076-147-E	"	4.75	
58	E27076-147-F	"	3.13	
59 EM II FINISHED PRODU				
60	4369-142-F	LAB R-900(4369-146)	2.98	5.00
61	E13730-119-B	LAB R-900(127-2)	2.34	3.15
62	E13730-119-C	LAB-R-900(127-4)	2.22	4.66
63	E13730-147-A	LAB R-900(108-3)	2.45	3.50
64	R-101 8268		3.07	
65	E27076-15-A	R-101 HIGH TS	2.76	4.04
66	E27076-15-B	R-101 MEDIUM TS	2.22	3.49
67 JVI BASES				
68	4369-40		4.72	6.75
69	4346-124	.16%COOXSIO2	3.26	6.44
70	E27076-109-C		5.07	
71	E27076-109-D		3.48	
72	E27076-109-K		5.17	
73	E27076-3-D	10" FLUE LEG	3.42	
74	E27076-3-B	12" FLUE LEG	3.14	
75	E21826-107-1		3.13	
76	E21826-107-2	EMII CONDITIONS	3.68	
77	E21826-107-3	"W/.35% COOX SIO2	4.36	
78	E21826-107-4	"W/.35% COOX SIO2	3.97	
79	E21826-107-5	"W/.70% COOX SIO2	3.28	
80 JV I PRODUCTS				
81	4369-57-4	LAB R-900(4369-40)	2.24	3.63
82	E27076-115-D	" LAB MZ 4 S/P	2.78	

TABLE DPF-12 CONT'D

AGGREGATE COUNTS

0 SAMPLE TYPE	1 CODE	2 DESCRIPTION	3 MEAN AGG SIZE DUPONT	4 MEAN AGG SIZE ARI
83 JVII BASES				
84	4369-84	8" FLUE LEG	3.18	
85	4369-79	8" FLUE LEG	2.81	4.79
86	E13730-123-C	12" FLUE LEG	2.55	5.20
87	E27076-3-E	MUFFLER FLUE	2.31	
88	E27076-123-A		3.09	
89	E27076-123-B		3.85	
90	E32949-1-1		3.46	
91	E32949-1-2		3.65	
92	E32949-1-7	FINNED FLUE PIPE	3.58	
93	E32949-1-8	FINNED FLUE PIPE	3.68	
94	E32949-9-9		2.55	
95	E32949-9-10		3.47	
96	E27076-132-B		2.50	
97	E27076-109-G		2.61	
98	E27076-109-H	HIGH SCRUBS	3.97	
99	E27076-109-I		3.79	4.87
100	E27076-109-A		3.70	
101	E27076-109-B		4.64	
102	E32949-9-5	COOX P	4.16	
103	E32949-9-4	COOX P	3.29	
104	E32949-9-6	COOX P	3.16	
105	E32949-9-7	COOX P	3.24	
106	E32949-9-8	COOX P	3.52	
107	E32949-9-3	COOX P	4.25	
108 JV II PRODUCTS				
109	4369-85	LAB R-900 (4369-79)	1.73	2.49
110	E13730-124-C	LAB R-900 (E13730-123-G)	1.63	2.47
111	R-900 LOT 4193		2.49	2.89
112	R-900 LOT 4193		2.73	
113 MISCELLANEOUS BASES				
114	E27076-38-1	KERR-MCGEE DRY	3.00	2.94
115	E27076-38-1	KERR-MCGEE WASHED	2.42	
116	E29027-19-A	GEMMELL'S LAB BASE	4.03	
117 MISCELLANEOUS PRODUC				
118	E27076-118-A	TIOXIDE RHD6	2.89	2.96
119	E27076-118-B	TIOXIDE RTC90	3.75	4.20
120	E27076-118-C	KM CR-800	2.99	2.79
121	E27076-118-D	NJZ RF-30	2.62	2.41
122	E27076-118-E	GLIDDEN RCL-9	3.01	2.53
123	E27076-118-F	AM CY OR-600	2.82	2.65
124	E27076-118-G	NL 2090	2.36	2.84
125 VINYL FILM SECTIONS				
126	E27076-35-A	LAB R-900 SNOMLD ANT BAS	1.68	2.07
127	E27076-35-B	LAB R-900 SNOMLD JVII BA	1.90	2.96
128	E27076-35-C	LAB R-900 SNOMLD JVI BAS	1.69	2.38
129	E27076-35-D	LAB R-900 SNOMLD EMII BA	1.95	2.87
130	E27076-35-E	LAB R-900 SNOMLD EMII CO	1.87	3.03
131	E27076-118-A	TIOXIDE RHD6	1.56	
132	E27076-118-B	TIOXIDE RTC90	1.84	
133	E27076-118-C	KM CR-800	1.51	

TABLE DPF-12 CONT'D

AGGREGATE COUNTS

0 SAMPLE TYPE	1 CODE	2 DESCRIPTION	3 MEAN AGG SIZE DUPONT	4 MEAN AGG SIZE ARI
134	E27076-118-E	GLIDDEN RCL-9	1.51	
135	E27076-118-G	NL 2090	1.72	
136	E27076-118-I	R-900 LOT 4193	1.59	
137	E27076-115-A	JVI R-101DD	2.69	
138	E27076-115-B	ABOVE LAB MZ 1 S/P	1.98	
139	E27076-115-C	ABOVE LAB MZ 2 S/P	1.53	
140	E27076-115-D	ABOVE LAB MZ 4 S/P	1.95	
141	E27076-115-E	ABOVE LAB MZ 6 S/P	1.91	
142	E27076-115-F	ABOVE LAB MZ 6 S/P W/TEA	1.71	
143	E27076-115-G	ABOVE LAB MZ 12 S/P	1.77	
144	E27076-115-H	ABOVE LAB MZ <1 S/P	1.81	
145	E32949-52-I	R-900 4193 1 PVC	1.50	
146	E32949-144-A	R-900 4193 1PVC	1.80	
147	E32949-144-B	R-900 4193 5PVC	1.90	
148	E32949-144-C	R-900 4193 17.1PVC	2.60	
149	E32949-144-D	R-900 4193 23.6PVC	3.40	
150	E32949-144-E	R-900 4193 1PVC	1.90	
151	E32949-144-F	R-900 4193 1PVC	1.70	2.45
152	E32949-144-G	R-900 4193 1PVC	1.70	
153 30J PAINT FILM SECTI				
154	ED 446-8	LAB R-900 56 GLOSS	2.01	
155	ED-446-10	LAB R-900 67 GLOSS	1.96	
156	ED-447-4	LAB R-900 78 GLOSS	1.85	2.45
157	ED-447-4	ABOVE CROSS CHECK	1.71	
158	R-900 4193	18.2 PVC	1.84	
159	ABOVE	18.2 PVC	1.85	
160 TFW -180 PAINT SECTI				
161	ED-468-12	LAB R-900 52 GLOSS	5.52	
162	ED-468-14	LAB R-900 69 GLOSS	2.83	
163	ED-468-13	LAB R-900 78 GLOSS	2.74	3.37
164	ED-468-13	ABOVE CROSS CHECK	2.45	
165	ABOVE	22.8 PVC	2.96	
166				
167				
168				

TABLE DPF-13
AGGREGATE COUNTS

0 SAMPLE TYPE	1 CODE	2 DESCRIPTION	3 MEAN AGG SIZE DUPONT	4 MEAN AGG SIZE ARI
1 ANTIOCH BASES				
2	4369-87		3.84	4.40
3	4369-87	LEACHED NAOH (SONIC)	2.81	
4	4369-87	LEACHED NAOH	2.92	
5	4369-87	SANDMILLED	2.46	4.10
6	4369-87	BALL MILLED 4 WKS	2.04	
7	4369-87	BALL MILLED 12 WKS	2.19	
8	E21826-130-A	0% COOX AL203 NO Q	2.28	4.34
9	E21826-130-B	0% COOX AL203 W/Q	2.56	3.92
10	4383-159-1	HIGH CBU	3.10	4.85
11	E32949-16	HIGH CBU	3.13	
12	E32949-109-E		4.60	
13	E32949-109-F	W/ LOW COOX P	3.50	
14	4369-51	PURGED REACTOR	6.65	6.80
15	ANTIOCH #48	HIGH Q	2.08	
16	ANTIOCH #50	LOW Q	2.51	
17	E32949-67-A	300 PPH CL2	3.01	
18	E32949-67-B	600 PPH CL2	3.30	
19	E32949-67-C	900 PPH CL2	3.09	
20	E32949-67-D	1200 PPH CL2	2.48	
21	E32949-67-E	300 PPH CL2	3.20	
22	OPAR	SMALL PARTICLE SIZE	3.68	
23	OPAR (RAW)	SMALL PARTICLE SIZE	4.68	
24	4369-138	VIBRATING MILL	2.14	
25 ANTIOCH PRODUCTS				
26	4369-86-F	LAB R-900 (4369-87)	2.01	2.57
27	R-900 1868	PLANT R-900	2.26	2.75
28 DELISLE BASES				
29	E18746-27		3.74	5.91
30	E27076-16		3.11	
31	E32949-99		2.73	
32 DELISLE PRODUCTS				
33	R-900 10510	PLANT R-900	2.78	2.40
34 EDGE MOOR I BASES				
35	4369-81-A	0.6% COOX AL203	3.81	
36	4369-81-B	1.12% COOX AL203	3.85	
37	4369-81-E	2.43% COOX AL203	3.62	
38 EDGE MOOR II BASES				
39	E13730-1-4		3.70	
40	E13728-7-10	HIGH Q	3.05	
41	E13728-10-4	LOW Q	3.12	
42	4369-146		6.23	7.04
43	4369-146	SANDMILLED	3.53	5.67
44	E13730-18-A		4.62	5.51
45	130-2	DFR REACTOR	3.33	
46	E13730-18-B	.18%COOX SIO2 (SLOT)	5.23	7.52
47	E13730-18-C	.18% COOX SIO2 (RECYCLE	5.00	6.29
48	127-4	CONTAM W/COOX SIO2	3.82	6.06

TABLE DPF-13 CONT'D

AGGREGATE COUNTS

0 SAMPLE TYPE	1 CODE	2 DESCRIPTION	3 MEAN AGG SIZE DUPONT	4 MEAN AGG SIZE ARI
49	127-2	W/COOX SIO2	3.43	4.36
50	E21826-97-B	COOX P RPS	3.01	
51	ABOVE	CROSS CHECK	3.10	
52	E21826-97-B	SANDMILLED		4.17
53	108-3	COOX P (HIGH P206)	3.16	6.32
54	E27076-116-A	COOX P RPS	4.68	
55	E27076-116-B	"	7.83	
56	E27076-116-C	"	4.06	
57	E27076-116-D	"	6.42	
58	E27076-116-E	"	4.88	
59	E27076-116-F	"	5.39	
60	E32949-90-A	"	3.28	
61	E32949-90-B	"	4.11	
62	E32949-90-C	"	3.02	
63	E32949-90-D	"	2.84	
64	E27076-147-A	"	4.09	
65	E27076-147-B	"	3.92	
66	E27076-147-C	"	3.31	
67	E27076-147-D	"	4.19	
68	E27076-147-E	"	4.76	
69	E27076-147-F	"	3.13	
70	4369-144	VIBRATING MILL	3.48	
71 EM II FINISHED PRODU				
72	4369-142-F	LAB R-900(4369-146)	2.98	5.00
73	E13730-119-B	LAB R-900(127-2)	2.34	3.15
74	E13730-119-C	LAB-R-900(127-4)	2.22	4.66
75	E13730-147-A	LAB R-900(108-3)	2.45	3.50
76	R-101 B268		3.07	
77	R-101 B268	LEACHED NAOH	3.12	
78	E27076-15-A	R-101 HIGH TS	2.76	4.04
79	E27076-15-B	R-101 MEDIUM TS	2.22	3.49
80 JVI BASES				
81	4369-40		4.72	5.75
82	4369-40	SANDMILLED	3.44	5.74
83	4346-124	.16%COOXSIO2	3.26	6.44
84	E27076-109-C		5.07	
85	E27076-109-D		3.48	
86	E27076-109-K		6.17	
87	E27076-3-D	10" FLUE LEG	3.42	
88	E27076-3-B	12" FLUE LEG	3.14	
89	E21826-107-1		3.13	
90	E21826-107-2	EMII CONDITIONS	3.68	
91	E21826-107-3	"W/.35% COOX SIO2	4.36	
92	E21826-107-4	"W/.36% COOX SIO2	3.97	
93	E21826-107-5	"W/.70% COOX SIO2	3.28	
94	4346-120	VIBRATING MILL	2.82	
95 JV Y PRODUCTS				
96	4369-87-4	LAB R-900(4369-40)	2.24	3.63

TABLE DPF-13 CONT'D

AGGREGATE COUNTS

0 SAMPLE TYPE	1 CODE	2 DESCRIPTION	3 MEAN AGG SIZE DUPONT	4 MEAN AGG SIZE ARI
97	E27076-115-A	R-101 DD	2.70	
98	E27076-115-B	* LAB MZ 1 S/P	2.57	
99	E27076-115-C	* LAB MZ 2 S/P	3.05	
100	E27076-115-D	* LAB MZ 4 S/P	2.78	
101	E27076-115-E	* LAB MZ 6 S/P	2.32	
102	E27076-115-F	* ABOVE W/TEA	3.60	
103	E27076-115-G	* LAB MZ 12 S/P	2.74	
104	E27076-115-H	* LAB MZ <1 S/P	2.42	
105 JVII BASES				
106	4369-84	8" FLUE LEG	3.18	
107	4369-79	8" FLUE LEG	2.81	4.79
108	4369-79	SANDMILLED	2.92	4.48
109	E13730-123-G	12" FLUE LEG	2.55	5.20
110	E27076-3-E	MUFFLER FLUE	2.31	
111	E27076-123-A		3.09	
112	E27076-123-B		3.85	
113	E32949-1-1		3.46	
114	E32949-1-2		3.65	
115	E32949-1-7	FINNED FLUE PIPE	3.58	
116	E32949-1-8	FINNED FLUE PIPE	3.68	
117	E32949-9-9		2.55	
118	E32949-9-10		3.47	
119	E27076-132-B		2.80	
120	E27076-132-D-G	FLUE SAMPLE	4.35	
121	E27076-109-G		2.61	
122	E27076-109-H	HIGH SCRUBS	3.97	
123	E27076-109-I		3.79	4.87
124	E27076-109-J	FLUE SAMPLE	4.12	5.91
125	E27076-109-A		3.70	
126	E27076-109-B		4.64	
127	E32949-9-5	COOX P	4.16	
128	E32949-9-4	COOX P	3.29	
129	E32949-9-6	COOX P	3.16	
130	E32949-9-7	COOX P	3.24	
131	E32949-9-8	COOX P	3.52	
132	E32949-9-3	COOX P	4.25	
133 JV II PRODUCTS				
134	4369-85	LAB R-900 (4369-79)	1.73	2.49
135	E13730-124-G	LAB R-900 (E13730-123-G)	1.63	2.47
136	R-900 LOT 4193		2.49	2.89
137	R-900 LOT 4193	LEACHED IN NAOH	2.49	
138	R-900 LOT 4193	BALL MILLED 4 WKS	1.96	
139	R-900 LOT 4193	BALL MILLED 12 WKS	1.99	
140	R-900 LOT 4193	VIBRATING MILL	1.84	
141	R-900 LOT 4193		2.73	
142	ABOVE	LOW TIO2 GRID CONC	2.07	
143	ABOVE	ABOVE SONICATED	2.45	
144 MISCELLANEOUS BASES				

TABLE DPF-13 CONT'D

AGGREGATE COUNTS

0 SAMPLE TYPE	1 CODE	2 DESCRIPTION	3 MEAN AGG SIZE DUPONT	4 MEAN AGG SIZE ARI
145	E27076-38-1	KERR-MCGEE DRY	3.00	2.94
146	E27076-38-1	KERR-MCGEE WASHED	2.42	
147	E29027-19-A	GEMMELL'S LAB BASE	4.03	
148 MISCELLANEOUS PRODUC				
149	E27076-118-A	TIOXIDE RHD6	2.89	2.96
150	E27076-118-A	ABOVE LEACHED IN NAOH	2.78	
151	E27076-118-B	TIOXIDE RTC90	3.78	4.20
152	E27206-118-B	ABOVE LEACHED IN NAOH	3.14	
153	E27076-118-C	KM CR-800	2.99	2.79
154	E27076-118-C	ABOVE LEACHED IN NAOH	2.66	
155	E27076-118-D	NJZ RF-30	2.62	2.41
156	E27076-118-E	GLIDDEN RCL-9	3.01	2.53
157	E27076-118-E	ABOVE LEACHED IN NAOH	2.48	
158	E27076-118-F	AM CY DR-600	2.82	2.68
159	E27076-118-F	ABOVE LEACHED IN NAOH	2.52	
160	E27076-118-G	NL 2090	2.36	2.84
161 VINYL FILM SECTIONS				
162	4346-20	JV I BASE	3.11	
163	4383-166-A	ABOVE SANDMILLED	1.55	2.02
164	E27076-35-A	LAB R-900 SNDMLD ANT BAS	1.68	2.07
165	E27076-35-B	LAB R-900 SNDMLD JVII BA	1.90	2.96
166	E27076-35-C	LAB R-900 SNDMLD JVI BAS	1.69	2.38
167	E27076-35-D	LAB R-900 SNDMLD EMII BA	1.95	2.87
168	E27076-35-E	LAB R-900 SNDMLD EMII CO	1.87	3.03
169	E27076-118-A	TIOXIDE RHD6	1.56	
170	E27076-118-B	TIOXIDE RTC90	1.84	
171	E27076-118-C	KM CR-800	1.51	
172	E27076-118-E	GLIDDEN RCL-9	1.51	
173	E27076-118-G	NL 2090	1.72	
174	E27076-118-I	R-900 LOT 4193	1.59	
175	E27076-115-A	JVI R-101DD	2.69	
176	E27076-115-B	ABOVE LAB MZ 1 S/P	1.98	
177	E27076-115-C	ABOVE LAB MZ 2 S/P	1.53	
178	E27076-115-D	ABOVE LAB MZ 4 S/P	1.95	
179	E27076-115-E	ABOVE LAB MZ 6 S/P	1.91	
180	E27076-115-F	ABOVE LAB MZ 6 S/P W/TEA	1.71	
181	E27076-115-G	ABOVE LAB MZ 12 S/P	1.77	
182	E27076-115-H	ABOVE LAB MZ <1 S/P	1.81	
183	E32949-52-H	R-900 4193 .5 PVC	1.50	
184	E32949-52-I	R-900 4193 1 PVC	1.50	
185	E32949-52-J	R-900 4193 9.3 PVC	2.37	
186	E32949-144-A	R-900 4193 1PVC	1.80	
187	E32949-144-B	R-900 4193 5PVC	1.90	
188	E32949-144-C	R-900 4193 17.1PVC	2.60	
189	E32949-144-D	R-900 4193 23.6PVC	3.40	
190	E32949-144-E	R-900 4193 1 PVC	1.90	
191	E32949-144-F	R-900 4193 1PVC	1.70	
192	E32949-144-G	R-900 4193 1PVC	1.70	

TABLE DPF-13 CONT'D

AGGREGATE COUNTS

0 SAMPLE TYPE	1 CODE	2 DESCRIPTION	3 MEAN AGG SIZE DUPONT	4 MEAN AGG SIZE ARI
193 30J PAINT FILM SECTI				
194	ED 446-8	LAB R-900 56 GLOSS	2.01	
195	ED-446-10	LAB R-900 67 GLOSS	1.96	
196	ED-447-4	LAB R-900 78 GLOSS	1.85	2.45
197	ED-447-4	ABOVE CROSS CHECK	1.71	
198	R-900 4193	18.2 PVC	1.84	
199	ABOVE	48.7 PVC	2.64	
200	ABOVE	26.5 PVC	1.95	
201	ABOVE	18.2 PVC	1.85	
202	ABOVE	11.2 PVC	2.00	
203	ABOVE	6.4 PVC	1.73	
204 TFW -180 PAINT SECTI				
205	ED-468-12	LAB R-900 52 GLOSS	6.62	
206	ED-468-14	LAB R-900 69 GLOSS	2.83	
207	ED-468-13	LAB R-900 78 GLOSS	2.74	3.37
208	ED-468-13	ABOVE CROSS CHECK	2.45	
209	R-900 4193	37.3 PVC	2.81	
210	ABOVE	22.8 PVC	2.95	
211	ABOVE	12.9 PVC	2.87	
212	ABOVE	6.9 PVC	2.34	

TABLE DPF-14

MIT BOND INVESTIGATIONS (TEM)
OXIDATION LINE DIFFERENCES

OXIDATION LINE	PARTICLES PER AGGREGATE (MEAN)	BONDING	PARTICLE GROWTH AFTER INITIAL AGGREGATION	OTHER
JV LINE II	5	MANY GEL BRIDGES, FEW SINTER BONDS	NONE	PARTICLES WITH NO APPARENT POINT CONTACT ARE GEL BRIDGED
JV LINE I	6	MORE SINTER BONDS THAN JV II (35% GEL - 65% SINTER)	LIMITED	
EM LINE II	7	MOSTLY SINTER BONDS (10% GEL - 90% SINTER)	EXTENSIVE	LINEAR CLUMPS

TABLE DPF-15

AGGREGATE COUNTS
ANTIOCH BASE INVESTIGATION

	BONDING	MEAN*	MEDIAN BY #	MEDIAN BY WT
STD BASE	GEL BRIDGES	4.4	2.2	6.6
NO CO-OX AL_2O_3 NO "Q"	SINTER	4.3	1.6	6.4
NO CO-OX AL_2O_3 WITH "Q"	SINTER	3.9	2.0	5.6

*TOTAL # OF PARTICLES
TOTAL # OF CLUMPS

TABLE DPF-16

AGGREGATE SIZE MEASUREMENTS*

VARIABLE OXIDATION BASES

	OXID. BASE	SANDMILLED BASE	R-900 PRODUCT	R-900 PRODUCT FROM SANDMILLED BASE
ANTIOCH	4.4	4.1	2.6	2.1
JV LINE II	4.8	4.5	2.5	3.0
JV LINE I	5.8	5.7	3.6	2.4
EM LINE II	7.0	6.1	5.0	2.9
EM LINE II W/CO-OX P_2O_5	5.3	4.2	3.5	3.0

*ARI VALUES

FIGURE DPF-22

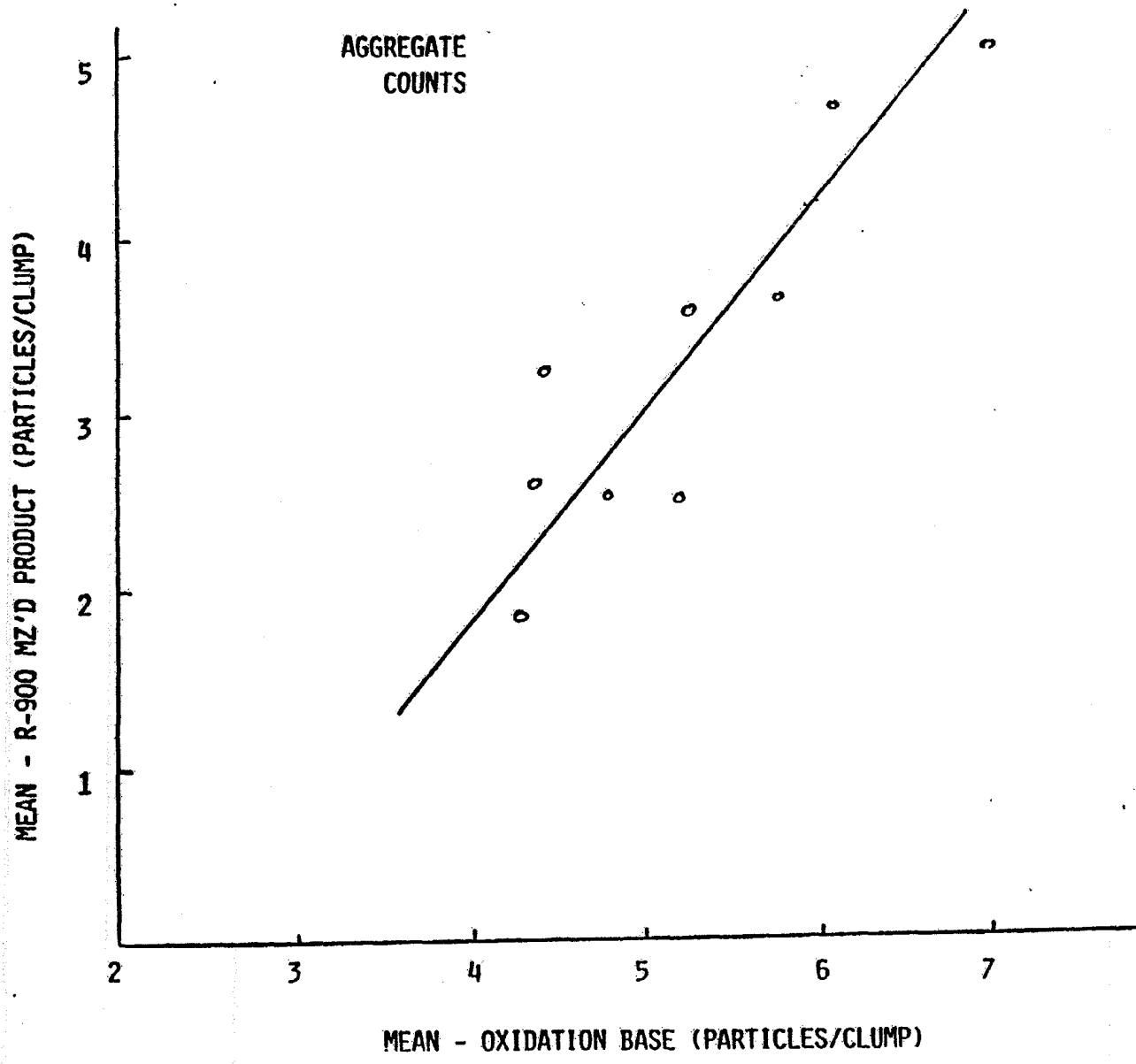

TABLE DPF-17

CLUMP SUMMARY

OXIDATION BASE	PARTICLES PER CLUMP MEAN	MEDIAN BY NUMBER	MEDIAN BY WEIGHT
AS IS (SEDIGRAPH)	-	-	16.5
SONICATED (SEDIGRAPH)	-	-	7.5
PETRONATE (TEM)	4.4	1.6	6.4
R-900 MZ'D PRODUCT (TEM)	2.6	1.2	3.1
END USE SYSTEMS			
EMULSION GLOSS PAINT (R-900-78 GLOSS)	3.4	1.9	4.2
AUTOMOTIVE GLOSS PAINT (R-900-78 GLOSS)	2.5	1.2	2.8
VINYL PLASTICS (R-100)	2.0	1.2	2.1

AGGREGATION IS A COARSE TAIL PROBLEM AND NOT A PRIMARY AGGREGATION PROBLEM (LOW MEDIAN BY NUMBER)

TABLE DPF-18

HIDING POWER - AGGREGATION

SERIES II

COMMERCIAL HIGH GLOSS R-900 PRODUCTS

PRODUCT*	PROCESS	AUTO. GLOSS	EMULSION GLOSS	EMULSION HP	EMULSION CBU	AGGR. SIZE	VINYL TS	VINYL Δ UT**
TIOXIDE RHD-6X	S	82	78	102	13.5	3.0	109	-0.016
TIOXIDE RTC-90	C	79	76	102	13.5	4.2	107	-0.007
K-M CR-800	C	77	74	103	15.7	2.8	110	0.000
NJZ RF-30	C	75	71	99	11.7	2.4	106	-0.017
GLIDDEN RCl-9	C	78	71	102	13.3	2.5	107	-0.016
AM CYAN OR-600	S	79	74	98	11.3	2.6	99	-0.028
NL 2090	S	78	72	99	14.2	2.8	102	-0.014
DU P - ANTIOCH R-900	C	78	76	103	12.5	2.8	102	-0.024
DU P - JV R-900	C	81	79	102	12.8	2.9	105	-0.026
DU P - DeL R-900	C	79	77	101	13.5	2.4	103	-0.022

*SIGNIFICANT DIFFERENCES IN OA, HYDROUS Al_2O_3, SURFACE AREA, ETC.

**FROM R-101 STD

TABLE DPF-19

HIDING POWER - AGGREGATION STUDIES

SERIES III

JV R-101 DD - VARIABLE LAB MZ ENERGY

SAMPLE	DESCRIPTION	CBU	AGGREGATE SIZE*	VINYL TS	VINYL UT
1	NO MZ'ING	11.9	4.3	91.5	1.005
2		12.2	2.5	103	1.009
3		12.2	2.9	107	1.011
4	INCREASING GRINDING	12.1	1.5	108	1.010
5	ENERGY	12.2	2.9	109	1.015
6		12.1	2.7	110	1.016
7		12.6	2.2	111	1.017
8	S/P≅12	12.0	2.5	111	1.013

*IN VINYL

TABLE DPF-20

HIDING POWER - AGGREGATION STUDIES

JV R-101 WORK

ASSUMPTIONS

- ORIGINAL - IMPROVE HP BY DECREASING AGGREGATE SIZE (4→1)
- NEW - IMPROVE HP BY GETTING RID OF COARSE OVERSIZE
  ASSUME CLUMPS >0.5μ DO NOT SCATTER LIGHT

SERIES III

VINYL TS	% >0.5μ (SEDIGRAPH)
91.5	25.0
103.0	12.0
107.0	10.0
108.0	8.0
109.0	7.0
111.0	5.5

NORMALIZE DATA FOR 111 MAXIMUM HP

VINYL TS	% >0.5μ	NORMALIZED % >0.5μ	PREDICTED VINYL TS (MAX - NORMAL GRIT)
91.5	25.0	19.5	91.5
103.0	12.0	6.5	104.5
107.0	10.0	4.5	106.5
108.0	8.0	2.5	108.5
109.0	7.0	1.5	109.5
111.0	5.5	0.0	111.0

TABLE DPF-21

AGGREGATE COUNTS - PAINT FILMS
(DUPONT)

AUTOMOTIVE GLOSS (30J) ~15 PVC	MEAN CLUMP SIZE	EST. ARI CLUMP SIZE
56 GLOSS	2.0	3.0
67 GLOSS	2.0	2.9
78 GLOSS	1.9 1.7	2.6 2.5A
EMULSION GLOSS (TFW-180) ~22.8 PVC		
52 GLOSS	5.5	7.6
69 GLOSS	2.8	4.5
78 GLOSS	2.7 2.5	4.4 3.4A

AACTUAL ARI COUNT

AGGREGATE COUNTS - PLASTIC FILMS
(DUPONT)

MEDIUM HARD POLYVINYLCHLORIDE (~1 PVC)		
R-900, COMPETITIVE PRODUCTS	MEAN CLUMP SIZE	EST. ARI CLUMP SIZE
TIOXIDE RHD6X TC 9635	1.6	2.0
TIOXIDE RTC-90 TC 9533	1.8	2.6
KERR-MCGEE CR-800 TC 9548	1.5	1.7
GLIDDEN RCL-9 TC 9482	1.5	1.7
N L 2090 TC 9621	1.7	2.3
R-900 4193	1.6	2.0
VARIABLE PVC		
R-900 4193 @ 0.5 PVC	1.5	1.7
R-900 4193 @ 1.0 PVC	1.5	1.7
R-900 4193 @ 9 PVC	2.4	3.9

TABLE DPF-22

AGGREGATE MEASUREMENTS
TEM COUNTING

	AGGREGATE SIZE (PARTICLES/CLUMP)
TIO2 PIGMENT (ENAMEL TYPE)	
RAW TIO2	3 - 4
FINISHED PRODUCTS	2 - 3
TIO2 END-USES (R-900)	
EMULSION ENAMEL (23 PVC)	2.7
AUTOMOTIVE ENAMEL (17 PVC)	2.0
VINYL FILM (1 PVC)	1.5

FIGURE DPF-23

COMPUTER SIMULATION OF "RANDOM AGGREGATION"

2 DIMENSIONS (RANDOM X-Y GENERATOR)

CALCULATED PVC	
2.8	
5.7	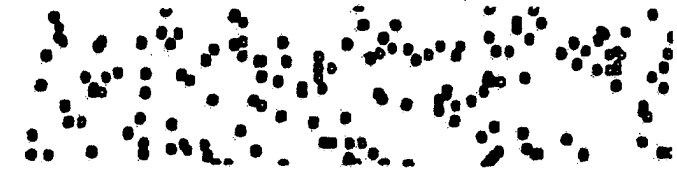
8.6	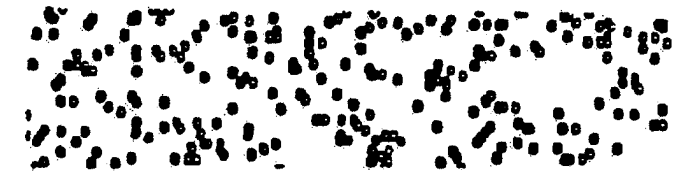
11.3	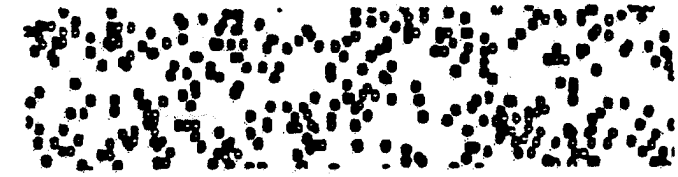
13.7	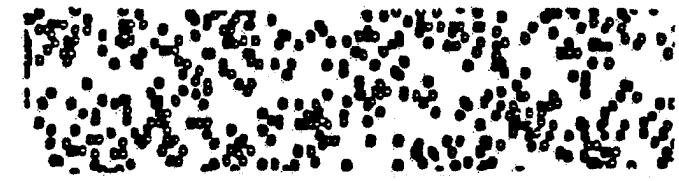
25.6	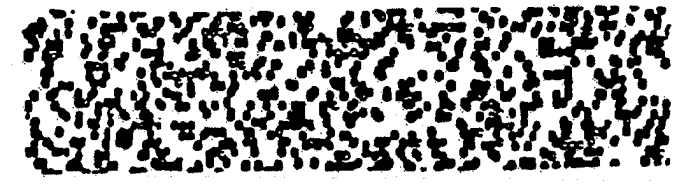
48.2	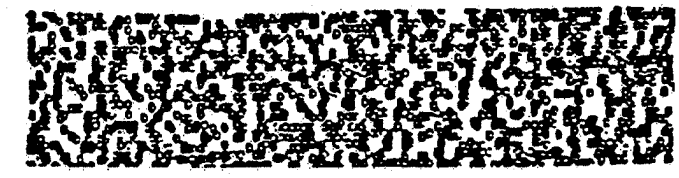

FIGURE DPF-24

RANDOM AGGREGATION AS F(PIGMENT VOLUME CONCENTRATION)

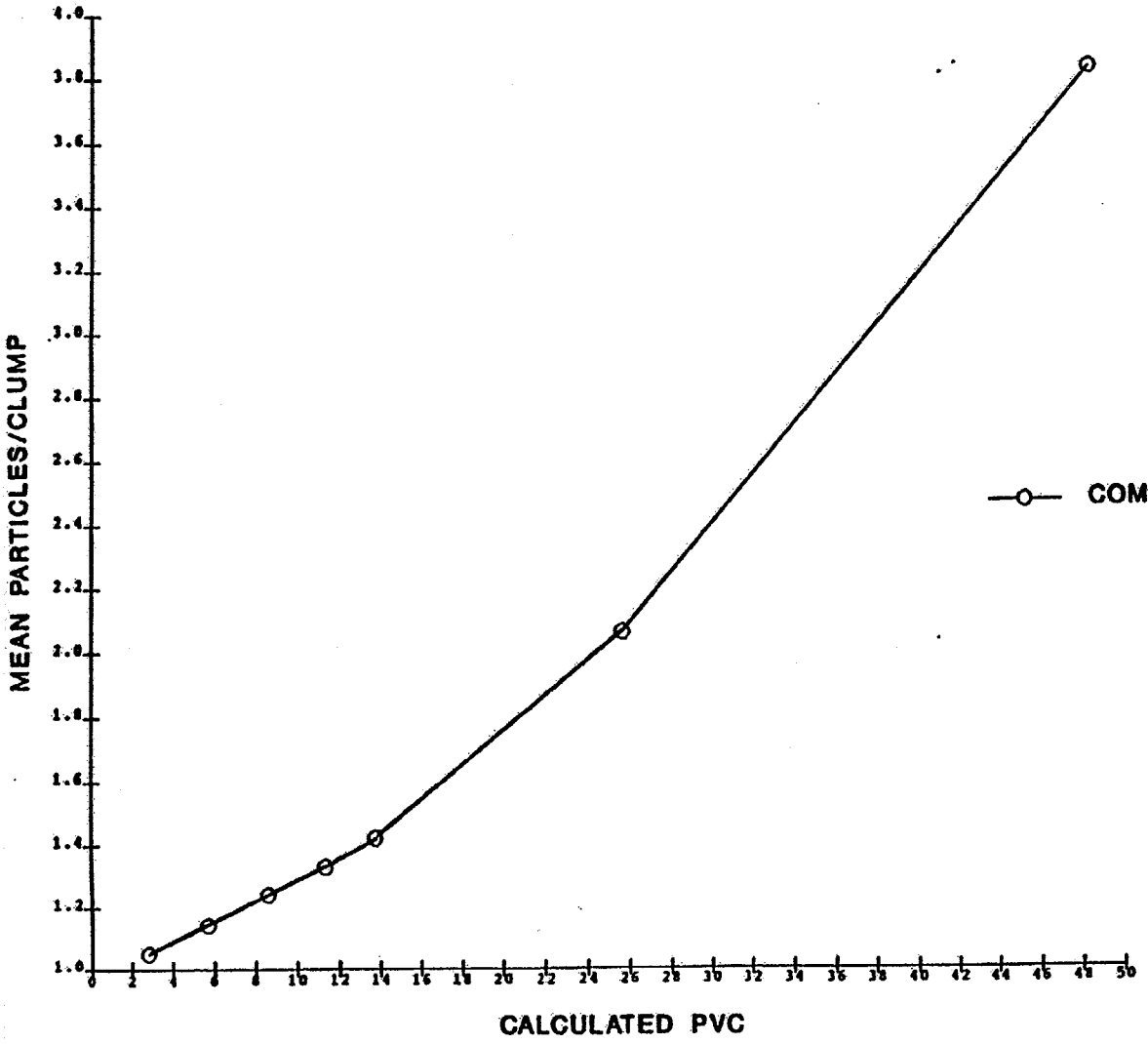

FIGURE DPF-25

TIO2 AGGREGATION AS F(PIGMENT VOLUME CONCENTRATION)

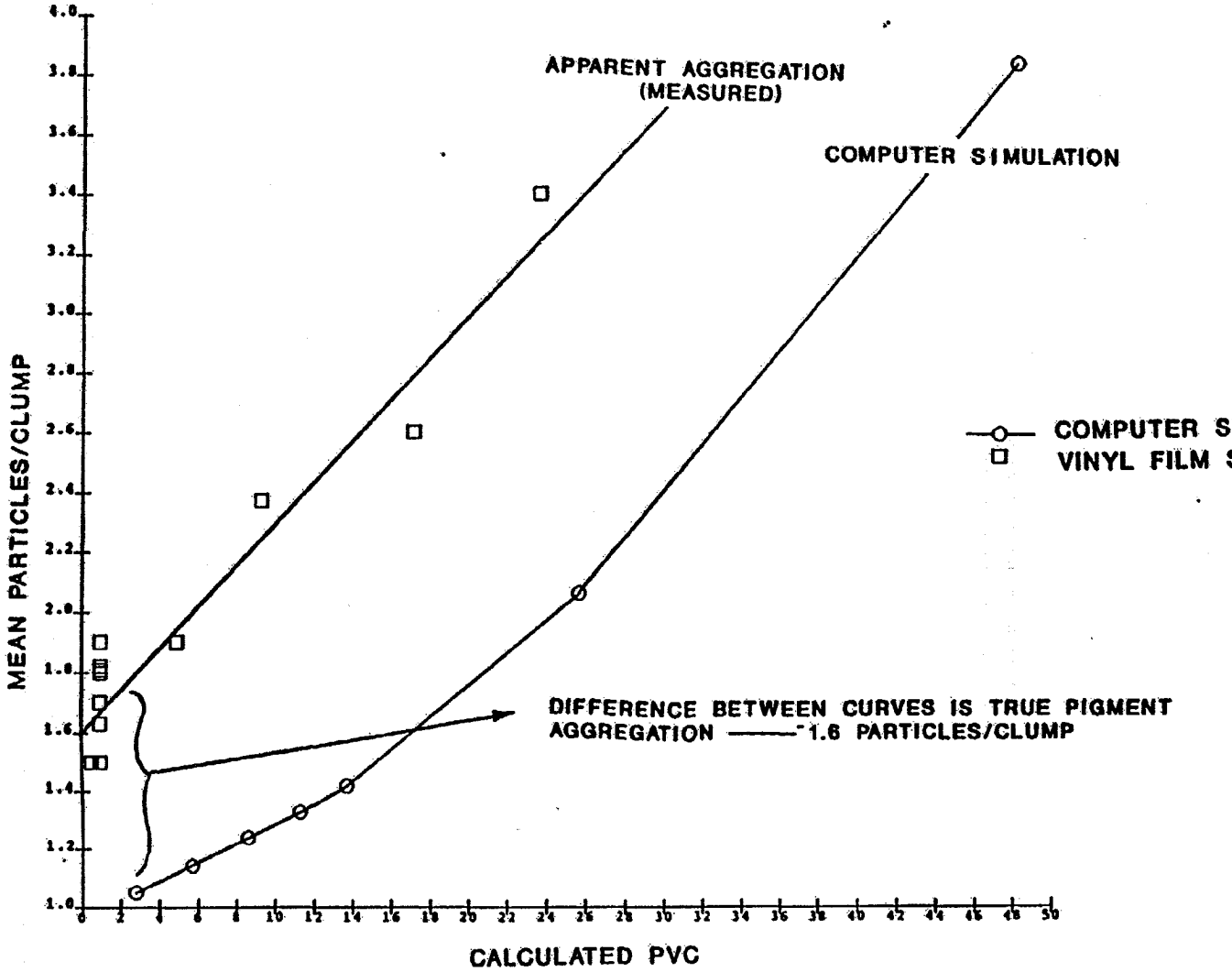

FIGURE DPF-26

TIO2 AGGREGATION AS F(PIGMENT VOLUME CONCENTRATION)

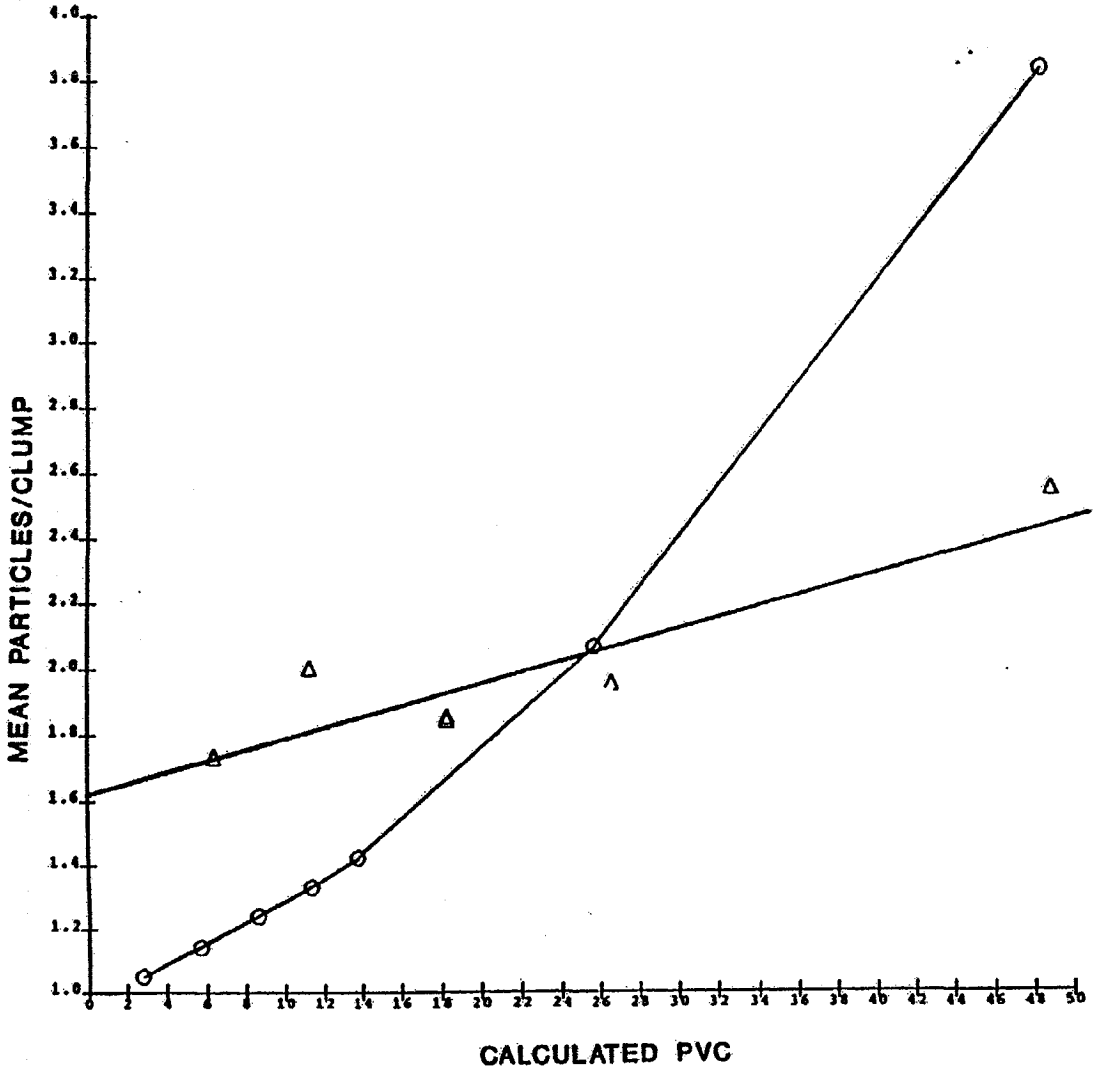

FIGURE DPF-27

TIO2 AGGREGATION AS F(PIGMENT VOLUME CONCENTRATION)

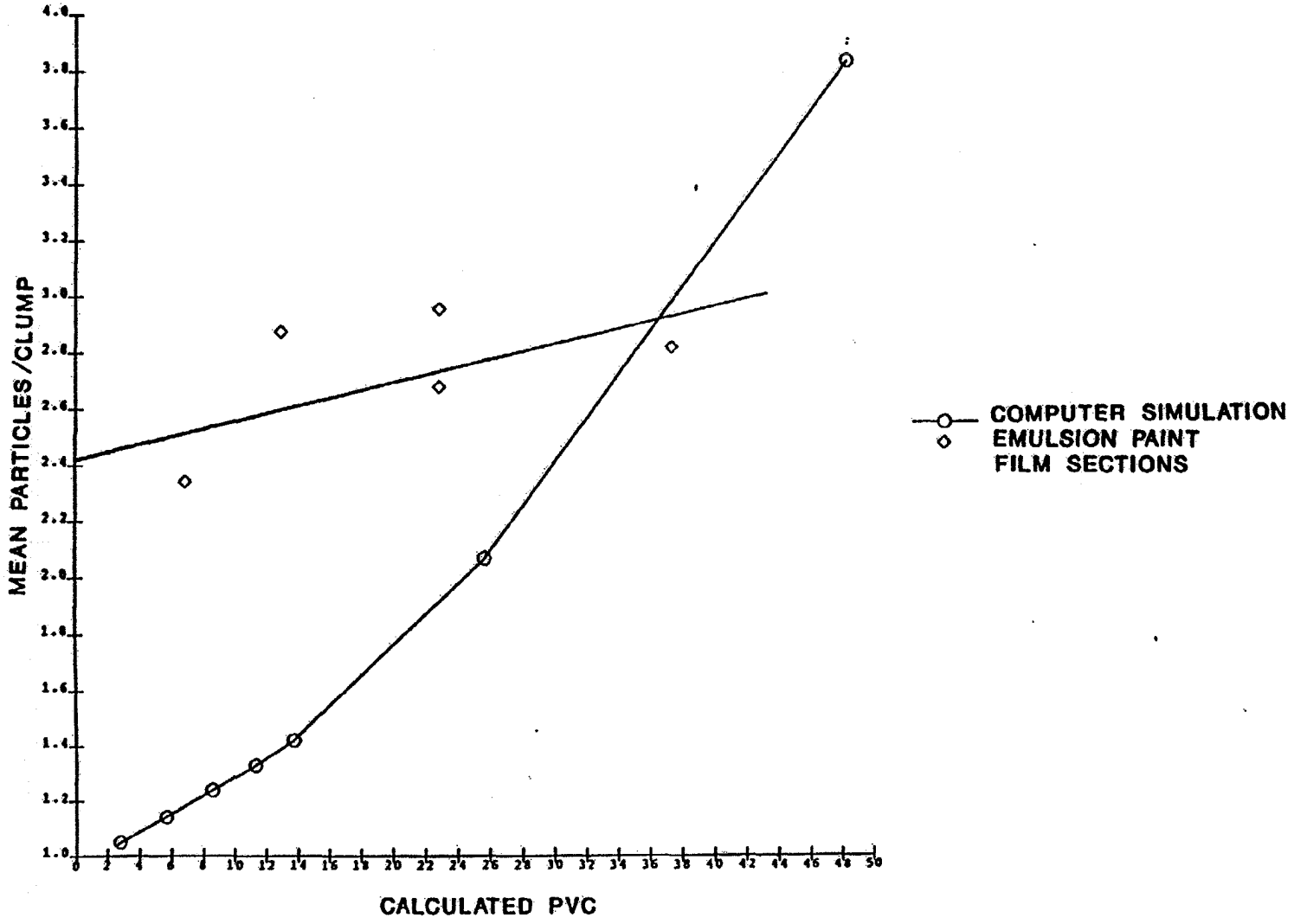

FIGURE DPF-28

PARTICLE SIZE DISTRIBUTION

SAMPLE IDENTIFICATION

Density ..... g/cc LIQUID

Preparation

Density . g/cc Viscosity . . . cp

DATE

BY

TEMPERATURE °C

RATE START DIA. µm

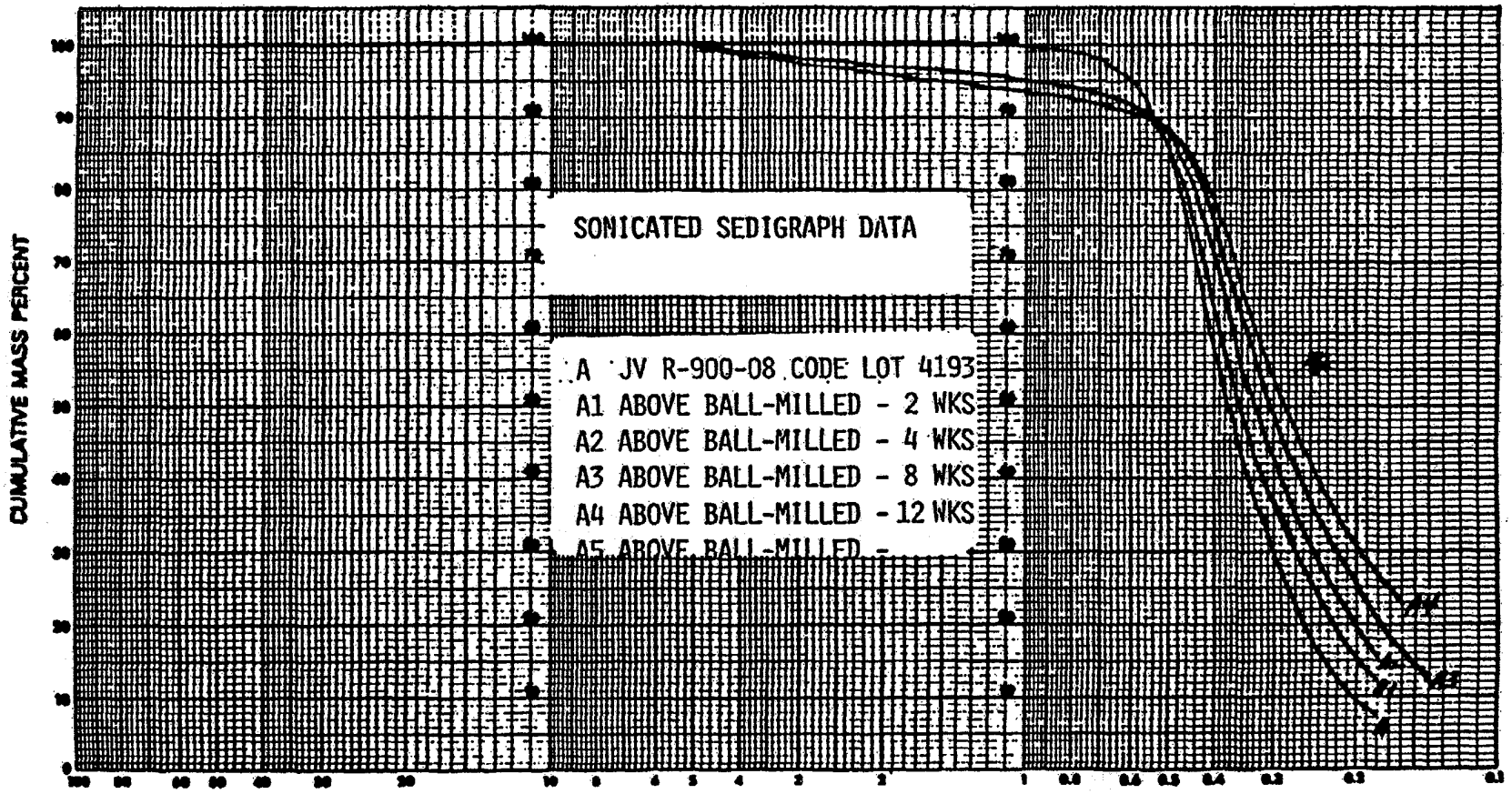

micromeritics instrument corporation

FIGURE DPF-29

PARTICLE SIZE DISTRIBUTION

SAMPLE IDENTIFICATION _____ DATE _____

Density .. ___ g/cc LIQUID. _____ Density . . g/cc Viscosity . . ___ cp BY _____

Preparation _____ TEMPERATURE _____ °C

RATE ___ START DIA. ___ µm

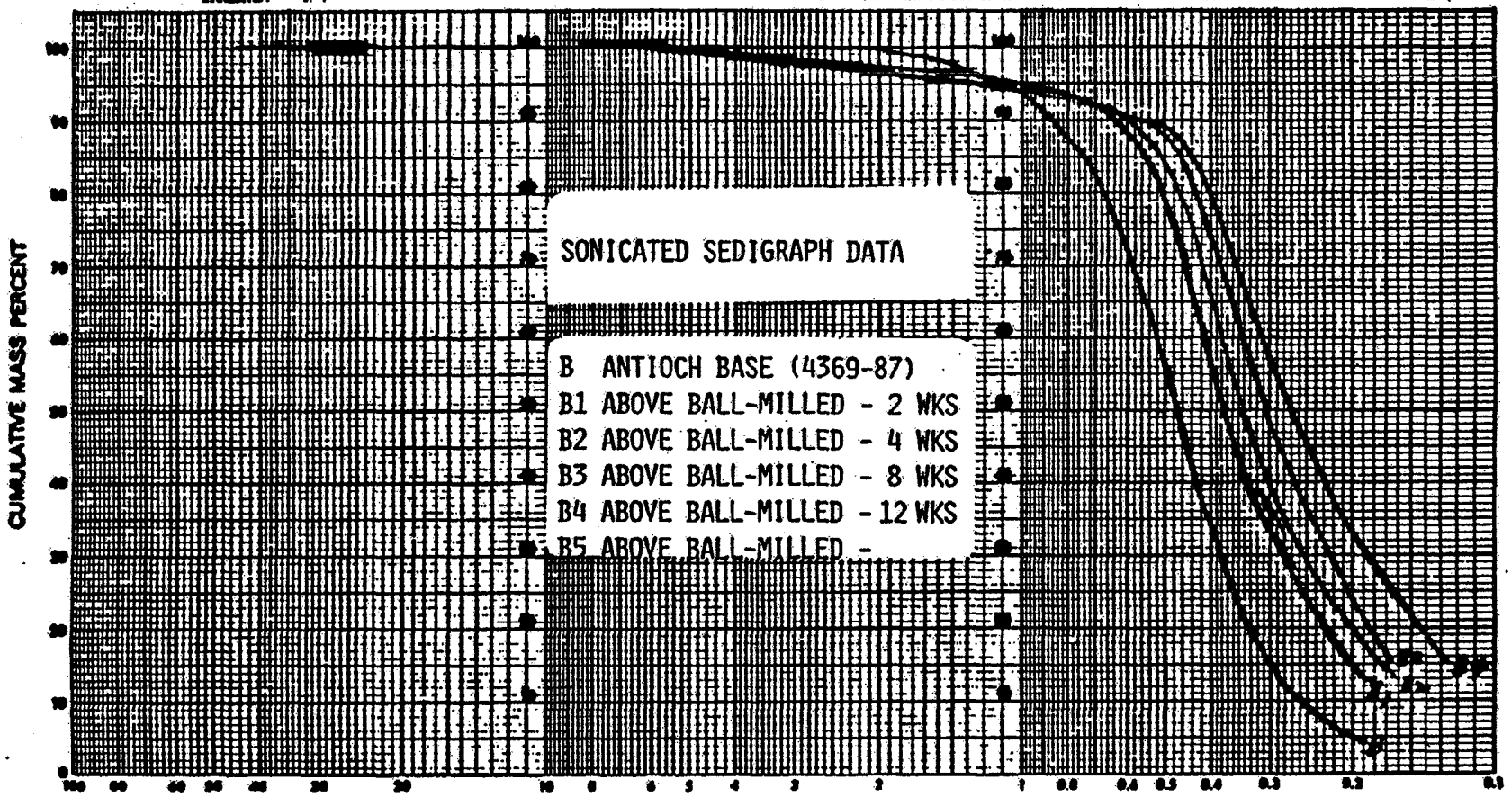

micromeritics instrument corporation

FIGURE DPF-30

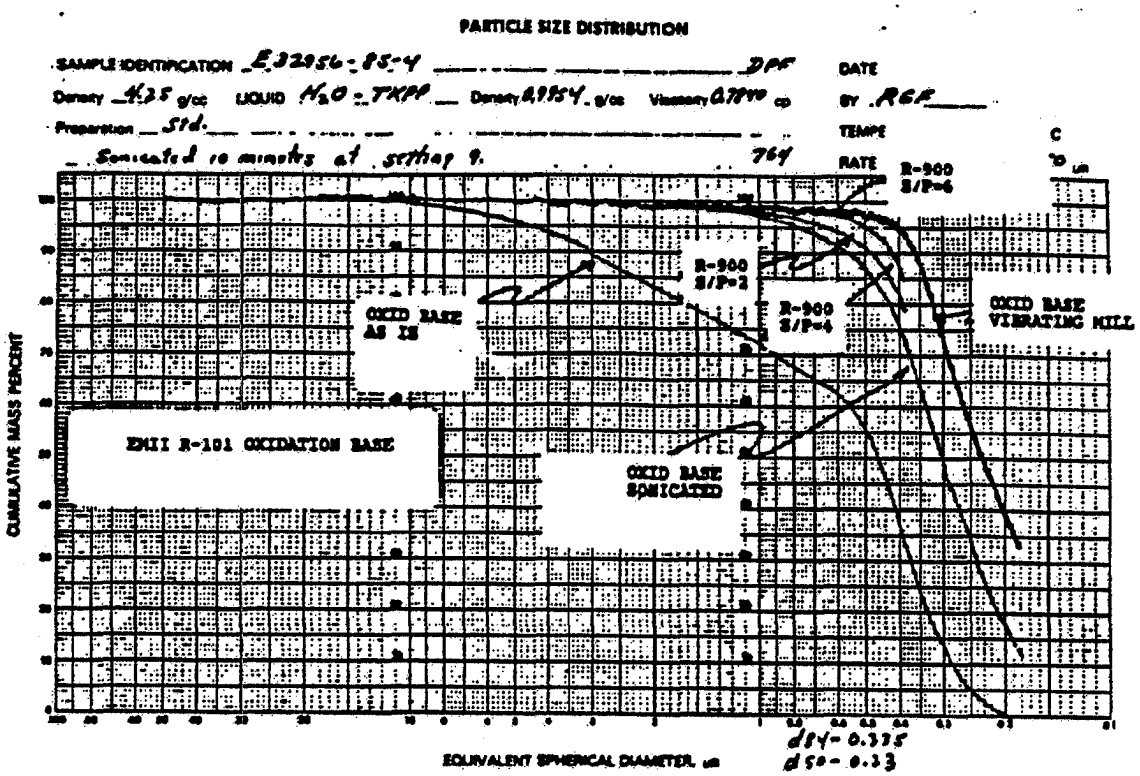

FIGURE DPF-31

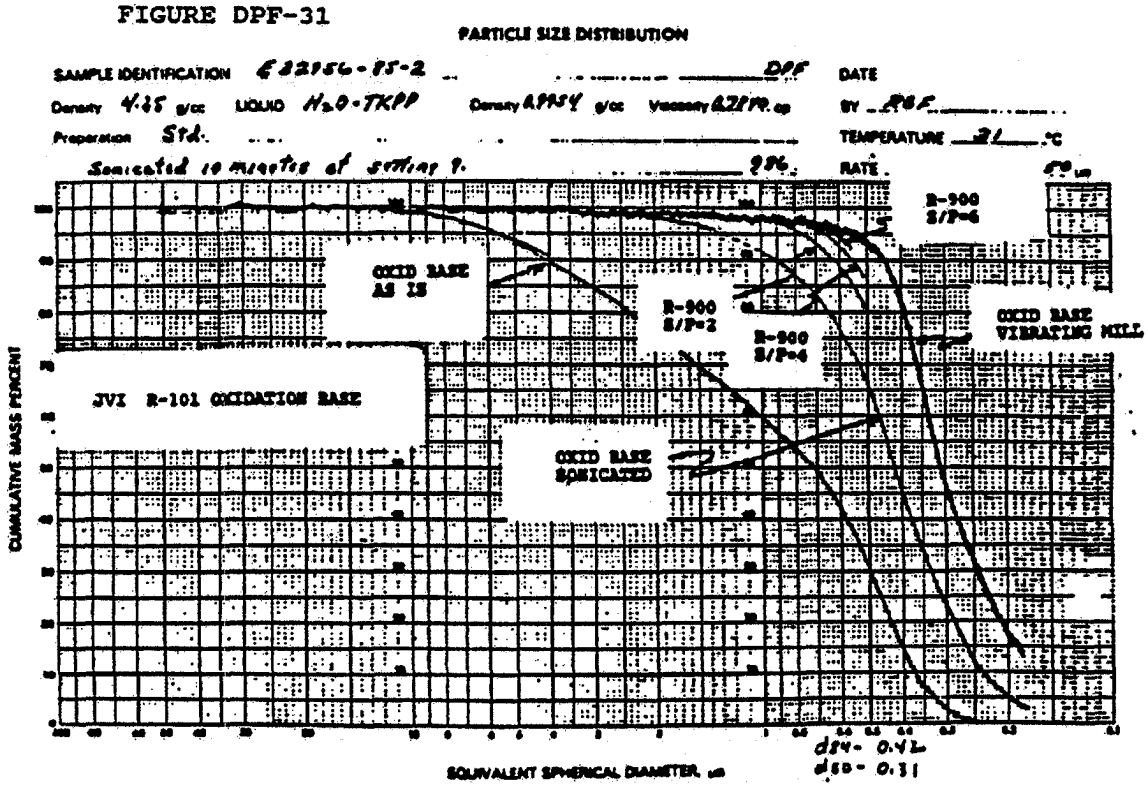

FIGURE DPF-32

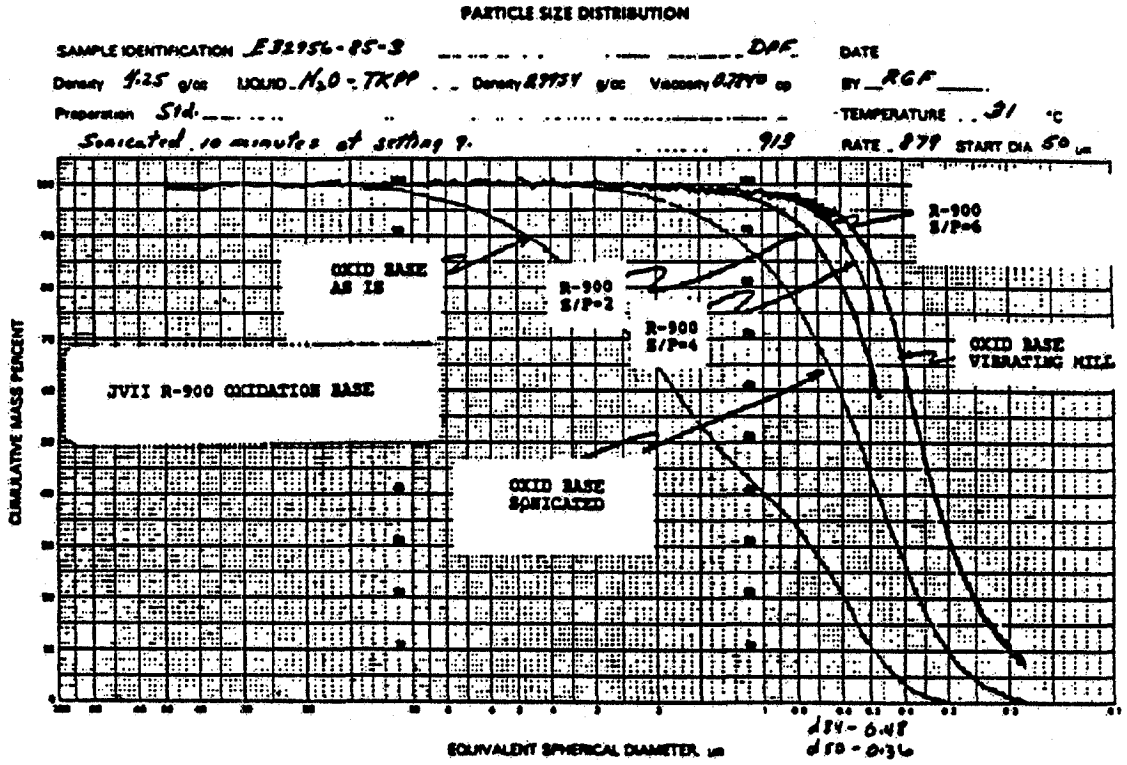

FIGURE DPF-33

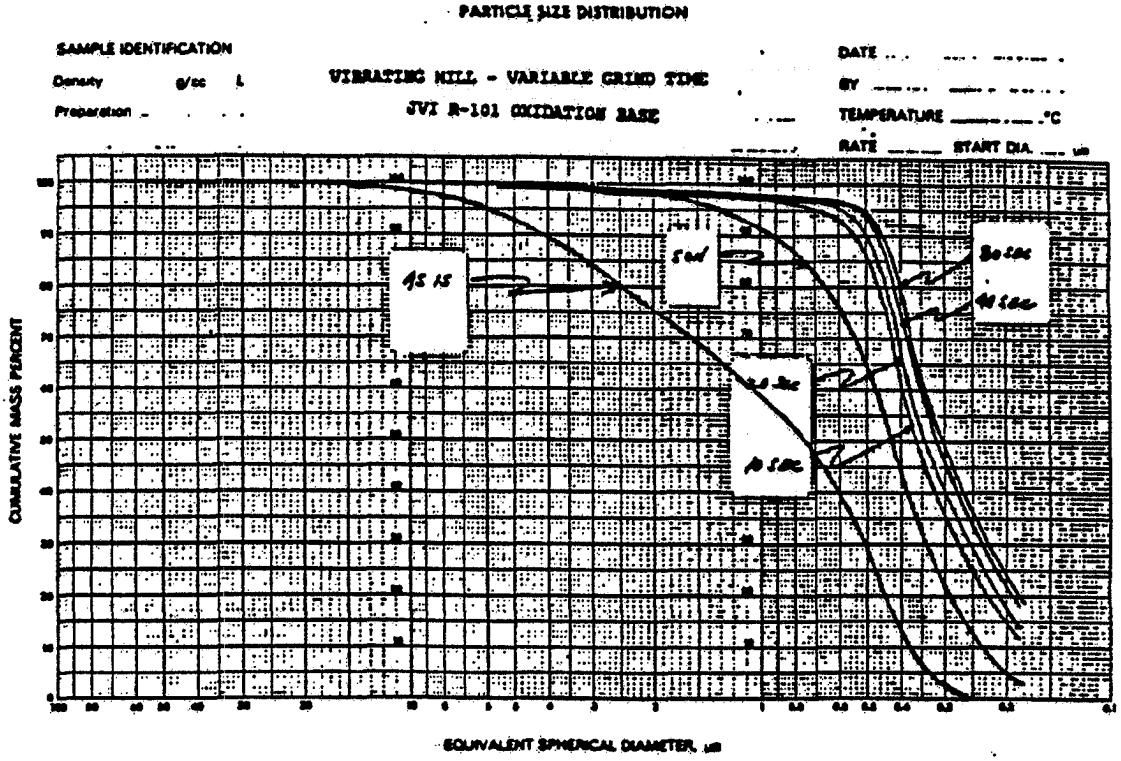

FIGURE DPF-34

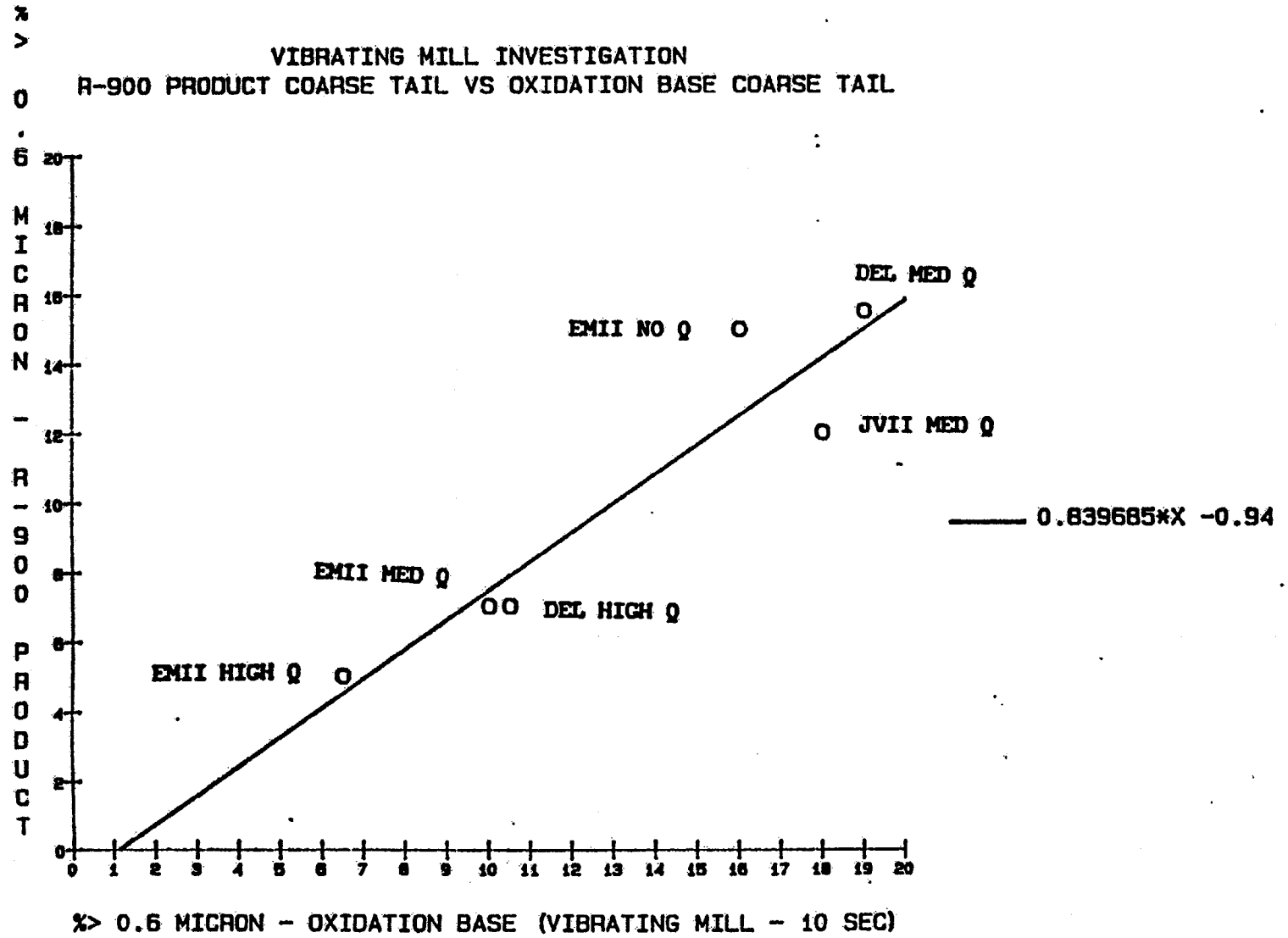

FIGURE DPF-35

R-900 FINISHED PRODUCT SIZE DISTRIBUTIONS

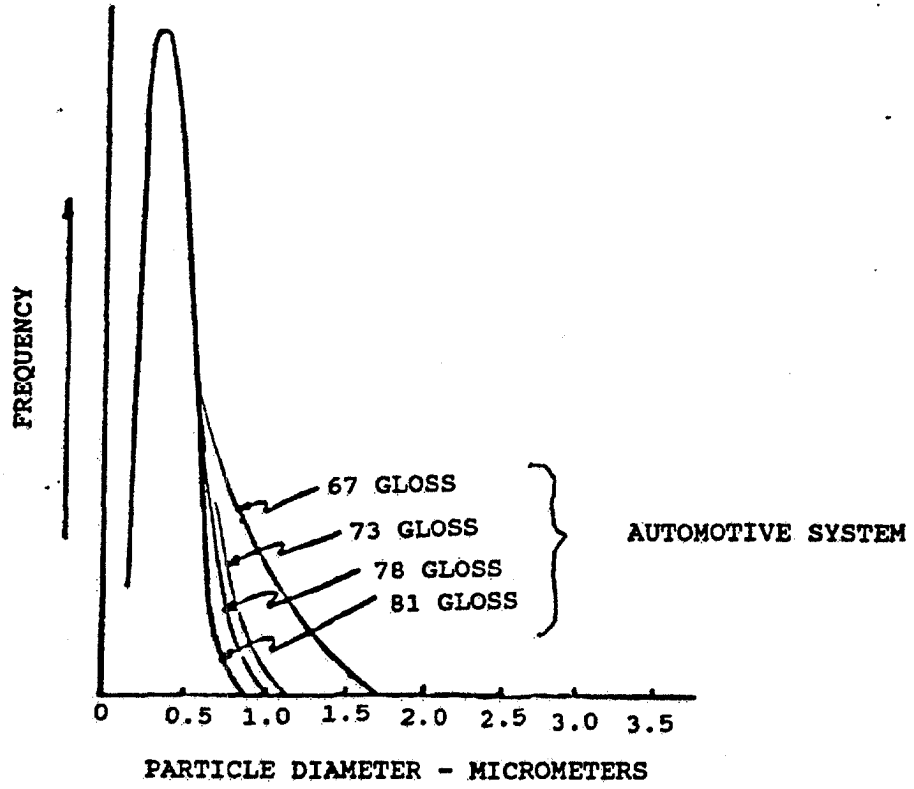

R-900 EMULSION GLOSS (TFW-180) VS. PARTICLE SIZE COARSE TAIL

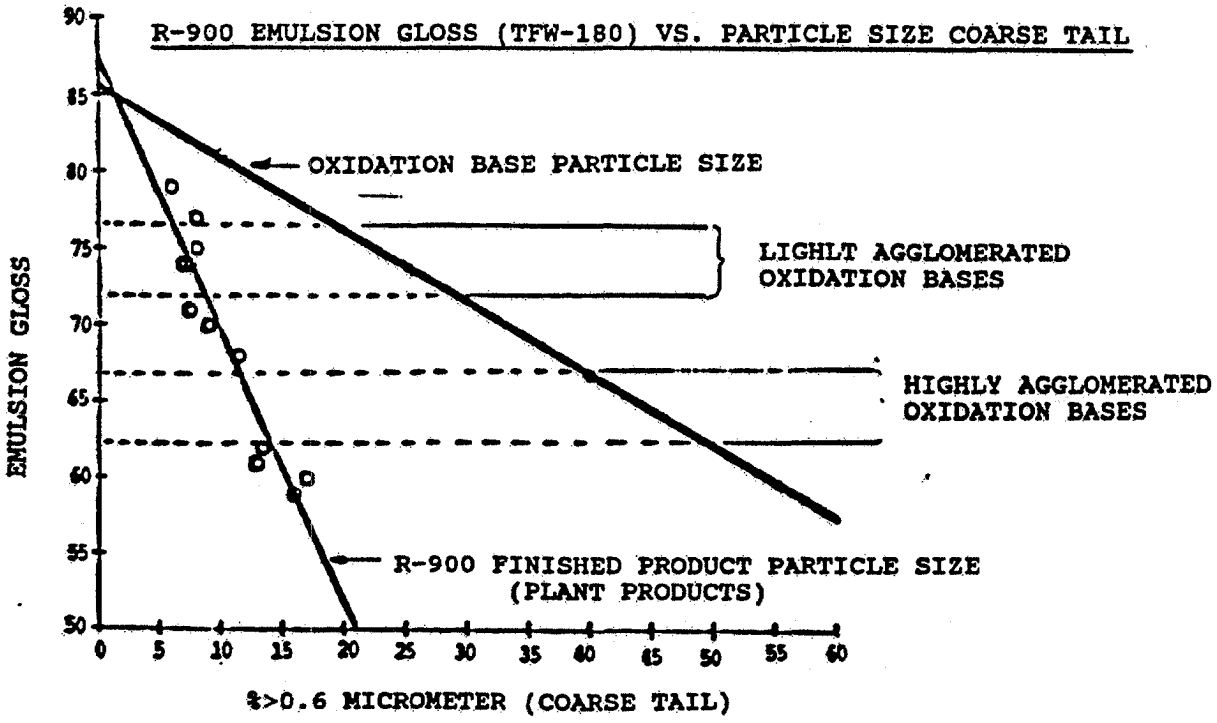

FIGURE DPF-36

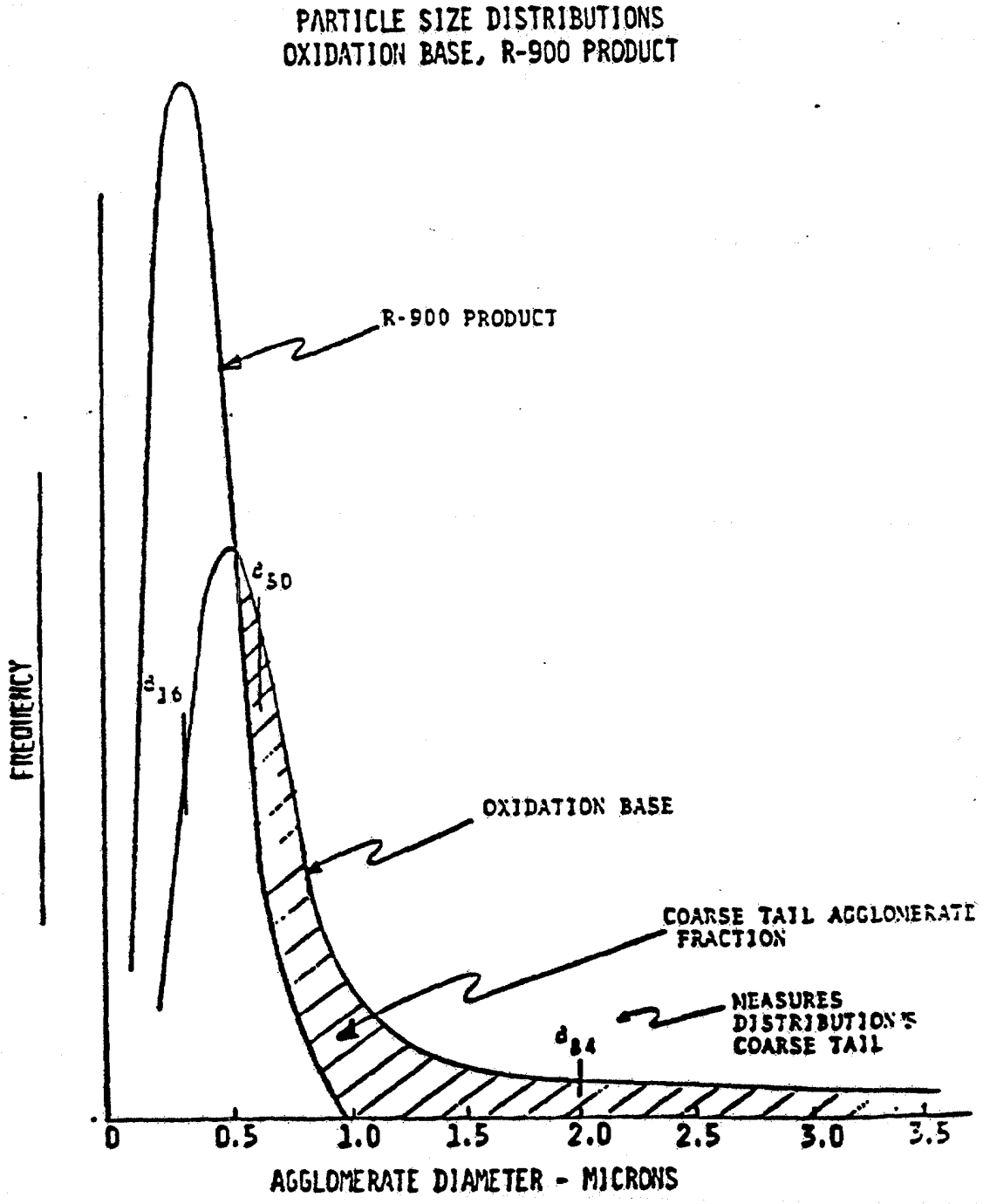

FIGURE DPF-37

OXIDATION BASE PARTICLE SIZE
EM LINE II VARIABLE CBU

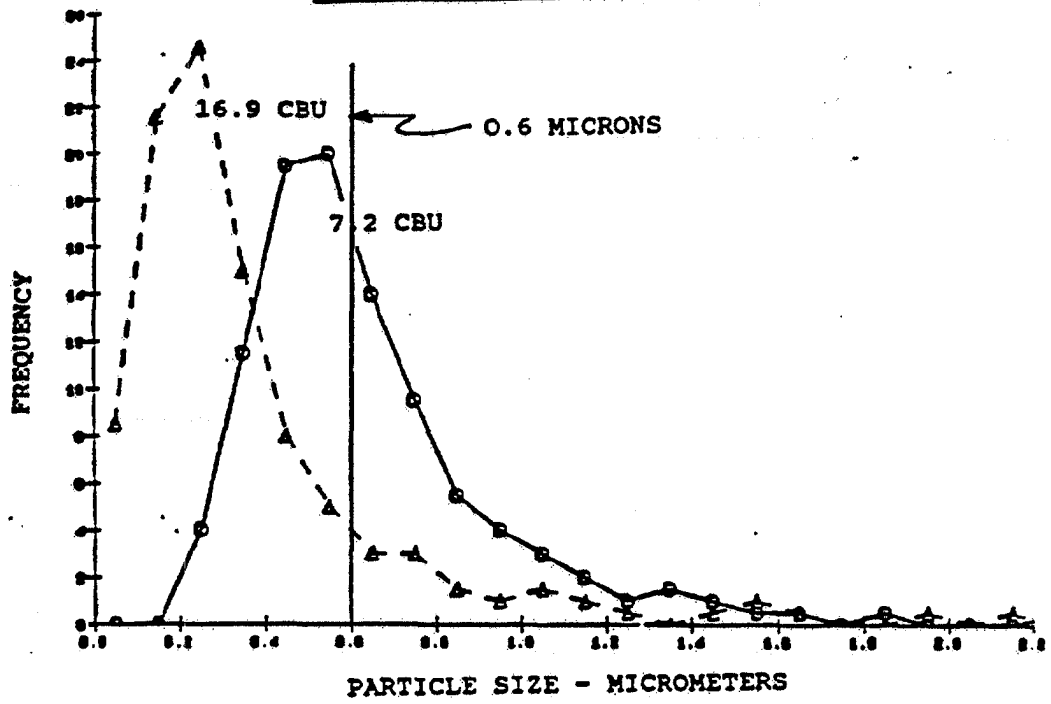

PARTICLE SIZE DISTRIBUTIONS
SEDIGRAPH DATA - VARIABLE OXIDATION LINE, CBU

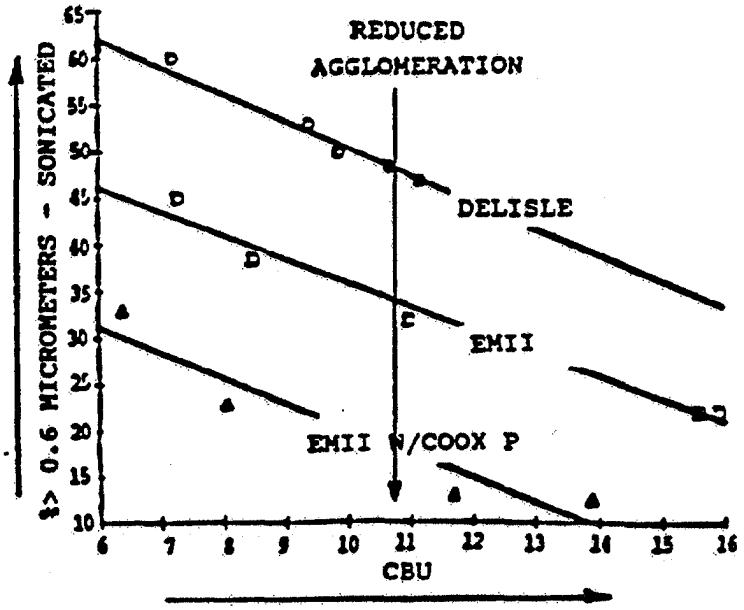

FIGURE DPF-38

OXIDATION BASE EVALUATION
COARSE TAIL VS OXIDATION RATE

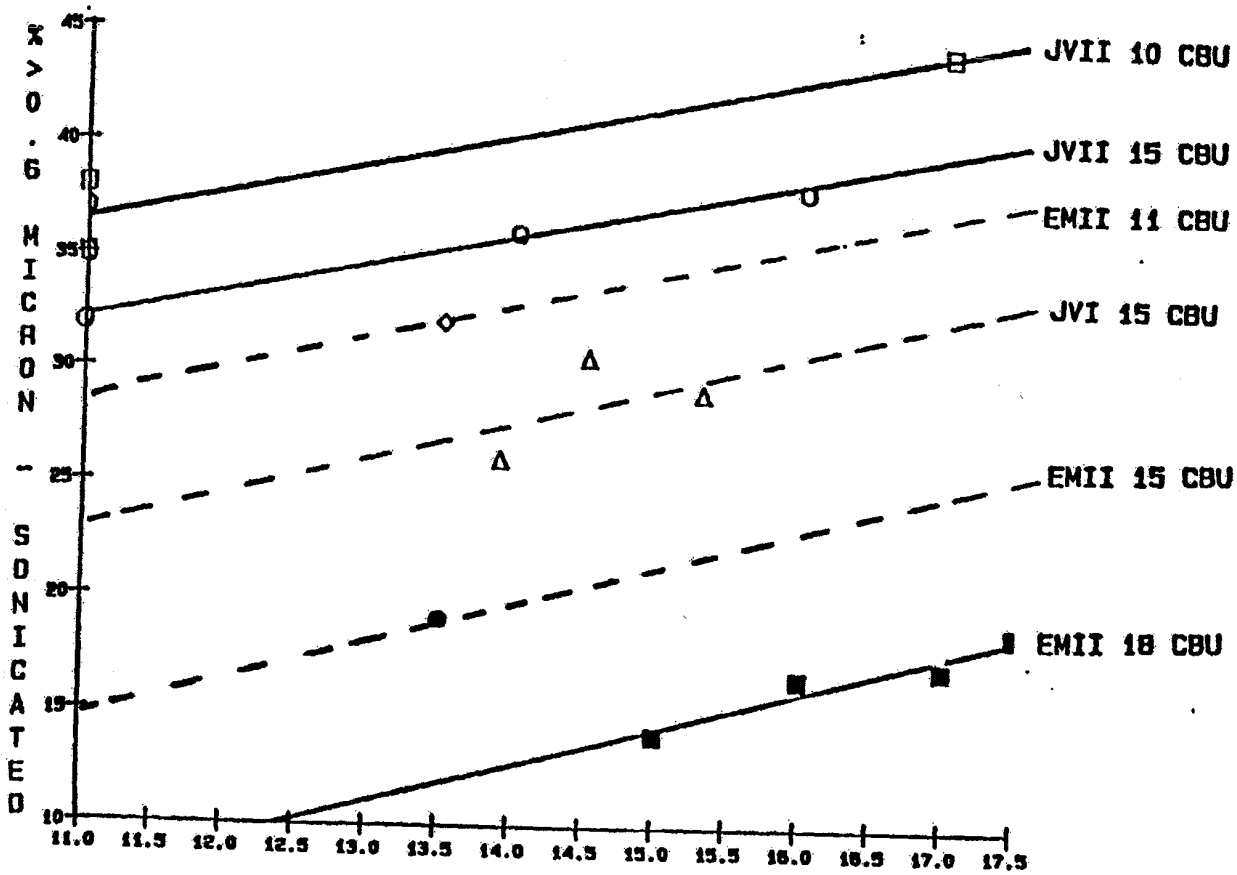

TABLE DPF-23

OXIDATION BASE WET GRINDING

SANDMILL TIME (MIN)	COARSE TAIL (%>0.6 MICRONS)	
	DEAGGLOM BASE	AGGLOM BASE
0	32	43
5	20	29
15	13	23

FIGURE DPF-39

TIO2 HIDING POWER
EFFECT OF REFRACTIVE INDEX

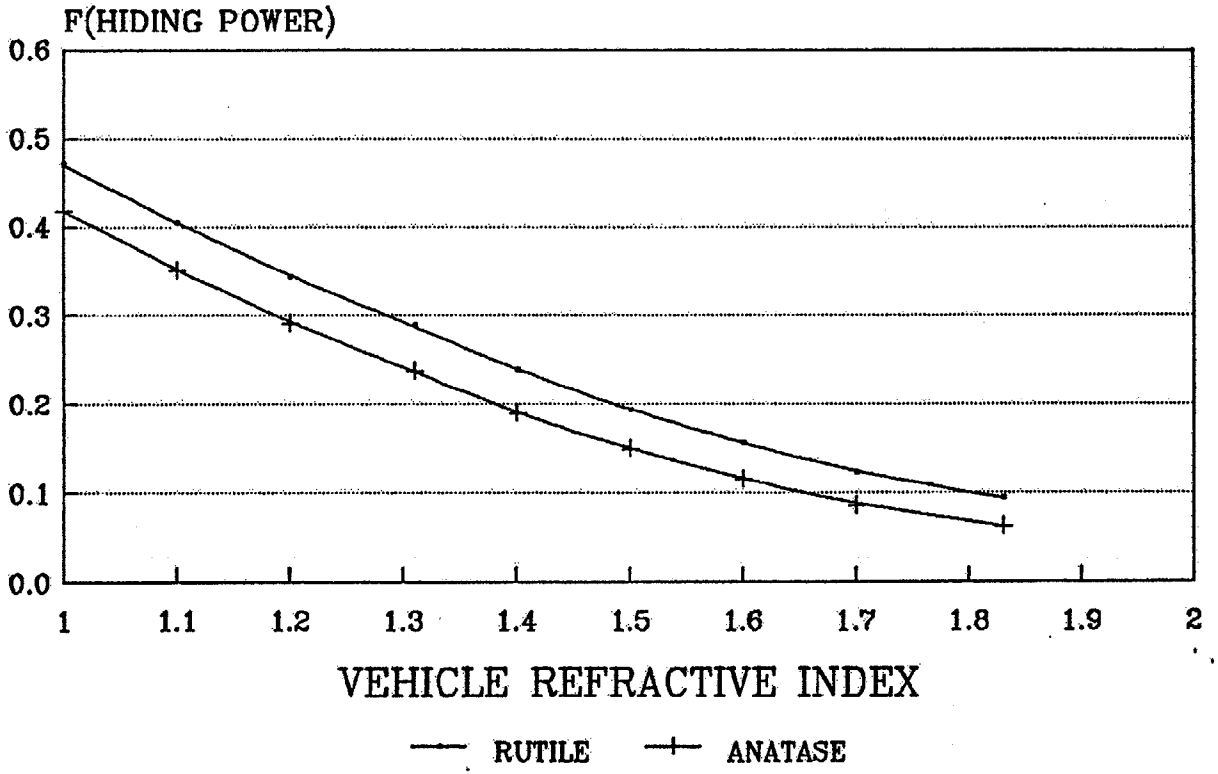

CALCULATED

FIGURE DPF-40

RUTILE TIO2 HIDING POWE

EFFECT OF REFRACTIVE INDEX

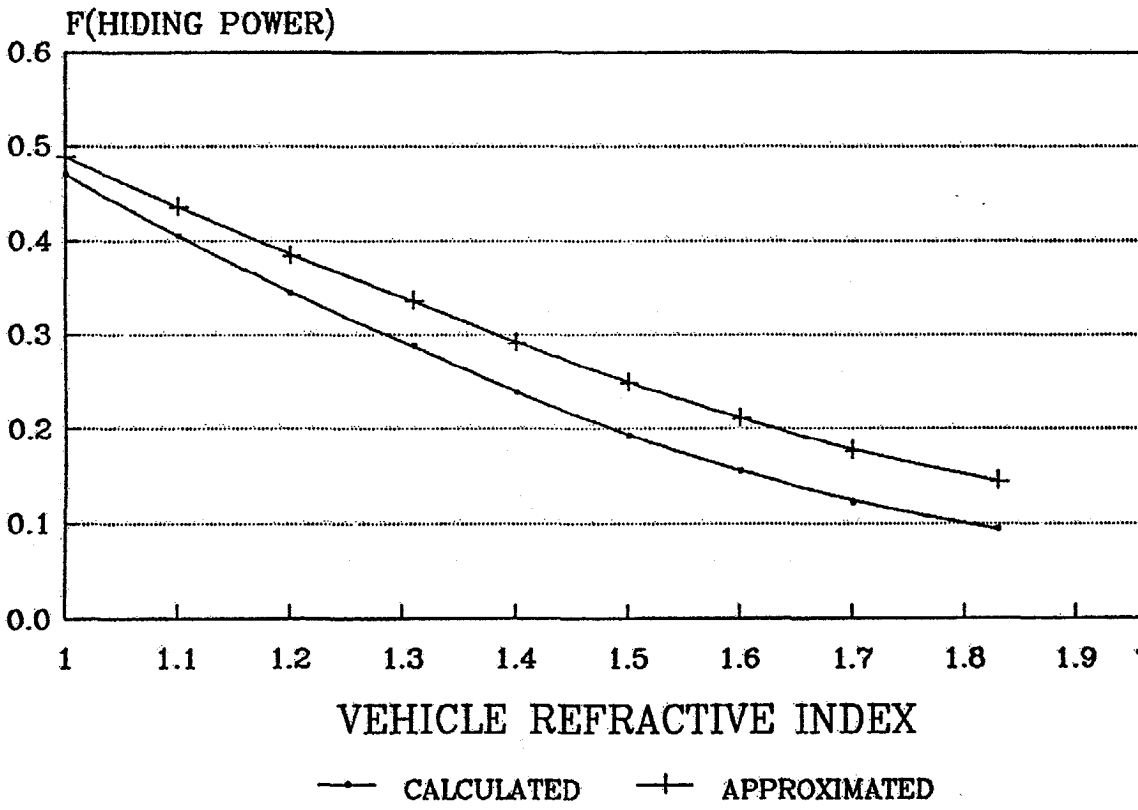

FIGURE DPF-41

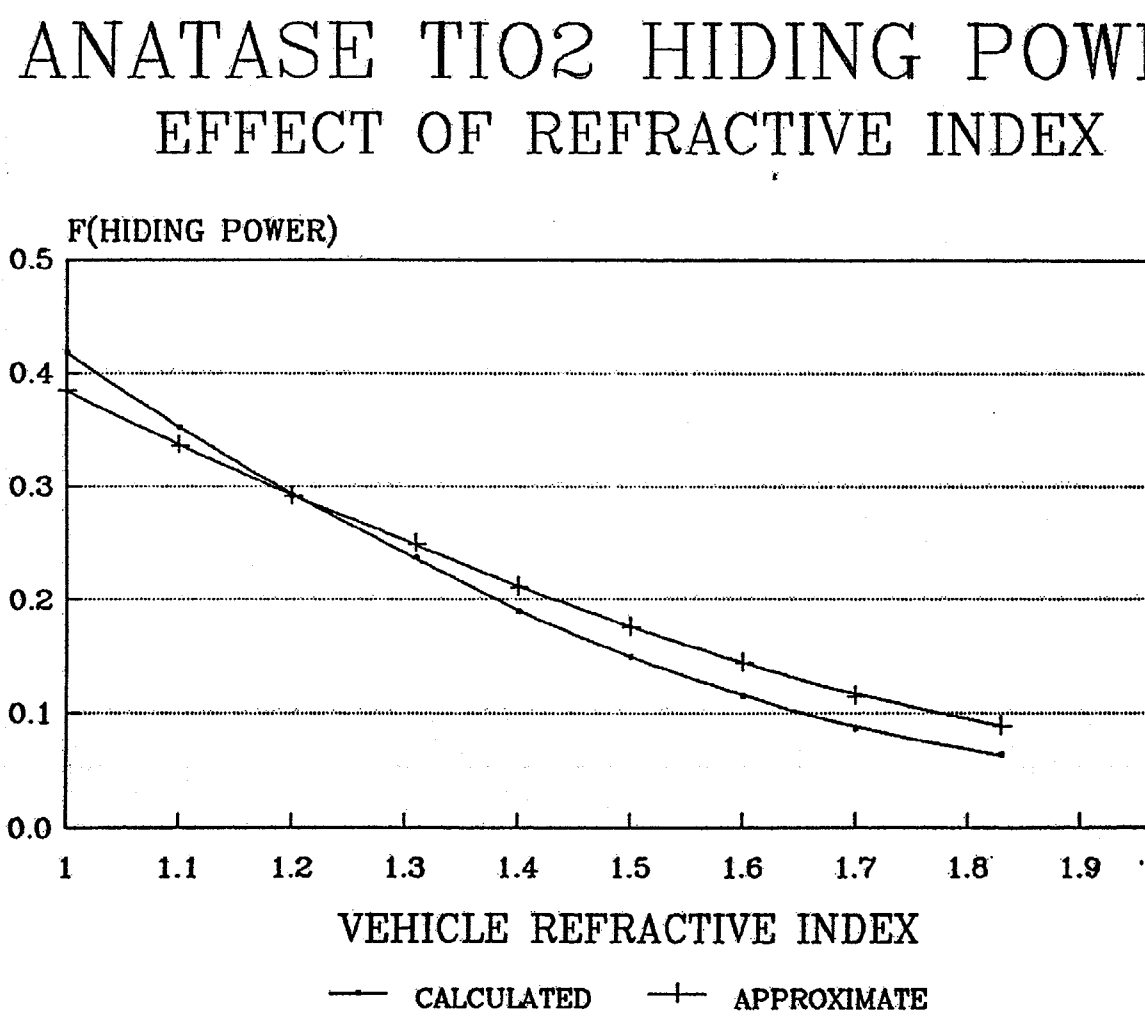

FIGURE DPF-42

OPTIMUM RUTILE DIAMETE
VARIABLE VEHICLE REFRACTIVE IND

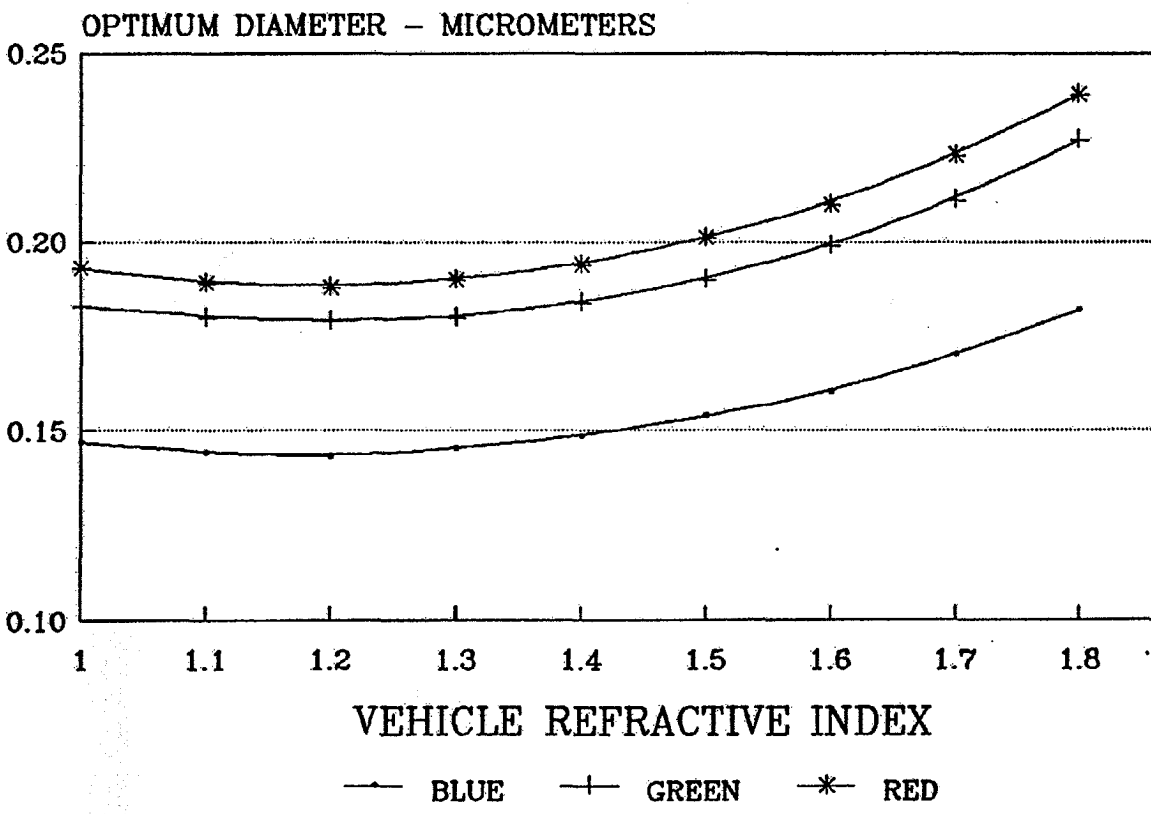

FIGURE DPF-43

TIO2 SCATTERING RELATIONSHIPS
OPTIMUM DIAMETER - REFRACTIVE INDEX

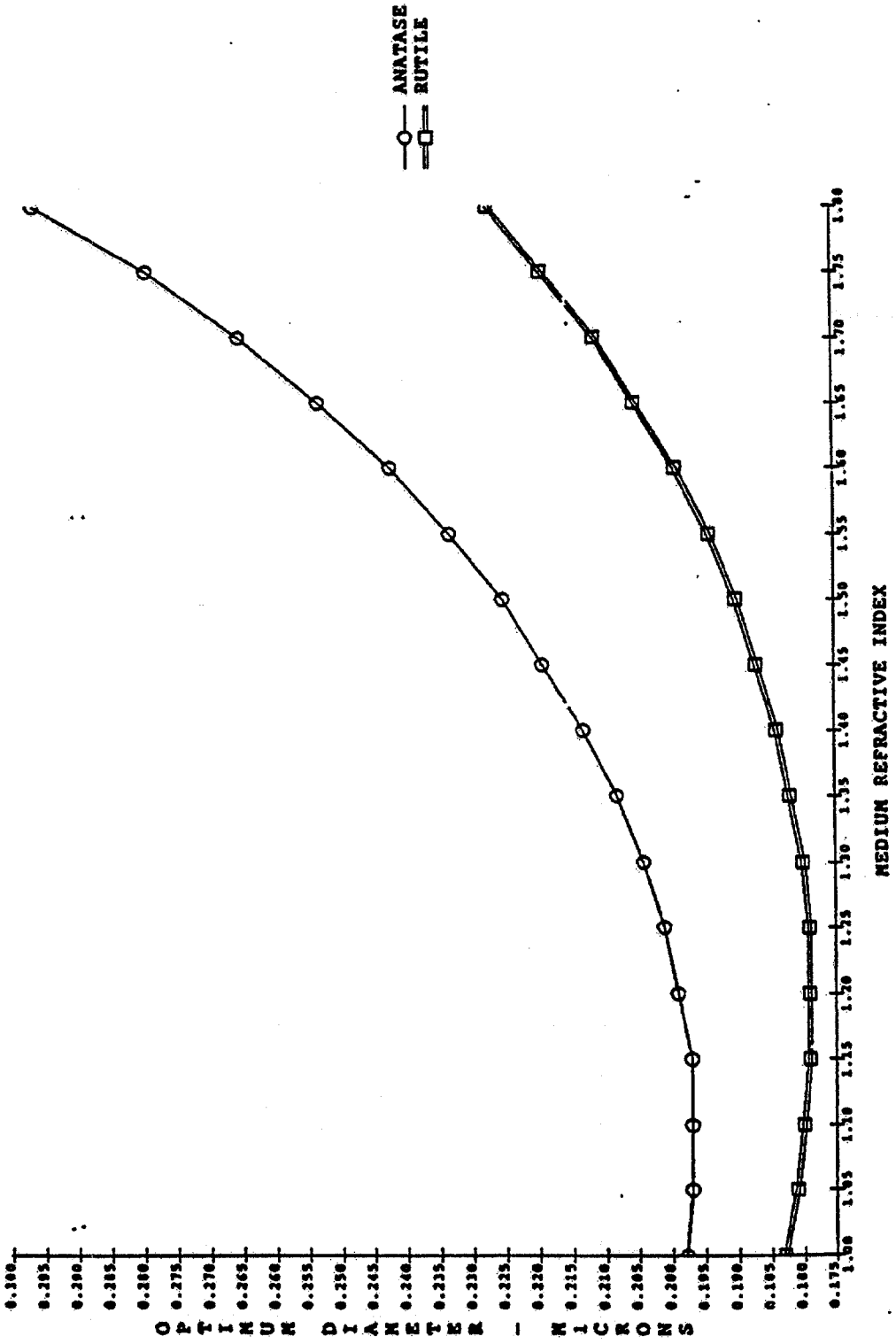

FIGURE DPF-44

OPTIMUM RUTILE DIAMETE
VARIABLE REFRACTIVE INDEX

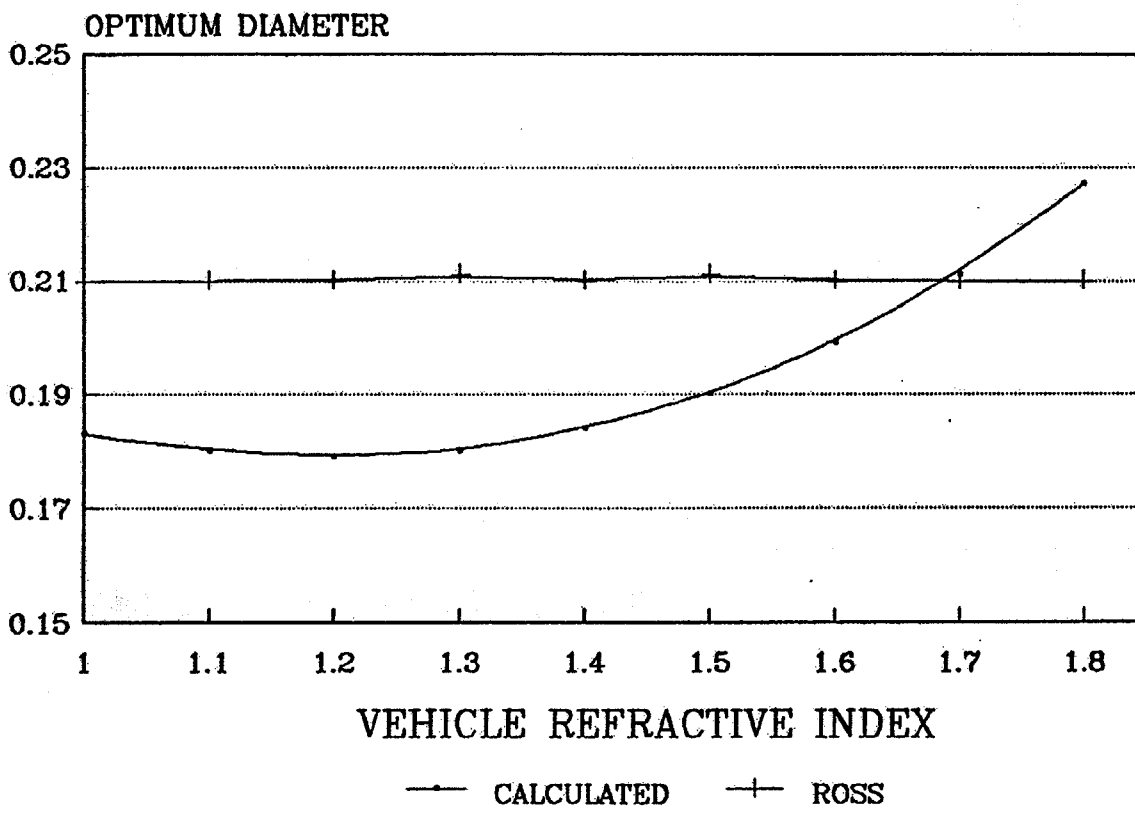

FIGURE DPF-45

MIE SCATTERING CALCULATIONS
ROSS CURVE FITS

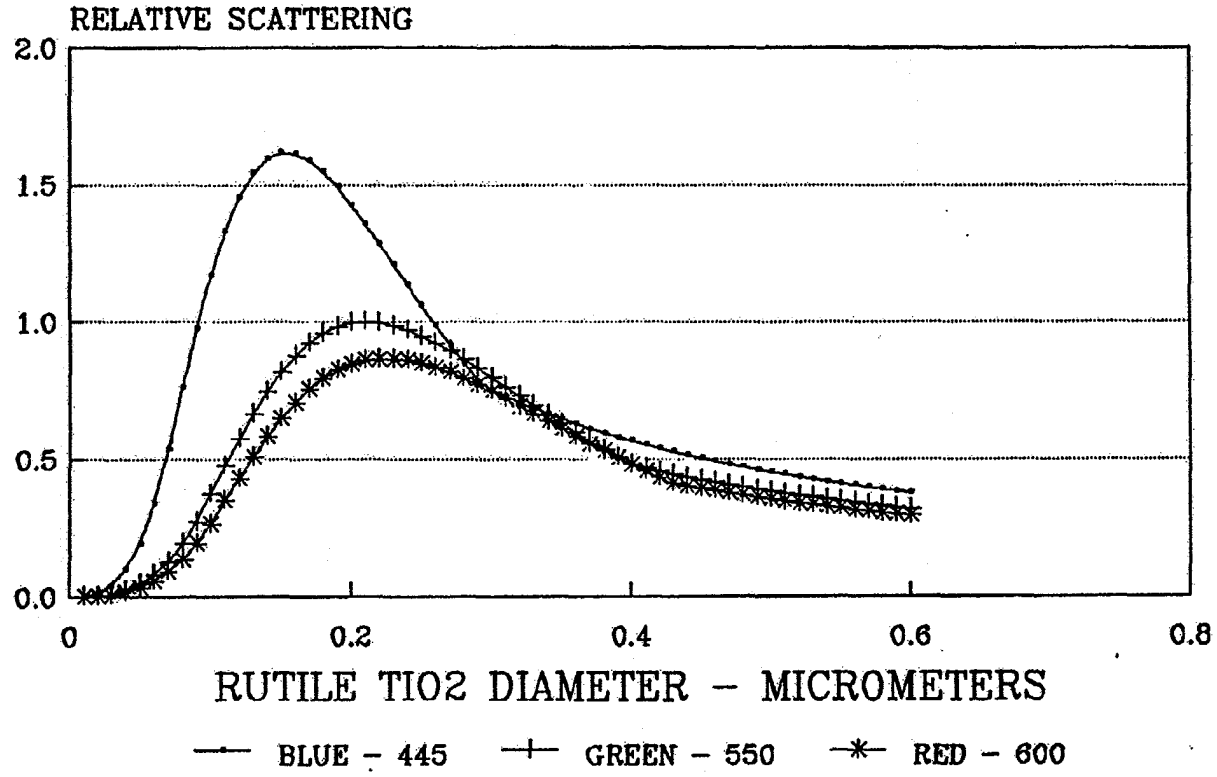

1.514 MEDIUM RI

FIGURE DPF-46

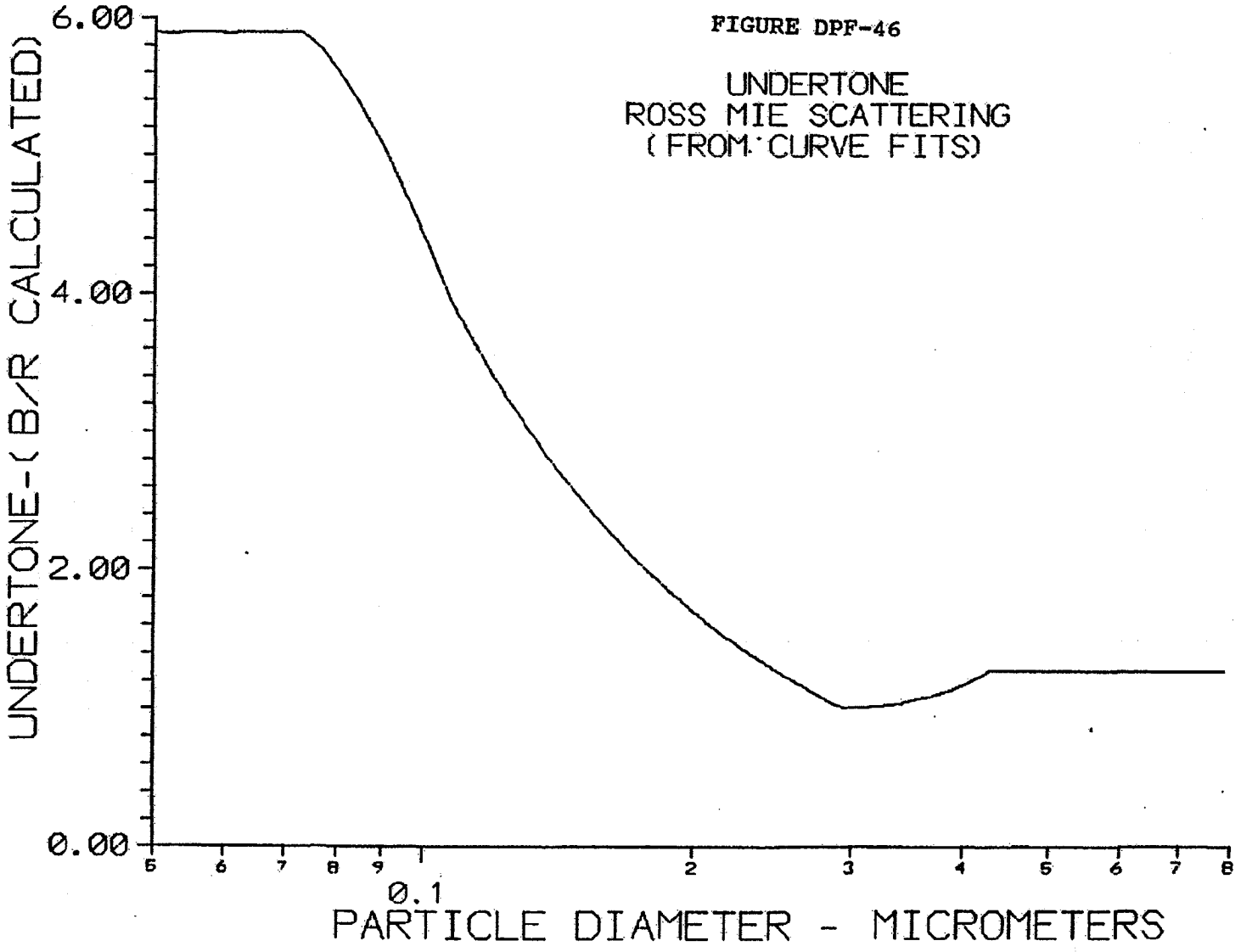

FIGURE DPF-47

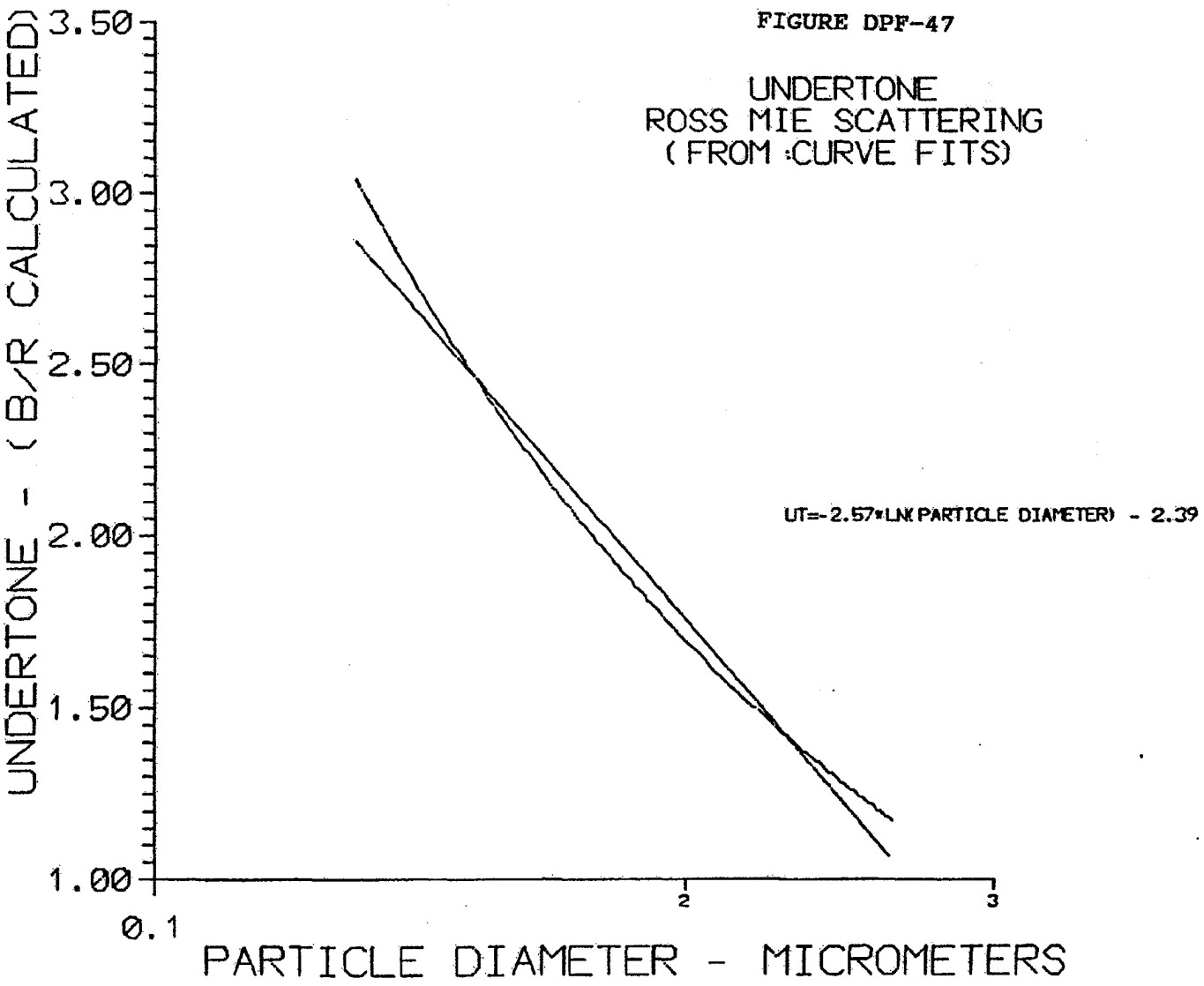

FIGURE DPF-48

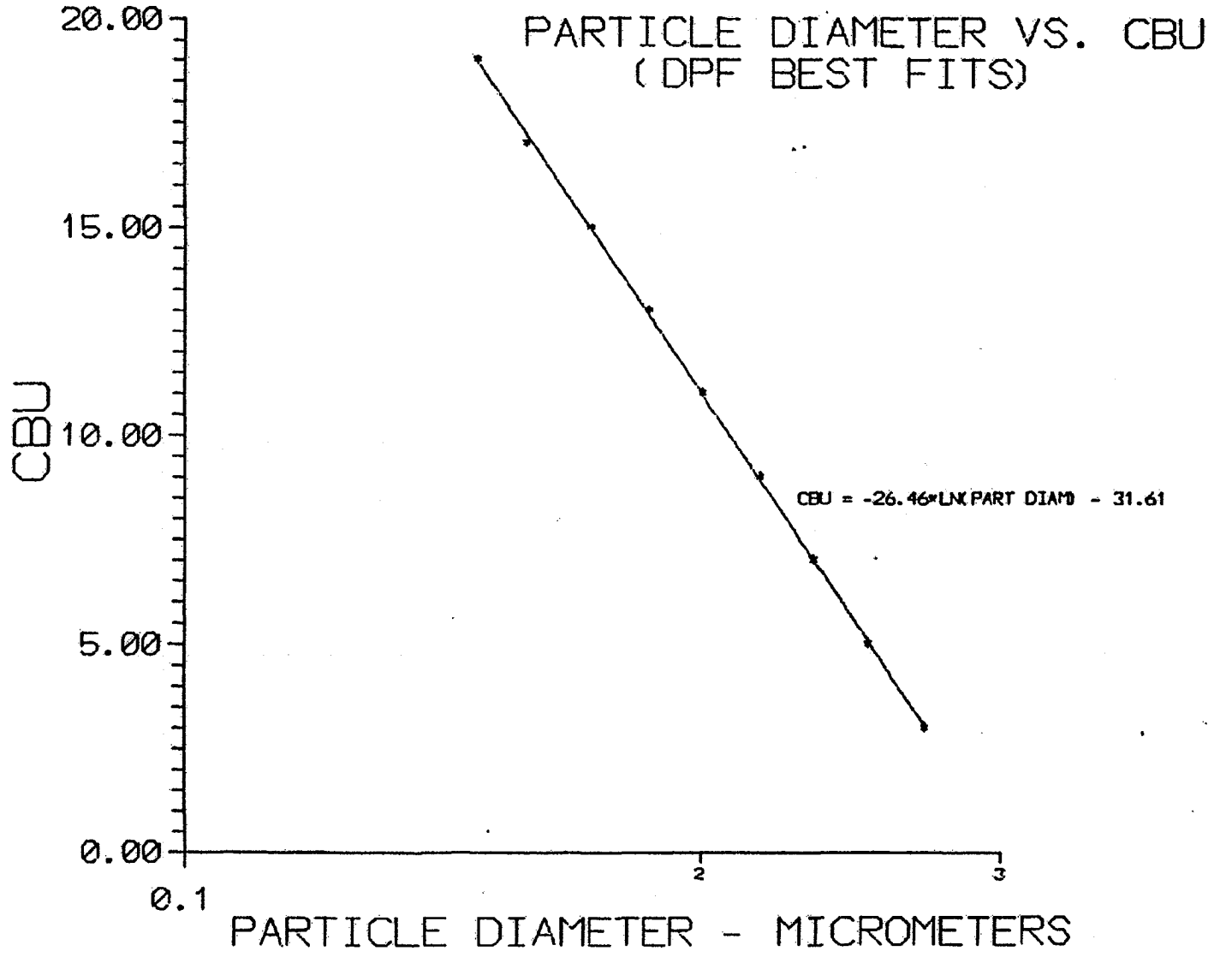

FIGURE DPF-49

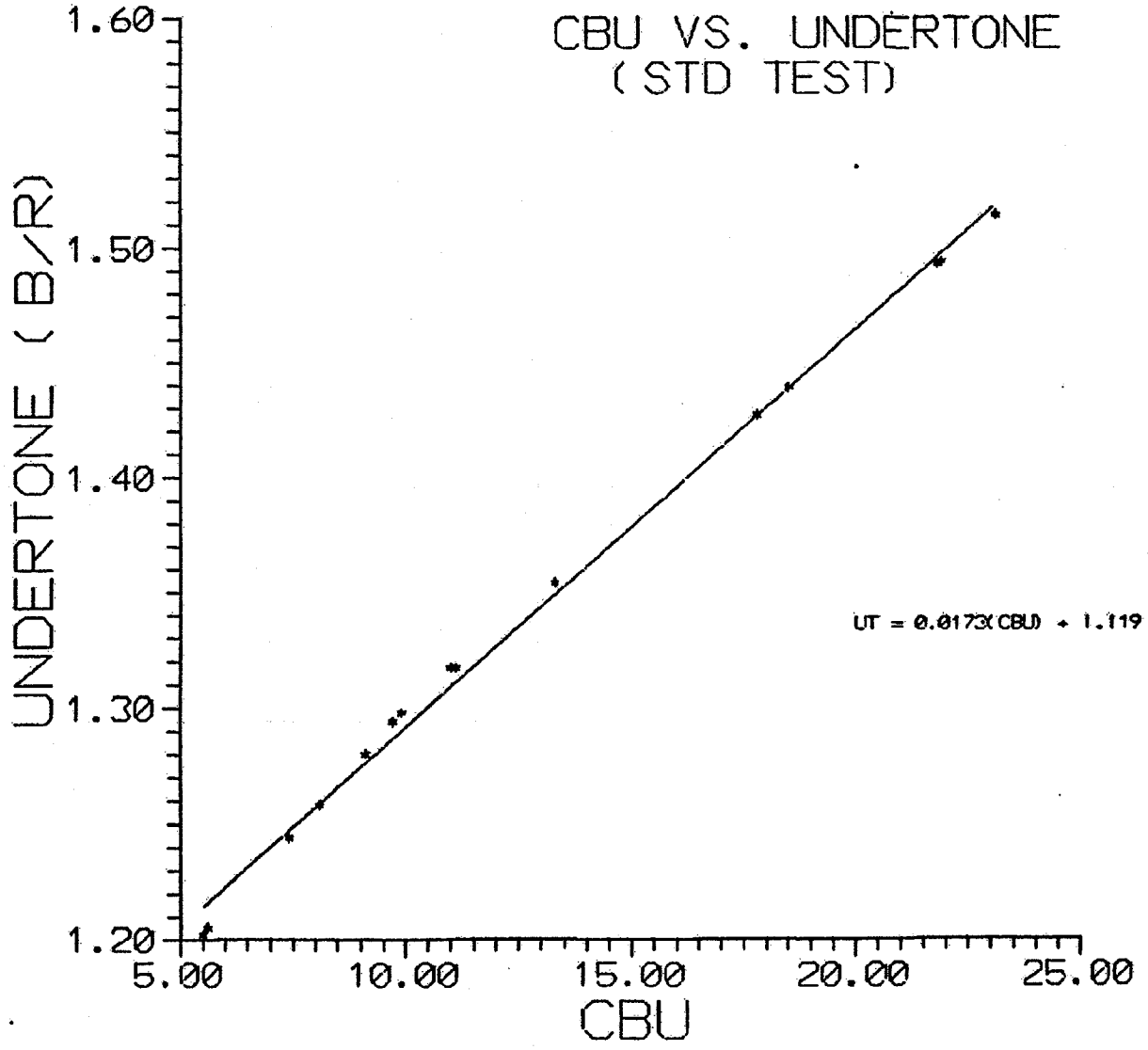

FIGURE DPF-50

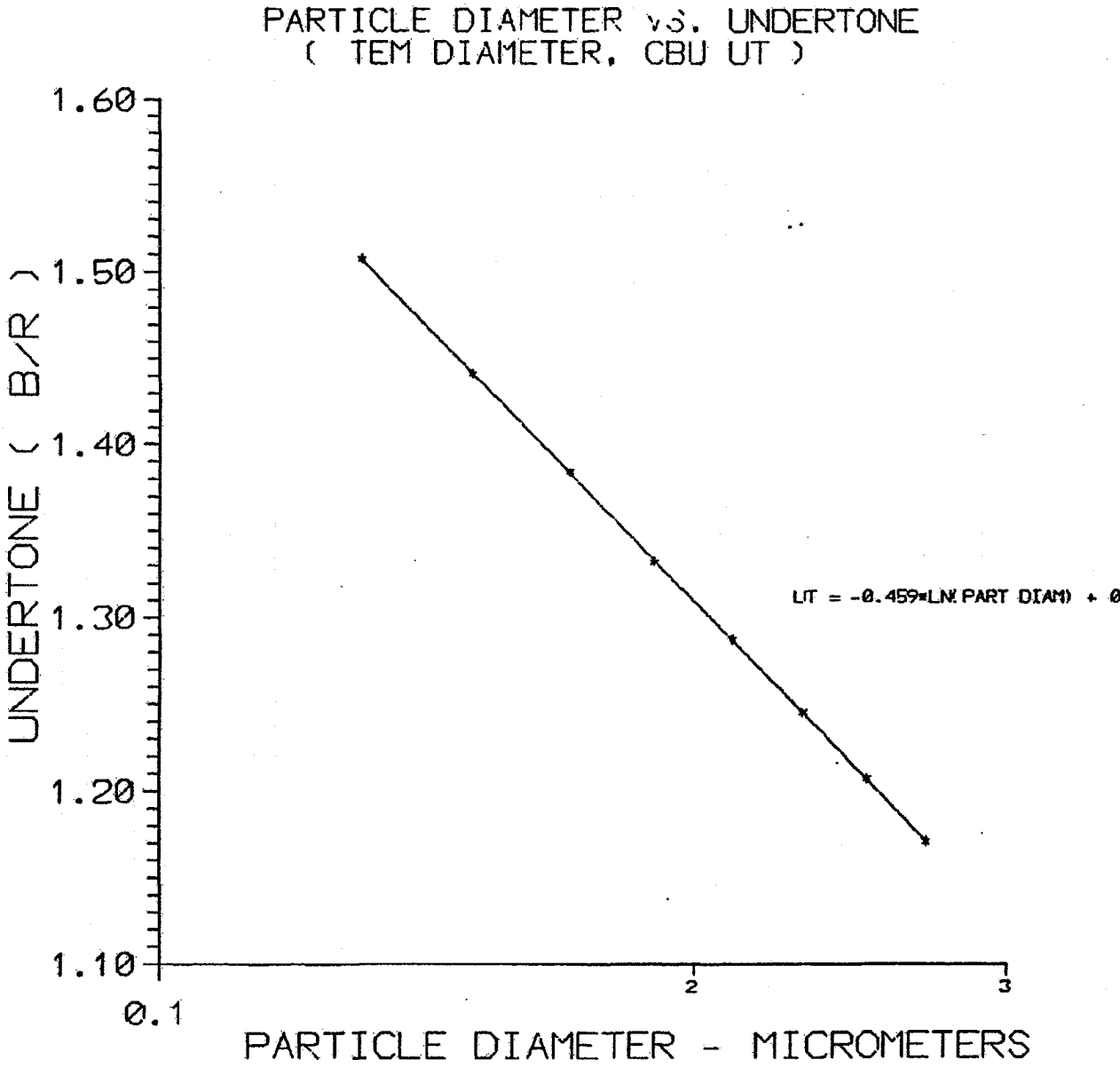

FIGURE DPF-51

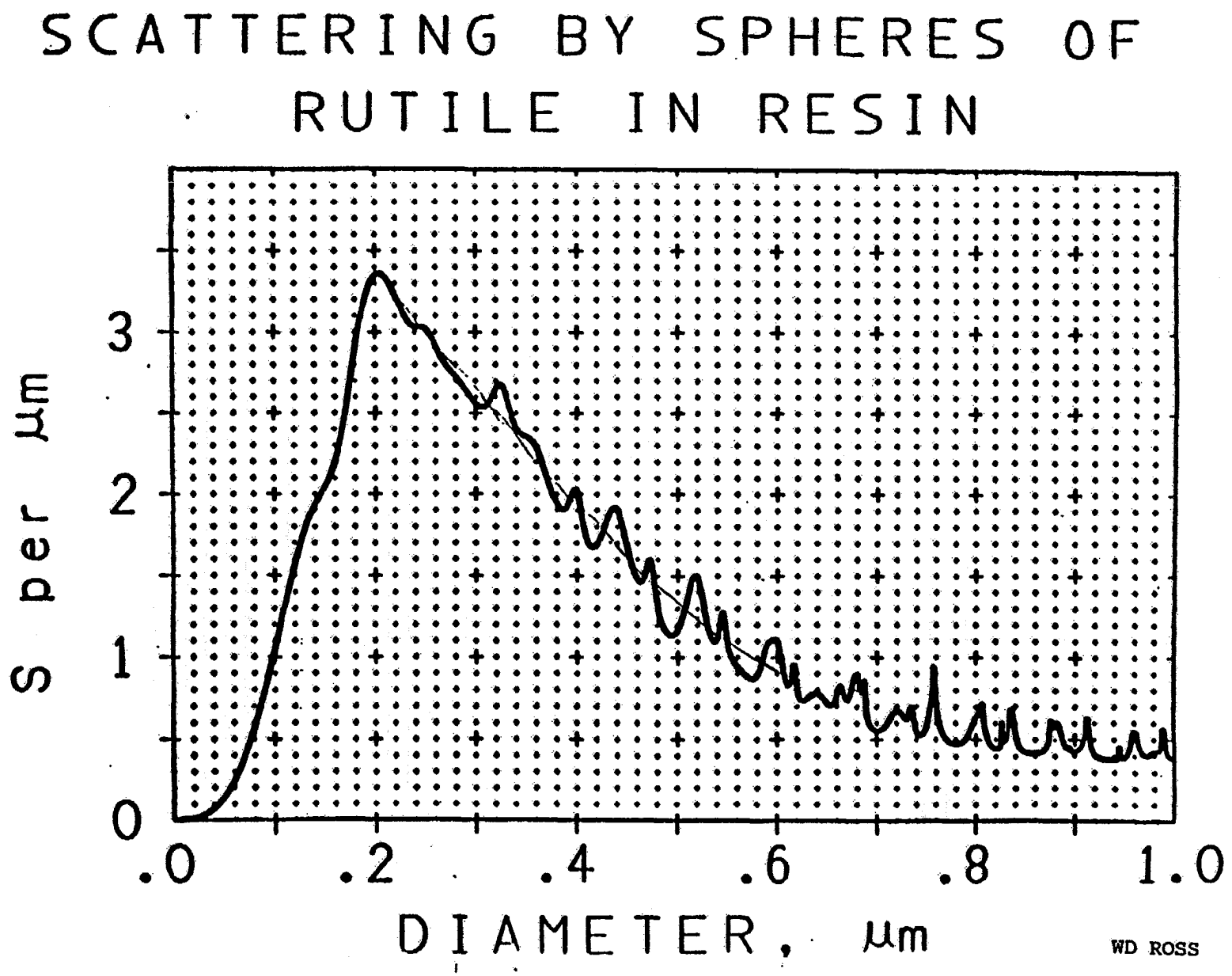

FIGURE DPF-52

RUTILE, LOG NORMAL DISTRIBUTIONS

IN MEDIUM OF REFRACTIVE INDEX 1.524, λ = .560 μm

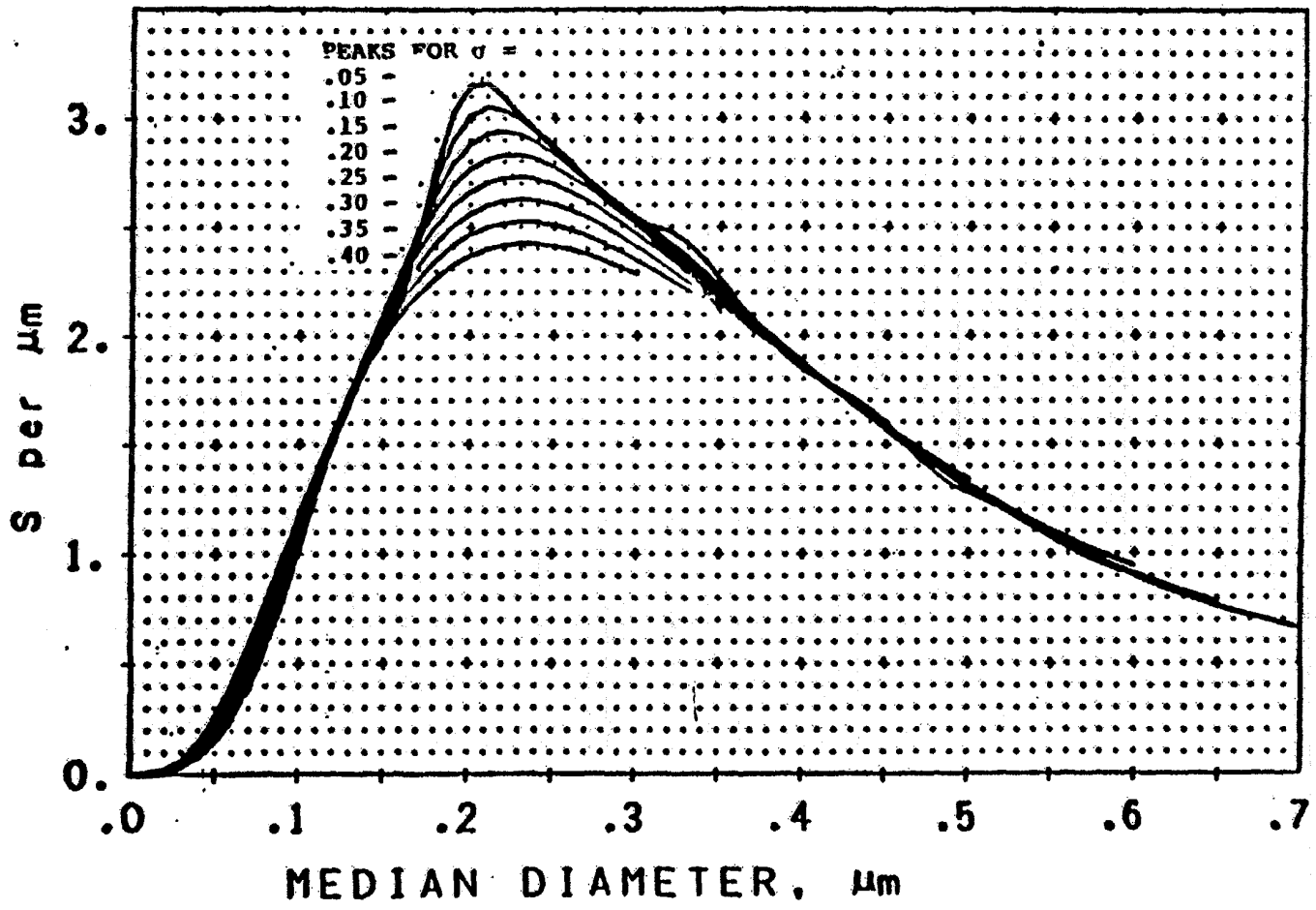

FIGURE DPF-53

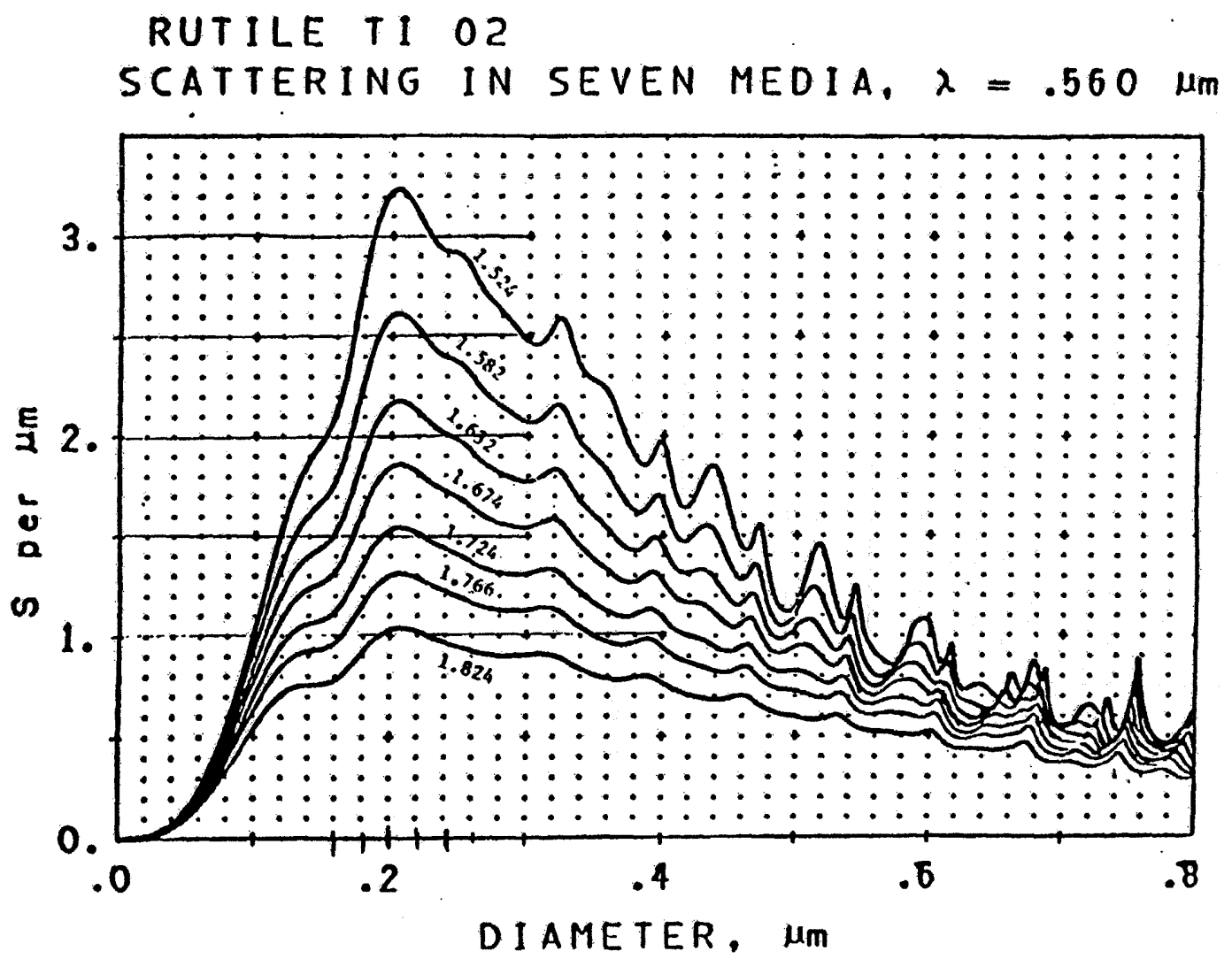

CP-JL-87-08

FIGURE DPF-54

SCATTERING AS F(REFRACTIVE IND
0.20 DIAMETER RUTILE PARTICLE

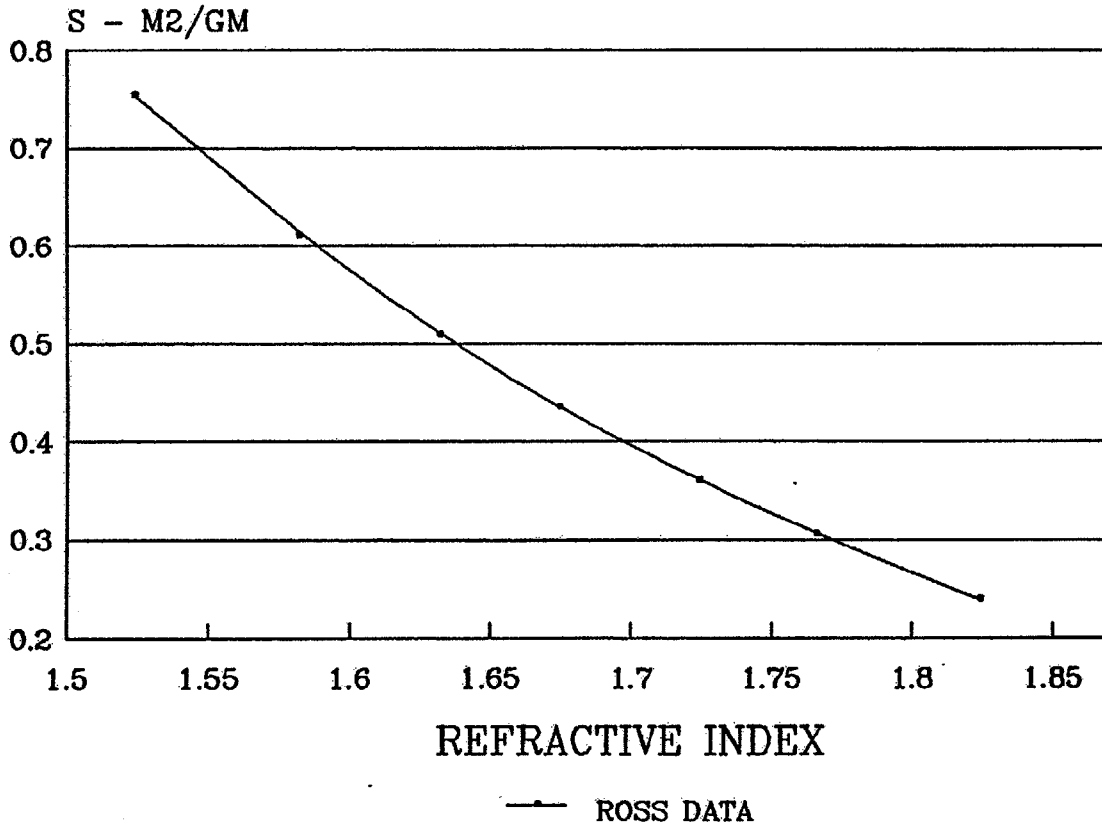

FIGURE DPF-55

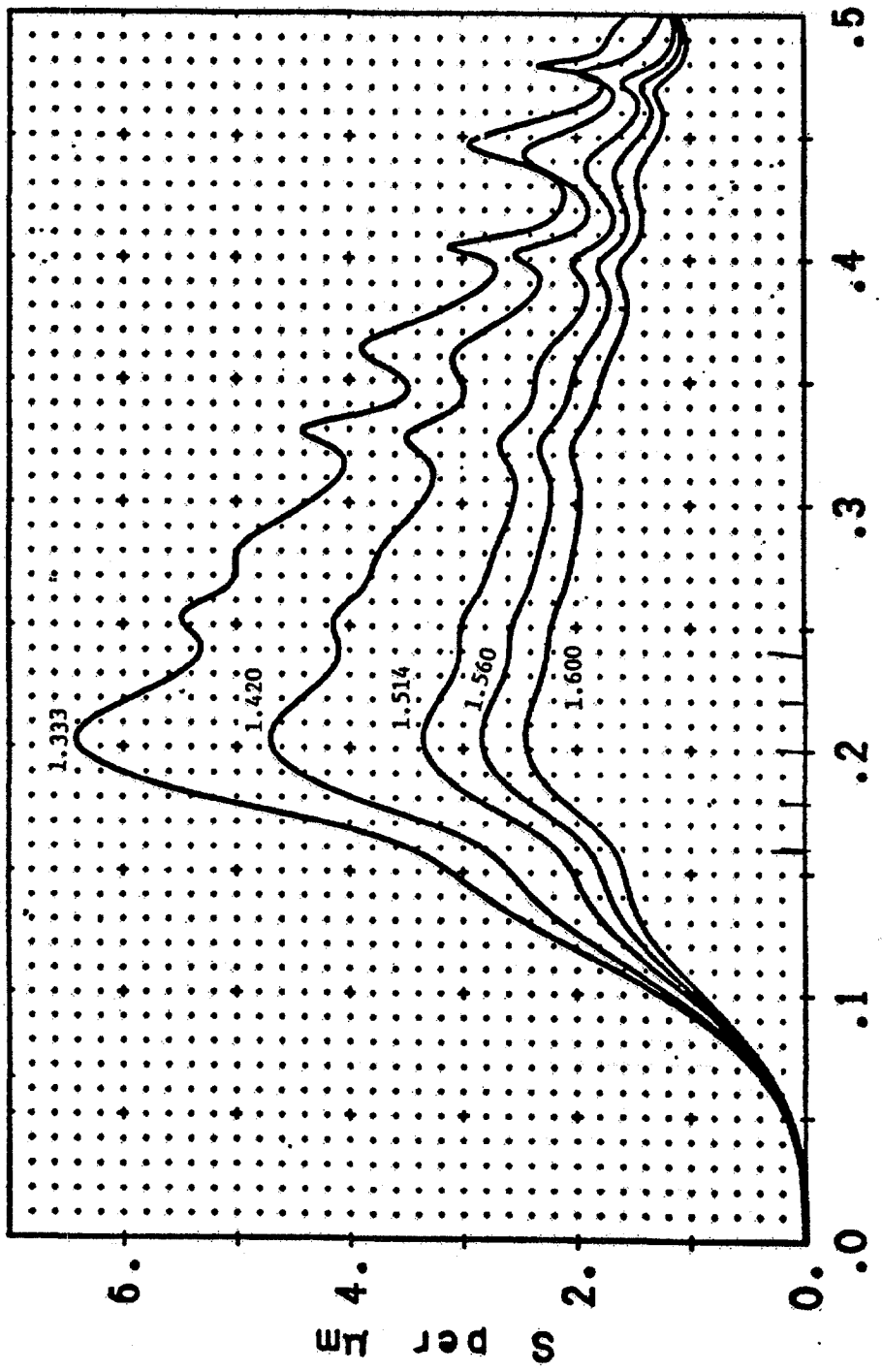

FIGURE DPF-56

SCATTERING AS F(REFRACTIVE INI
0.20 DIAMETER RUTILE PARTICLI

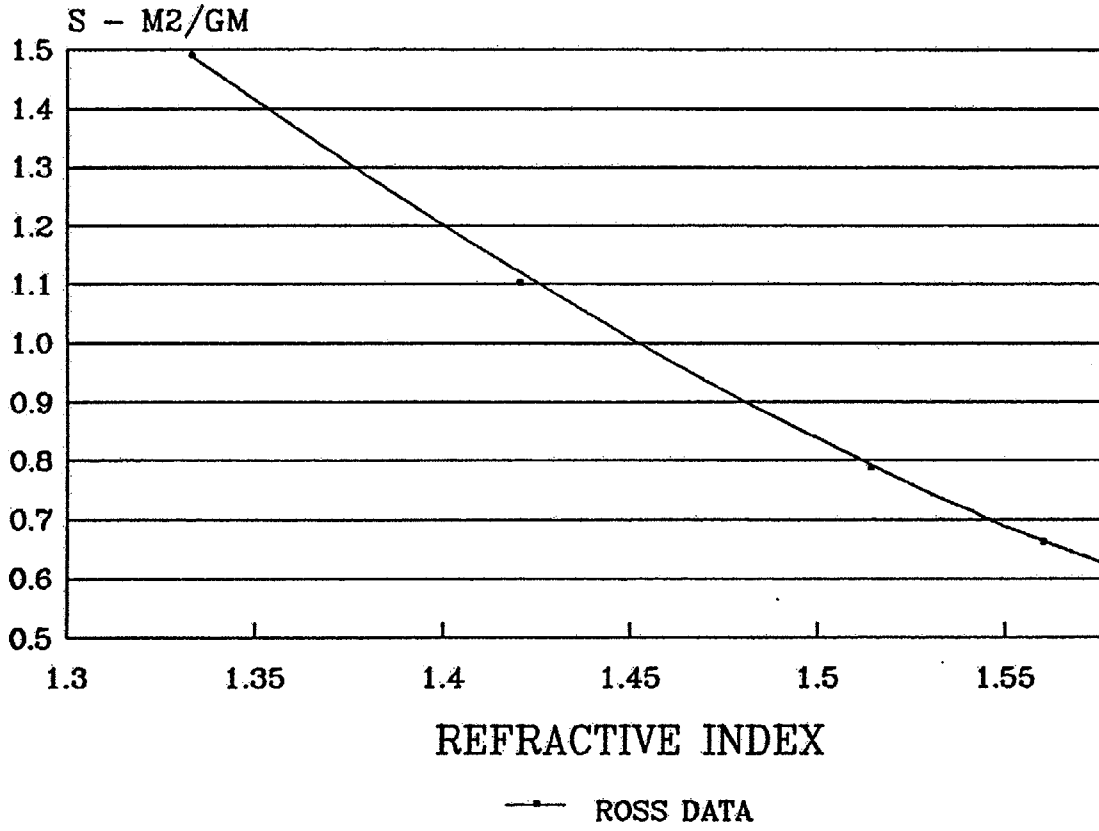

FIGURE DPF-57

SCATTERING AS F(REFRACTIVE IND
0.20 DIAMETER RUTILE PARTICLE

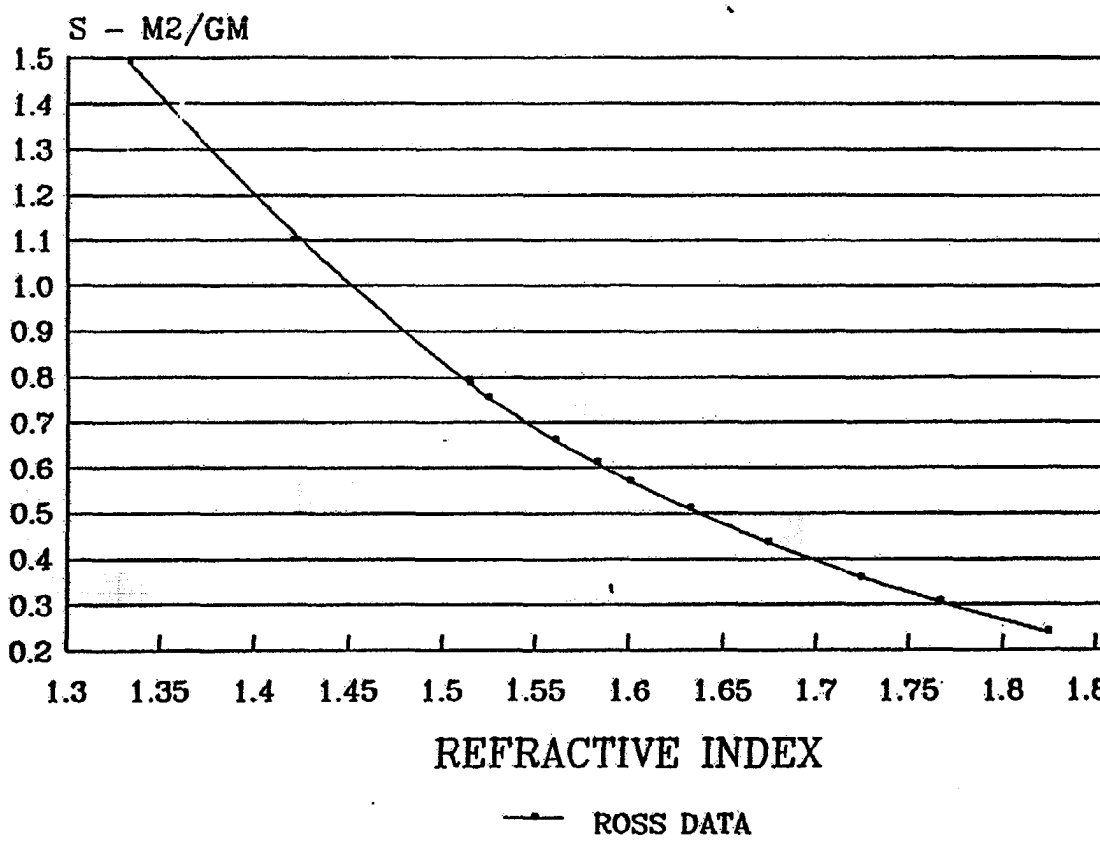

COMPOSITE OF WD

FIGURE DPF-58

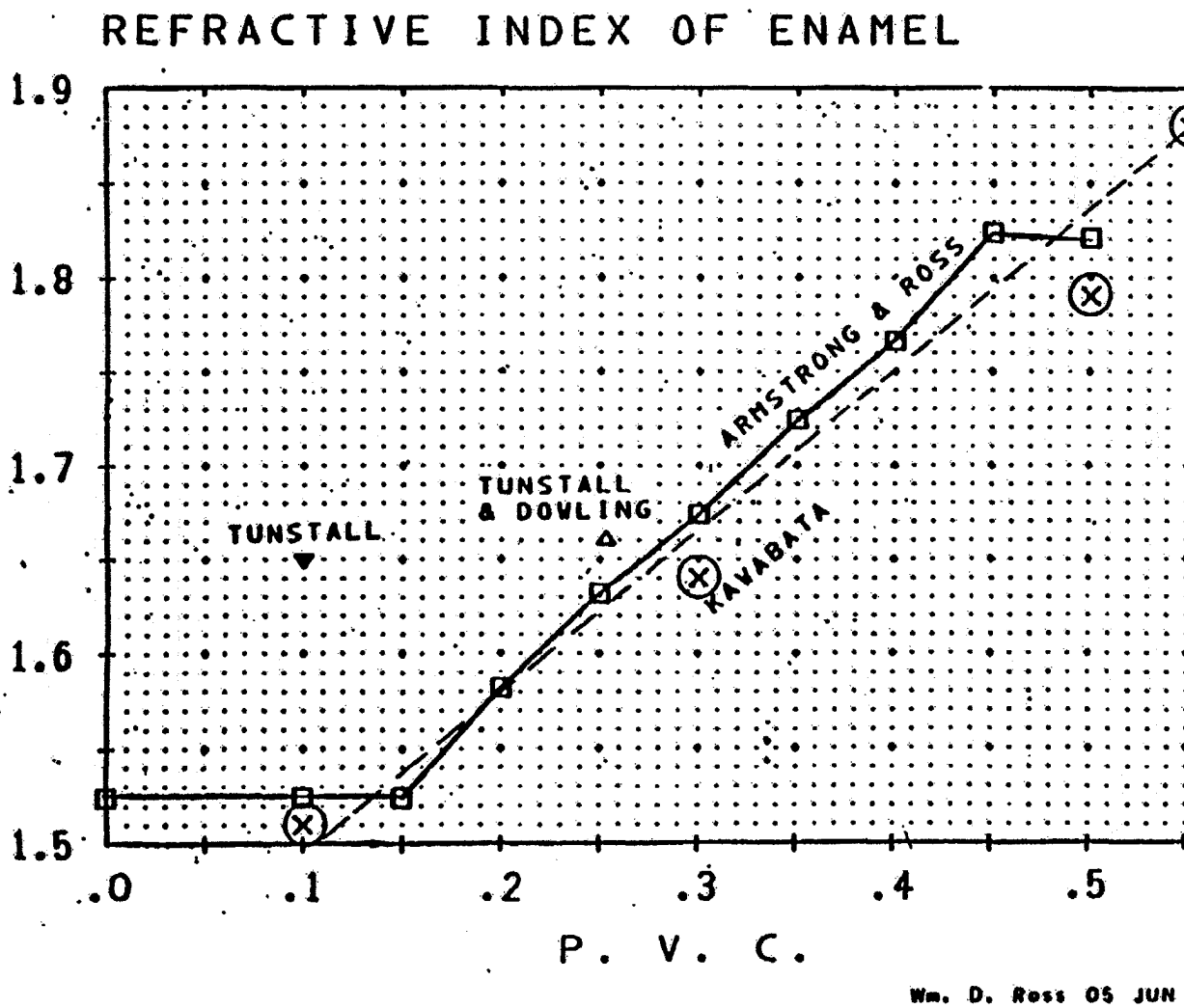

FIGURE DPF-59

ENAMEL REFRACTIVE INDEX VS. ROSS DATA

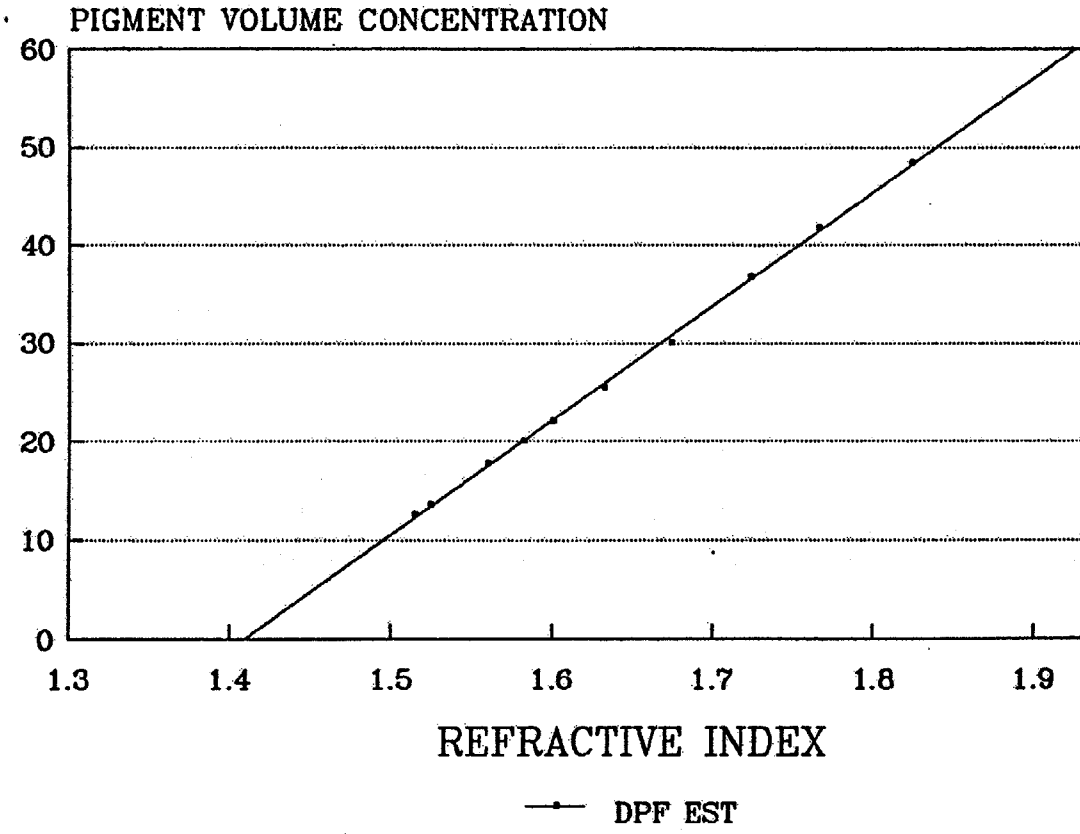

FIGURE DPE-60

M2/GM DATA)

MONOSIZE DISTRIBUTION (ROSS

TIO2 SCATTERING -

FIGURE DPF-61

TIO2 SCATTERING DATA
ROSS DATA - 0.20 DIAMETER

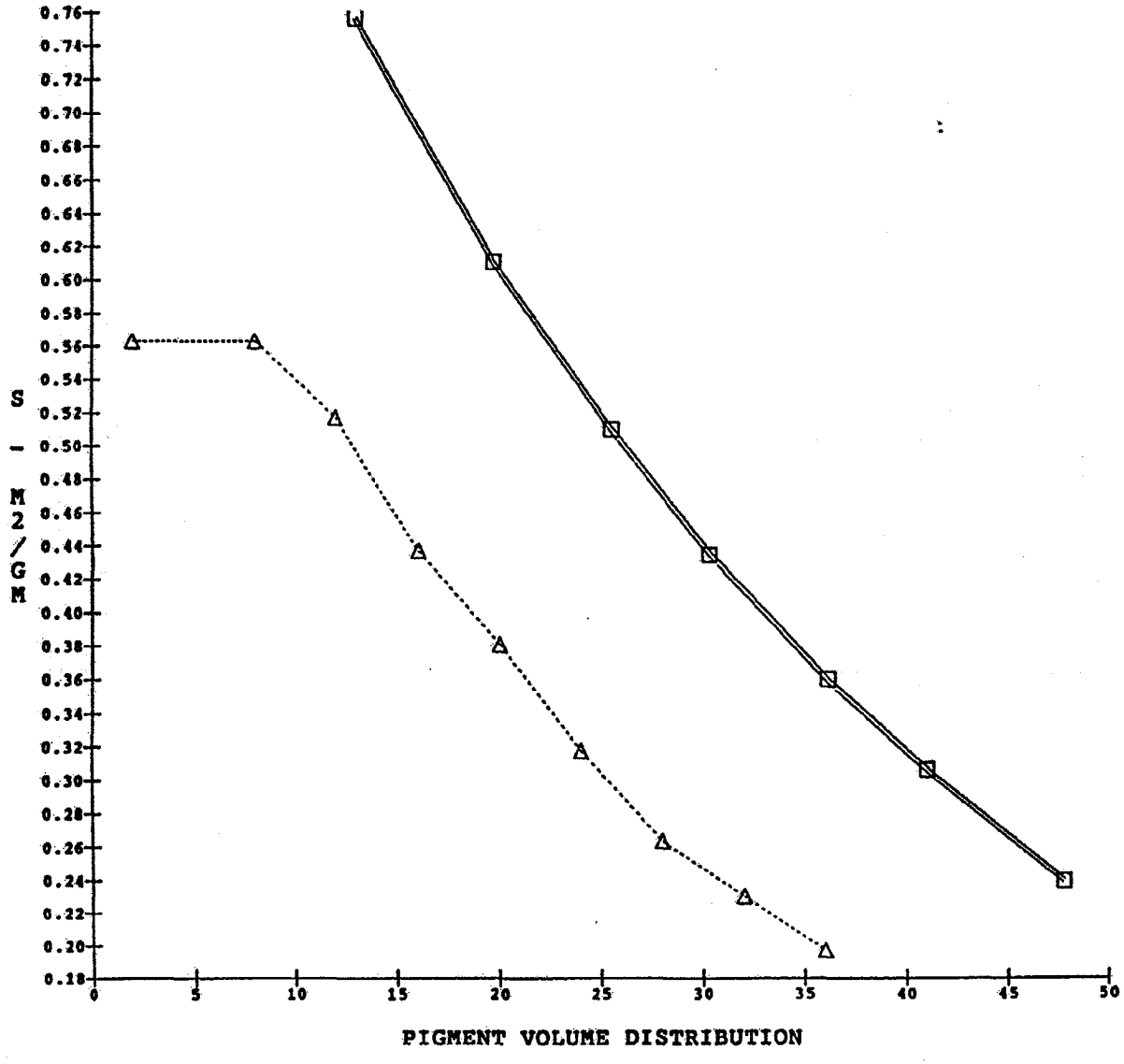

FIGURE DPF-62

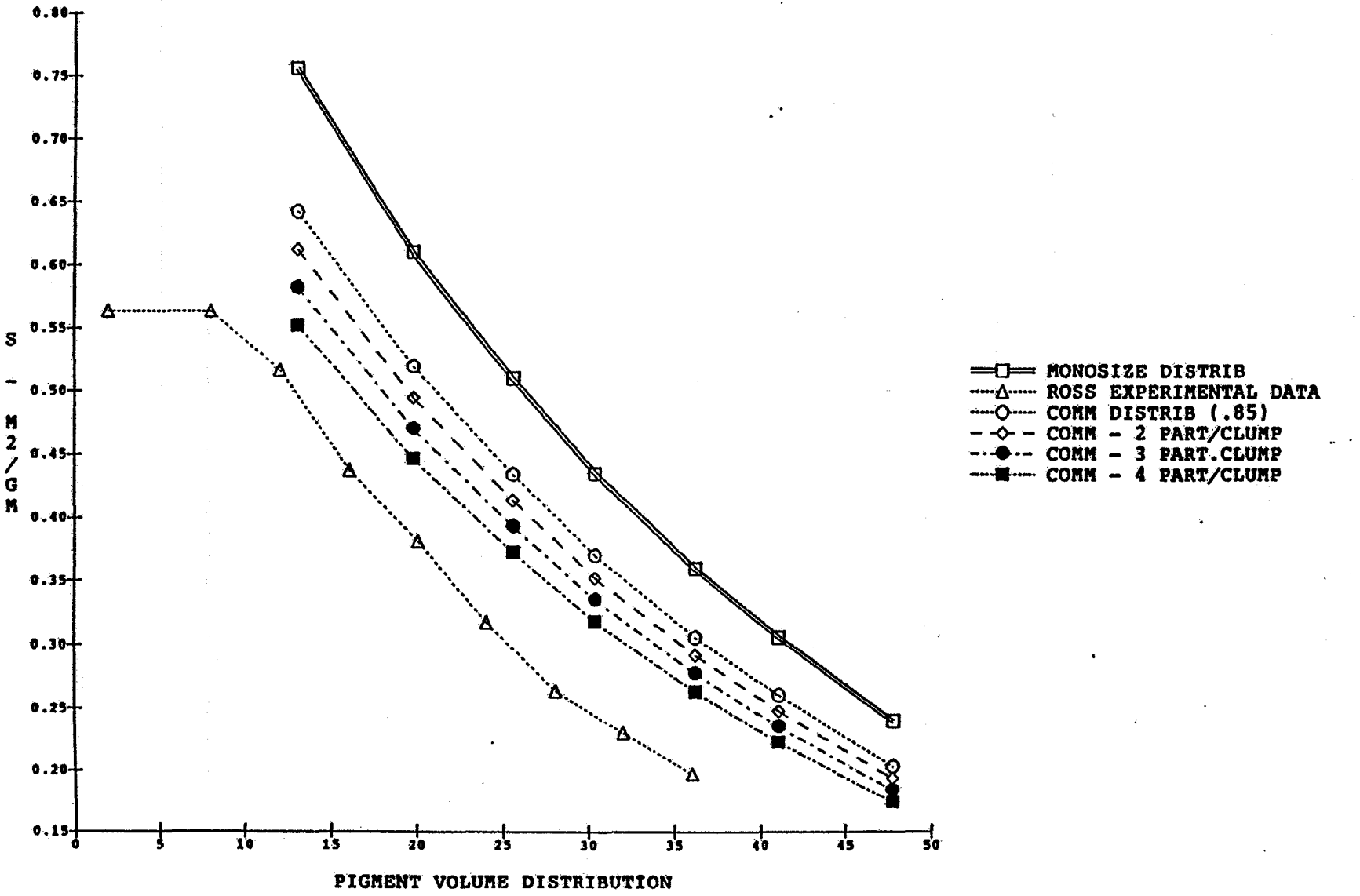

TABLE DPF-24

ROSS/BRUEHLMAN (R&D TIO2) - 1969

TIO2 S VALUE (MEASURED) - 0.52 M^2/GM

MIE SCAT MAX S FOR 1.514 REFRACTIVE INDEX - 0.785 M^2/GM

```
  0.785
 -0.520          0.265/0.785*100 = 34% LOSS IN S (HP)
 ------
  0.265
```

KNOWN - 15% HP LOSS FOR COMMERCIAL PRIMARY PARTICLE SIZE DISTRIBUTION (VS. OPTIMUM MONOSIZE)

- 5% HP LOSS FOR AGGREGATION

UNKNOWN - 14% REMAINING UNACCOUNTED FOR

NOTE: NO SIGNIFICANT HP INCREASE HAS BEEN OBSERVED DURING THE LAST 25 YEARS (LOW PVC SYSTEMS)

TABLE DPF-25

SPOONER/CAIRNS (TECHNICAL SERVICE COLORS) - 1975

TIO2 S VALUE (MEASURED) - 0.70 M^2/GM

MIE SCAT MAX S FOR 1.48 REFRACTIVE INDEX - 0.885 M^2/GM

```
  0.885
 -0.700          0.185/0.885*100 = 21% LOSS IN S (HP)
 ------
  0.185
```

KNOWN - 15% HP LOSS FOR COMMERCIAL PRIMARY PARTICLE SIZE DISTRIBUTION (VS. OPTIMUM MONOSIZE)

- 5% HP LOSS FOR AGGREGATION

20% OR ESSENTIALLY ALL HP ACCOUNTED FOR

APPENDIX

ATT-1

"INDXREFI.BAS"

```
'INDEX OF REFRACTION CALCULATIONS
CLS
LPRINT "INDEX OF REFRACTION CALCULATIONS"
LPRINT : LPRINT
PRINT "SINGLE [1] OR MULTIPLE [2] CALCULATIONS"
INPUT Z%
SELECT CASE Z%
    CASE 1
    GOTO SING
    CASE 2
    GOTO MULT
END SELECT
SING:
INPUT "PIGMENT INDEX OF REFRACTION"; NP
INPUT "VEHICLE INDEX OF REFRACTION"; NV
A = (NP / NV)
B = NP - NV
M = (A ^ 2 - 1) / (A ^ 2 + 2)
MAPPROX = .4 * B
LPRINT "PIGMENT INDEX OF REFRACTION, NP = "; NP
LPRINT "VEHICLE INDEX OF REFRACTION, NV = "; NV
LPRINT "M CALCULATED = "; M
LPRINT "M APPROX = "; MAPPROX
LPRINT "M SQUARED (CALC) = "; M ^ 2.
LPRINT "M SQUARED (APPROX) = "; MAPPROX ^ 2
LPRINT "OPTIMUM DIAMETER FOR BLUE LIGHT  - (0.45 MICRONS)"; "    "; FIX(.45 * 1000 / (4.443 * NV * M)) / 1000; " MICRONS"
LPRINT "OPTIMUM DIAMETER FOR GREEN LIGHT - (0.56 MICRONS)"; "    "; FIX(.56 * 1000 / (4.443 * NV * M)) / 1000; " MICRONS"
LPRINT "OPTIMUM DIAMETER FOR RED LIGHT   - (0.59 MICRONS)"; "    "; FIX(.59 * 1000 / (4.443 * NV * M)) / 1000; " MICRONS"
LPRINT : LPRINT
INPUT "RUN ANOTHER CALCULATION? - Y/N"; YN$
IF YN$ = "Y" THEN GOTO SING ELSE END
MULT:
LPRINT CHR$(27); CHR$(40); CHR$(115); CHR$(50); CHR$(48); CHR$(72)
WIDTH LPRINT 160
LPRINT "PIGMENT", "VEHICLE", , "M", "M", "M^2", "M^2", "D opt", "D opt", "D opt", "ADIF M^2"
LPRINT "INDEX", "INDEX", , "CALC", "APPROX", "CALC", "APPROX", "BLUE", "GRN", "RED", "APPROX VS. CALC"
LPRINT : LPRINT
INPUT "PIGMENT INDEX OF REFRACTION START"; NPS!
INPUT "PIGMENT INDEX OF REFRACTION END"; NPE!
INPUT "PIGMENT INDEX OF REFRACTION INCREMENT"; NPI!
INPUT "VEHICLE INDEX OF REFRACTION START"; NVS!
INPUT "VEHICLE INDEX OF REFRACTION END"; NVE!
INPUT "VEHICLE INDEX OF REFRACTION INCREMENT"; NVI!
FOR NP! = NPS! TO NPE! STEP NPI!
FOR NV! = NVS! TO NVE! STEP NVI!
A! = (NP! / NV!)
B! = NP! - NV!
M! = (A! ^ 2 - 1) / (A! ^ 2 + 2)
MAPPROX! = .4 * B!
X! = (FIX(.45 / (4.443 * NV! * M!) * 1000)) / 1000
Y! = (FIX(.56 / (4.443 * NV! * M!) * 1000)) / 1000
Z! = (FIX(.59 / (4.443 * NV! * M!) * 1000)) / 1000
LPRINT NP!, NV!, , FIX(M! * 1000) / 1000, FIX(MAPPROX! * 1000) / 1000, FIX(M! ^ 2 * 1000) / 1000, FIX(MAPPROX! ^ 2 * 1000) / 1000, X!, Y!, Z!, ((FIX(M! ^ 2 * 10
NEXT NV!
LPRINT
NEXT NP!
END
```

APPENDIX

ATT-2

OUTPUT FROM

"INDXREF1.BAS"

INDEX OF REFRACTION CALCULATIONS

PIGMENT INDEX OF REFRACTION, NP = 2.75
VEHICLE INDEX OF REFRACTION, NV = 1.5
N CALCULATED = .4404145
N APPROX = .5
N SQUARED (CALC) = .1939649
N SQUARED (APPROX) = .25
OPTIMUM DIAMETER FOR BLUE LIGHT - (0.45 MICRONS) .151 MICRONS
OPTIMUM DIAMETER FOR GREEN LIGHT - (0.56 MICRONS) .19 MICRONS
OPTIMUM DIAMETER FOR RED LIGHT - (0.59 MICRONS) .201 MICRONS

APPENDIX

ATT-3

OUTPUT FROM "INDXREF1.BAS

INDEX OF REFRACTION CALCULATIONS

PIGMENT INDEX	VEHICLE INDEX	N CALC	N APPROX	N^2 CALC	N^2 APPROX	D opt BLUE	D opt GRN	D opt RED	%DIF N^2 APPROX VS. CALC
2.55	1	.647	.62	.418	.384	.156	.194	.205	8.133971
2.55	1.1	.593	.579	.351	.336	.155	.193	.203	4.273504
2.55	1.2	.539	.539	.291	.291	.156	.194	.205	0
2.55	1.3	.486	.499	.237	.249	.159	.199	.209	-5.063291
2.55	1.4	.435	.459	.189	.211	.165	.206	.217	-11.64021
2.55	1.5	.386	.419	.149	.176	.174	.217	.229	-18.12081
2.55	1.6	.339	.379	.115	.144	.186	.232	.244	-25.21739
2.55	1.7	.294	.339	.086	.115	.202	.252	.265	-33.72093
2.6	1	.657	.639	.432	.409	.154	.191	.201	5.324074
2.6	1.1	.604	.599	.365	.359	.152	.189	.199	1.643836
2.6	1.2	.551	.559	.304	.313	.152	.19	.2	-2.960526
2.6	1.3	.499	.519	.249	.27	.155	.193	.204	-8.433735
2.6	1.4	.449	.479	.201	.23	.16	.2	.211	-14.42786
2.6	1.5	.4	.439	.16	.193	.168	.209	.221	-20.625
2.6	1.6	.353	.399	.124	.159	.179	.222	.234	-28.22581
2.6	1.7	.308	.359	.095	.129	.193	.24	.253	-35.78947
2.65	1	.667	.659	.445	.435	.151	.188	.198	2.247191
2.65	1.1	.615	.619	.378	.384	.149	.186	.196	-1.587302
2.65	1.2	.563	.579	.317	.336	.149	.186	.196	-5.993691
2.65	1.3	.512	.539	.262	.291	.151	.189	.199	-11.0687
2.65	1.4	.462	.499	.214	.249	.156	.194	.205	-16.35514
2.65	1.5	.414	.459	.171	.211	.163	.202	.213	-23.39181
2.65	1.6	.367	.419	.135	.176	.172	.214	.225	-30.37037
2.65	1.7	.322	.379	.104	.144	.184	.229	.241	-38.46154
2.7	1	.677	.679	.458	.462	.149	.186	.196	-.8733624
2.7	1.1	.626	.639	.392	.409	.147	.182	.192	-4.336735
2.7	1.2	.575	.599	.33	.359	.146	.182	.192	-8.787879
2.7	1.3	.524	.559	.275	.313	.148	.184	.194	-13.81818
2.7	1.4	.475	.519	.226	.27	.152	.189	.199	-19.46903
2.7	1.5	.427	.479	.182	.23	.157	.196	.207	-26.37363
2.7	1.6	.381	.439	.145	.193	.166	.206	.217	-33.10345
2.7	1.7	.336	.399	.113	.159	.176	.22	.232	-40.70797
2.75	1	.686	.699	.47	.489	.147	.183	.193	-4.042553
2.75	1.1	.636	.659	.404	.435	.144	.18	.189	-7.673267
2.75	1.2	.586	.619	.343	.384	.143	.179	.188	-11.95335
2.75	1.3	.536	.579	.288	.336	.145	.18	.19	-16.66667
2.75	1.4	.487	.539	.238	.291	.148	.184	.194	-22.26891
2.75	1.5	.44	.499	.193	.249	.153	.19	.201	-29.01554
2.75	1.6	.394	.459	.155	.211	.16	.199	.21	-36.12903
2.75	1.7	.35	.419	.122	.176	.17	.211	.223	-44.26229

APPENDIX

ATT-4

'WDR1SCAT.BAS"

```
INPUT "START PARTICLE DIAMETER = ", A!
INPUT "INCREMENTAL PARTICLE SIZE = ", A1!
INPUT "PARTICLE SIZE CUT-OFF = ", A2!
'LPRINT "WAVELENGTH - 445nm"
D1! = .073
D2! = .1533
D3! = .292
C1! = 1563.1826!
C2! = 1.62
C3! = .22591
INPUT "ENTER BLUE DATA FILE NAME - SCAT/B   ", SB$
INPUT "ENTER GREEN DATA FILE NAME - SCAT/G  ", SG$
INPUT "ENTER RED DATA FILE NAME - SCAT/R    ", SR$
OPEN SB$ FOR OUTPUT AS #1
AA! = A!
IF AA! < D1! THEN GOTO A
IF AA! <= D3! THEN GOTO AA
IF AA! > D3! THEN GOTO AAA
A:
DO WHILE AA! < D1!
S! = AA! ^ 3 * C1!
WRITE #1, AA!, S!
AA! = AA! + A1!
IF AA! >= A2! GOTO AAAA
LOOP
AA:
DO WHILE AA! <= D3!
S! = C2! * (EXP((((LOG(AA! / D2!)) / .53) ^ 2) * -.5))
WRITE #1, AA!, S!
AA! = AA! + A1!
IF AA! >= A2! GOTO AAAA
LOOP
AAA:
DO WHILE AA! > D3!
S! = C3! / AA!
WRITE #1, AA!, S!
AA! = AA! + A1!
IF AA! >= A2! GOTO AAAA
LOOP
AAAA:
CLOSE #1
'LPRINT "WAVELENGTH - 550nm"
D1! = .1
D2! = .21
D3! = .4
C1! = 375.3732
C2! = 1
C3! = .19103
OPEN SG$ FOR OUTPUT AS #2
AA! = A!
IF AA! < D1! THEN GOTO B
IF AA! <= D3! THEN GOTO BB
IF AA! > D3! THEN GOTO BBB
B:
DO WHILE AA! < D1!
S! = AA! ^ 3 * C1!
WRITE #2, AA!, S!
AA! = AA! + A1!
```

```
IF AA! >= A2! GOTO BBBB
LOOP
BB:
DO WHILE AA! <= D3!
S! = C2! * (EXP((((LOG(AA! / D2!)) / .53) ^ 2) * -.5))
WRITE #2, AA!, S!
AA! = AA! + A1!
IF AA! >= A2! GOTO BBBB
LOOP
BBB:
DO WHILE AA! > D3!
S! = C3! / AA!
WRITE #2, AA!, S!
AA! = AA! + A1!
IF AA! >= A2! GOTO BBBB
LOOP
BBBB:
CLOSE #2
'LPRINT "WAVELENGTH - 600nm"
D1! = .107
D2! = .2247
D3! = .428
C1! = 265.0502
C2! = .865
C3! = .17681
OPEN SR$ FOR OUTPUT AS #3
AA! = A!
IF AA! < D1! THEN GOTO C
IF AA! <= D3! THEN GOTO CC
IF AA! > D3! THEN GOTO CCC
C:
DO WHILE AA! < D1!
S! = AA! ^ 3 * C1!
WRITE #3, AA!, S!
AA! = AA! + A1!
IF AA! >= A2! GOTO CCCC
LOOP
CC:
DO WHILE AA! <= D3!
S! = C2! * (EXP((((LOG(AA! / D2!)) / .53) ^ 2) * -.5))
WRITE #3, AA!, S!
AA! = AA! + A1!
IF AA! >= A2! GOTO CCCC
LOOP
CCC:
DO WHILE AA! > D3!
S! = C3! / AA!
WRITE #3, AA!, S!
AA! = AA! + A1!
IF AA! >= A2! GOTO CCCC
LOOP
CCCC:
CLOSE #3
END
```

APPENDIX

ATT-5

"PRTSCAT1.BAS"

```
CLS
PRT1$ = " #.###      #.####      #.###      #.####      #.###      #.####"
LPRINT "MD ROSS MIE SCATTERING CALCULATIONS - DPP PROGRAMS MDR1SCAT.BAS, PRTSCAT1.BAS"
LPRINT
INPUT "NAME OF BLUE SCATTERING DATA FILE  ", SS1$
INPUT "NAME OF GREEN SCATTERING DATA FILE  ", SS2$
INPUT "NAME OF RED SCATTERING DATA FILE   ", SS3$
OPEN SS1$ FOR INPUT AS #1
OPEN SS2$ FOR INPUT AS #2
OPEN SS3$ FOR INPUT AS #3
CLS
LPRINT SS$
LPRINT
LPRINT "     BLUE - 445nm     "; " "; "      GREEN - 550nm   "; "        RED - 600nm"
LPRINT
LPRINT "PARTICLE"; "    "; "CALCULATED"; "    "; "PARTICLE"; "    "; "CALCULATED"; "    "; "PARTICLE"; "    "; "CALCULATED"
LPRINT "DIAMETER"; "    "; "SCATTERING"; "    "; "DIAMETER"; "    "; "SCATTERING"; "    "; "DIAMETER"; "    "; "SCATTERING"

LPRINT "--------"; "    "; "----------"; "    "; "--------"; "    "; "----------"; "    "; "--------"; "    "; "----------"
DO WHILE (NOT EOF(1))
INPUT #1, VALUE1#
INPUT #1, VALUE2#
INPUT #2, VALUE3#
INPUT #2, VALUE4#
INPUT #3, VALUE5#
INPUT #3, VALUE6#
LPRINT USING PRT1$; VALUE1#; VALUE2#; VALUE3#; VALUE4#; VALUE5#; VALUE6#
LOOP
LPRINT CHR$(12)
```

APPENDIX

ATT-6

OUTPUT FROM "WRDSCAT1.BAS" & PRTSCAT.BA

MD ROSS MIE SCATTERING CALCULATIONS - DPF PROGRAMS MDR1SCAT.BAS, PRTSCAT1.BAS

BLUE - 445nm		GREEN - 550nm		RED - 600nm	
PARTICLE DIAMETER	CALCULATED SCATTERING	PARTICLE DIAMETER	CALCULATED SCATTERING	PARTICLE DIAMETER	CALCULATED SCATTERING
0.000	0.0000	0.000	0.0000	0.000	0.0000
0.010	0.0016	0.010	0.0004	0.010	0.0003
0.020	0.0125	0.020	0.0030	0.020	0.0021
0.030	0.0422	0.030	0.0101	0.030	0.0072
0.040	0.1000	0.040	0.0240	0.040	0.0170
0.050	0.1954	0.050	0.0469	0.050	0.0331
0.060	0.3376	0.060	0.0811	0.060	0.0573
0.070	0.5362	0.070	0.1288	0.070	0.0909
0.080	0.7630	0.080	0.1922	0.080	0.1357
0.090	0.9778	0.090	0.2736	0.090	0.1932
0.100	1.1706	0.100	0.3754	0.100	0.2651
0.110	1.3315	0.110	0.4751	0.110	0.3488
0.120	1.4560	0.120	0.5727	0.120	0.4294
0.130	1.5435	0.130	0.6641	0.130	0.5076
0.140	1.5964	0.140	0.7463	0.140	0.5807
0.150	1.6186	0.150	0.8175	0.150	0.6468
0.160	1.6147	0.160	0.8767	0.160	0.7045
0.170	1.5895	0.170	0.9236	0.170	0.7531
0.180	1.5473	0.180	0.9586	0.180	0.7925
0.190	1.4925	0.190	0.9823	0.190	0.8227
0.200	1.4284	0.200	0.9958	0.200	0.8444
0.210	1.3582	0.210	1.0000	0.210	0.8580
0.220	1.2842	0.220	0.9962	0.220	0.8643
0.230	1.2086	0.230	0.9854	0.230	0.8642
0.240	1.1329	0.240	0.9688	0.240	0.8583
0.250	1.0583	0.250	0.9473	0.250	0.8476
0.260	0.9858	0.260	0.9220	0.260	0.8328
0.270	0.9159	0.270	0.8937	0.270	0.8146
0.280	0.8492	0.280	0.8630	0.280	0.7936
0.290	0.7859	0.290	0.8307	0.290	0.7704
0.300	0.7530	0.300	0.7974	0.300	0.7455
0.310	0.7287	0.310	0.7634	0.310	0.7194
0.320	0.7060	0.320	0.7292	0.320	0.6924
0.330	0.6846	0.330	0.6951	0.330	0.6650
0.340	0.6644	0.340	0.6615	0.340	0.6374
0.350	0.6455	0.350	0.6285	0.350	0.6098
0.360	0.6275	0.360	0.5962	0.360	0.5825
0.370	0.6106	0.370	0.5649	0.370	0.5556
0.380	0.5945	0.380	0.5347	0.380	0.5292
0.390	0.5793	0.390	0.5055	0.390	0.5035
0.400	0.5648	0.400	0.4776	0.400	0.4785
0.410	0.5510	0.410	0.4659	0.410	0.4544
0.420	0.5379	0.420	0.4548	0.420	0.4311
0.430	0.5254	0.430	0.4443	0.430	0.4112
0.440	0.5134	0.440	0.4342	0.440	0.4018
0.450	0.5020	0.450	0.4245	0.450	0.3929
0.460	0.4911	0.460	0.4153	0.460	0.3844
0.470	0.4807	0.470	0.4064	0.470	0.3762
0.480	0.4706	0.480	0.3980	0.480	0.3684
0.490	0.4610	0.490	0.3899	0.490	0.3608
0.500	0.4518	0.500	0.3821	0.500	0.3536

0.510	0.4130	0.510	0.3746	0.510	0.3467
0.520	0.4344	0.520	0.3674	0.520	0.3400
0.530	0.4262	0.530	0.3604	0.530	0.3336
0.540	0.4184	0.540	0.3538	0.540	0.3274
0.550	0.4107	0.550	0.3473	0.550	0.3215
0.560	0.4034	0.560	0.3411	0.560	0.3157
0.570	0.3963	0.570	0.3351	0.570	0.3102
0.580	0.3895	0.580	0.3294	0.580	0.3048
0.590	0.3829	0.590	0.3238	0.590	0.2997

JACKSON LABORATORY
DUPONT CHEMICALS
RESEARCH AND DEVELOPMENT DIVISION

TECHNICAL REPORT (CT-JL-92-0θ

DISTRIBUTION LIST

COPY		
1.	D. P. FIELDS, SR. RESEARCH ASSOCIATE, AUTHOR	CR
2.	M. H. LEWIS, DEVELOPMENT & TECH SERVICE MANAGER	CR
3.	A. M. DOYLE, RESEARCH DIRECTOR	B-
4.	C. E. LORENZ, RESEARCH VICE PRESIDENT	B-
5.	A. H. REID, RESEARCH SUPERVISOR	JV
6.	R. L. FREED, SR. RESEARCH SUPERVISOR	EM
7.	J. M. STEED, RESEARCH MANAGER	JL
8.	P. A. TOOLEY, RESEARCH SUPERVISOR	DELISLE
9.	T. W. BOAZ, PRODUCT MANAGER, COATINGS	B-
10.	J. P. PRITCHARD, PRODUCT MANAGER, PLASTICS	BMP
11.	R. A. JOHNS, PRODUCT MANAGER, PAPER	B-
ABSTRACT ONLY		
12.	D. H. REILLEY, VICE PRESIDENT - WP&MP	B-
13.	J. P. JESSON, LABORATORY DIRECTOR	JL
14.	G. E. LYNSKEY, MANUFACTURING DIRECTOR	B-
15.	D. J. GOULD, GROUP COUNCIL, CHEMICALS	M-
16-17.	CENTRAL REPORT INDEX	BMP
18-22.	JACKSON LABORATORY FILES	JL
23.	T. M. TAYLOR (EDGE MOOR FILES)	EM
24.	J. F. MURRILL. TECHNICAL INDEX	EM
25.	S. V. R. MASTRANGELO	EM
26.	J. H. BRAUN	CR
27.	R. E. MARGANSKI	JL
28.	R. A. GONZALEZ	JL
29.	R. J. BUCHACEK	CR
30.	M. R. BALOGA	JV
31.	D. P. SCHUSSLER	DELISLE
32.	R. L. GOROWARA	EM
33.	B. W. SULLIVAN	JL
34.	A. BAIDINS	JL
37.	C. R. BETTLER	CR
38.	D.A. HOLTZEN	CR
39.	B. TECLE	CR
40.	J.D. LEE	EXP ST 357252